Selective non-Catalytic Reduction of NOx in a cyclone reactor

Ahli Gharamaleki, Mohammad

Publication date:
2018

Document Version
Publisher's PDF, also known as Version of record

Selective Non-Catalytic Reduction of NOx in a cyclone reactor

Mohammad Ahli-Gharamaleki

Kongens Lyngby 2018

Technical University of Denmark
Department of Chemical and Biochemical Engineering
Søltofts Plads, building 229,
2800 Kongens Lyngby, Denmark
Phone +45 45252800
kt@kt.dtu.dk
www.kt.dtu.dk

Summary (English)

This project is focused mainly on providing background knowledge of the cyclone reactors and mapping the effect of fluid dynamics involving flow pattern and transport phenomena on a chemical reaction. Targeting this main purpose, SNCR for NOx reduction with the injection of ammonia as a reductant has been chosen as the reaction to be studied. To follow the effect of fluid dynamics on reaction parameters, including temperature profile, residence time and mixing, this thesis presents a detailed study, both with experiments and CFD modeling.

Due to environmental demands and legislation, NOx emission control is becoming stricter worldwide. In some industries, NOx pass by cyclones before emission; therefore, it is essential to investigate the potential of applying cyclone as an SNCR reactor. This is a more available and cost-effective way to control the NOx emission as a process in the cyclones with some modifications before emission.

Considering all the practical and theoretical demands, a pilot set-up is designed and assembled for this study, providing broad measurement access. An extensive experimental design is developed with a focus on fluid dynamics and considering effective reaction parameters, including temperature profile, concentration distribution, injection zone, ammonia inlet velocity, molar ratio, and initial NOx. Finally, the effect of particle loading on cyclone is studied. In the next step, a CFD model is developed to map the flow pattern further and provide a supportive base to discuss mixing and residence time inside the cyclone. The model is applied to predict temperature profile and residence time distribution inside cyclone targeting SNCR reduction. In the final step of CFD modeling, the system worked well, including SNCR reaction, and was validated with pilot scale experiments.

This CFD model is highly predictive for effective parameters such as RTD, temperature profile, flow pattern, mixing conditions and reaction zone. The model has been validated with experiments and shows good agreement with experimental results of a detailed study.

The results show that cyclone is non-isothermal and the reactants need to be in a proper temperature zone of the cyclone to react. The cyclone swirl flow provides proper time for the reactants with a good chance of meeting the high-temperature zone in both downward and upward flow. Rapid mixing of injected ammonia into the flue gas is also necessary and is provided by turbulence.

The results also prove that cyclones ensure excellent heat transfer and provide proper mixing in a short time for SNCR reduction. Adding ammonia from different positions makes a tiny difference in reduction efficiency. The reaction mainly takes place in the upper part of the cyclone, called reaction zone, in this thesis and is the upper zone of the cyclone with proper temperature.

The results presented here provide the background knowledge about the cyclone reactor for SNCR and could be applied to scale-up, design and optimization studies.

Summary (Danish)

Dette projekt er primært fokuseret på at levere baggrundsviden om cyklonreaktorer og kortlægge effekten af fluid dynamik der involverer strømningsmønster og transport fænomener af kemisk reaktioner. SNCR for NOx reduktion med tilsætning af ammoniak som et reduktionsmiddel er blevet valgt som reaktionen, der skal undersøges. At følge fluid dynamik effekt på reaktionsparametre herunder temperaturprofil, opholdstid og blanding, denne afhandling præsenterer en detaljeret undersøgelse både med eksperimenter og CFD modellering.

På grund af de miljømæssige krav og lovgivning bliver NOx emissionskontrollen strengere på verdensplan. I nogle brancher passere NOx cyklonen før emissionen, derfor er det meget vigtigt at overvåge potentialet for at anvende cyklon som SNCR reaktor. Dette er mere tilgængelig og omkostningseffektivt at styre NOx emission som et procesled i de cykloner med nogle ændringer før emission.

I betragtning af alle de praktiske og teoretiske krav, er en pilot set-up lavet til denne undersøgelse og giver samlet set bred adgang til afmåling. Et omfattende eksperimentelt design er udviklet med fokus på fluid dynamik og overvejer effektive reaktionsparametre herunder temperaturprofil, koncentration distribution, injektion zone, ammoniak indløb hastighed, molforholdet og indledende NOx. Endelig effekten af partikelladning til cyklonen er undersøgt.

I det næste trin, er en CFD model udviklet til at kortlægge yderligere flow mønster og giver et fundament for at diskutere om blanding- og opholdstiden inde i cyklonen. Modellen anvendes til at forudsige temperaturprofil- og opholdstidsfordelingen inde cyklonen målrettet SNCR reduktion. I det sidste trin af CFD modellering af systemet løst herunder SNCR reaktion og valideret med pilotskala eksperimenter. Denne CFD model er yderst prædiktiv for effektive

parametre såsom RTD, temperaturprofil, strømningsmønster, blandingsbetingelser og reaktionszone. Modellen er valideret med eksperimenter og viser god overensstemmelse med eksperimentale resultater.

Resultater viser, at cyklonen er ikke-isoterm, reaktanterne skal være i den korrekte temperaturzone af cyklonen for at reagere. Cyklonens hvirvelstrømning giver høj opholdstid for reaktanterne og også chancen for at møde den høje temperaturzone i både nedadgående og opadgående strømning. Hurtig blanding af injiceret ammoniak i røggassen er også nødvendigt, som giver cyklonen turbulens.

Resultaterne beviser agså, at cykloner sikrer fremragende varmeoverførsel og giver en passende blanding på kort tid til SNCR reduktion. Tilføjelse ammoniak fra forskellige positioner gør en meget lille forskel i reduktions effektivitet. Reaktionen finder primært sted i den øverste del af cyklonen, kaldet reaktionszone i denne afhandling, og er den øverste zone af cyklonen med den rette temperatur. Resultaterne der er præsenteret her giver baggrundsviden om cyklonreaktoren til SNCR og kan anvendes til scale-up, design og optimeringsstudier.

Preface

The thesis has been conducted under the Ph.D. program supported by Technical University of Denmark (DTU). The dissertation is submitted as a partial requirement of acquiring a Ph.D. degree at the Combustion and Harmful Emission Control (CHEC) research center at the Department of Chemical and Biochemical Engineering in the period from December 2013 to January 2017. The project was supervised by Professor Kim Dam-Johansen and Associate Professor Weigang Lin. The project was financially supported by DTU.

The thesis proposed a new industrial challenge in application of cyclone as reactor in addition to its main separation purpose. A pilot set-up has been designed and constructed for pilot scale experiments, and Selective Non-Catalytic Reduction (SNCR) of NO_x is selected as reaction due to its importance in recent industrial emission controls. A Computational Fluid Dynamics (CFD) model is developed to provide knowledge about flow patterns, mixing and residence time in cyclone reactor. The model is validated with experiments. Results also show high reduction efficiency for SNCR NO_x reduction in cyclone reactor.

Results have potential to apply as a background knowledge for scale up, industrial design, industrial modifications and more specifically for NO_x reduction control with high efficiency. The CFD- model can be more developed for all mentioned purposes to support industrial scale studies.

Kgs. Lyngby, 31-January-2018
Mohammad Ahli-Gharamaleki

Acknowledgments

I would like to express my gratitude to my supervisors Professor Kim Dam-Johansen and Associate Professor Weigang Lin for advice and encouragement during this study.

During the design and construction of pilot scale set-up the workshop and technical staff at the department of Chemical and Biochemical Engineering department helped me with many ideas how to solve practical problems. I would like to thank specifically Nikolaj V. Nissen, Jens H.Poulsen and Ivan H. Pedersen.

I would like to thank all former and present colleagues in CHEC group which made my stay in CHEC group very pleasant. I have also appreciated during my study many discussions with my colleagues from CHEC group specifically Seyednezamaddin Azizaddini, Mohammadhadi Nakhaei.

I would like to thank my family: my parents, wife and son for supporting me during this Ph.D. study.

Abbreviations

BSLkw: Baseline k-ω
CFD: Computational Fluid Dynamics
CFB: Circulating Fluidized Bed
CHEMKIN: CHEMical KINetics
DNS: Direct Numerical Simulation
DEM: Discrete Element Method
DPM: Discrete phase Method
DCKM: Detailed Chemical Kinetic Model
EBFGT: Electron Beam Flue Gas Treatment
FCC: Fluid Catalytic Cracking
LDA: Laser Doppler Anemometry
LES: Large Eddy Simulation
LRR: Launder, Reece, Rodi
LRRG: Modification of Launder, Reece, Rodi by Gibson, implementation of a differential RSTM
LPS: Linear Pressure Strain
MUSCL: Monotone Upstream-Centered Schemes for Conservation Laws
NSCR: Non-Selective Catalytic Reduction
PVC: Processing Vortex Core
PSIC: Particle Source In Cell
PSR: Perfectly Stirred Reactor
PFR: Plug Flow Reactor
PRESTO: PREssure STaggered Option
QUICK: Quadratic Upstream Interpolation for Convective Kinetics
RANS: Reynolds Averaged Navier–Stokes equations
RNG: Re-Normalization Group
RSTM: Reynolds Stresses Transport Model

RSM: Reynold Stress Model
RTD: Time Distribution
rke: Realizable k-ε
SGS: SubGrid scale model
SSG: Speziale Sarkar Gatski
SCR: Selective Catalytic Reduction
SNCR: Selective Non-Catalytic Reduction
skw: Standard k-ω
ske: Standard k-ε
SW: Stress Omega
sstkw: Shear Stress Transport k-ω
SIMPLEC: Semi-Implicit Method Pressure-Linked Equations Consistent
QPS: Quadratic Pressure Strain
UDF: User Defined function

Contents

Chapter 1

Introduction

Cyclones are well-known due to their various applications in the industries for separation purposes, mostly solid particles from the gas stream. In addition, cyclones also have the ability to be applied as a reactor for reactions with a short reaction time that can enhance the conversion of the reactants for different applications. Studies have shown that cyclones seem to ensure excellent heat transfer efficiencies between carrier gas, solid particles and walls. Moreover, the residence time in cyclones is high enough to provide reaction time as a reactor. Consequently, it can be anticipated that cyclones would be well suited for carrying out fast reactions. In addition, turbulent flow inside cyclone provides better mixing conditions. There is need to provide more knowledge in different aspects, e.g., mixing and residence time, to achieve a better understanding of the reaction inside the cyclone.

To develop the idea, SNCR reaction of NOx is chosen due to its importance in recent industrial emission controls and also because most of the industrial outflow path goes through a cyclone to get rid of solid particles. Therefore, the perspective of this study on cyclone reactor is to support real case design, modifications and optimizations in current industries.

1.1 Background

In cyclone separators, a strong swirling turbulent flow is formed to separate phases with different densities. The typical geometrical layout of a gas cyclone is used to separate particles from a gaseous stream. As in many confined swirling flow systems, the hydrodynamics in a cyclone can be of a complex nature. Flow reversal, quasi-periodic fluctuations and strong anisotropic turbulence are some of the characteristics.

Cyclones are energy-efficient and low-maintenance separation devices; they contribute in a very economical manner to dust emission reduction and air quality improvement [1].

Numerous investigations have been carried out on increasing the separation efficiency of the cyclones by describing fine particles moving with a carrier gas inside the cyclones. Less work was focused on considering a cyclone as a reactor.

The potential applications of this type of reactor are now being extended to various chemical reactions such as in the cement industry, CFB boilers, reduction of iron [2], coal pyrolysis [3], combustion and gasification [4, 5] and fluid catalytic cracking [6]. When used as a gas solid reactor, this type of device can enhance the conversion of the reactants by increasing the residence time due to swirling motion. With this approach, residence time distribution (RTD) is a new challenge. Calculation of the performance parameters of the cyclone reactors generally needs accurate information about the flow pattern, the heat and mass transfer efficiencies, and thermodynamics and kinetics of the chemical reactions to be carried out in the process.

The lack of fundamental understanding of the fluid dynamics and chemical reactions is because the fluid dynamics within a cyclone is complex. Also, the inclusion of parameters, such as residence time, reactant interaction, reactant concentrations and other relevant physical properties, add further complexities to the conservation equations. Computational fluid dynamics (CFD) simulations of the fluid flows in cyclones can provide a good understanding of the details of the flow and reaction patterns within the cyclones [7].

The main aim of this project is to map the relative importance of fluid dynamics and chemical reactions in a high-temperature process that involves flow pattern, transport phenomena and chemical reactions and to propose a methodology for process simplification. It could also be developed as an application for the systems such as mineral processing or biomass conversion.

1.2 Scope of Work

To provide a comprehensive study on reaction inside cyclone, the present work is divided into three practical phases including pilot design/ construction, experiments and CFD modeling.

In phase 1, the pilot setup is designed for this study and assembled considering all the practical and theoretical demands. Special efforts have been made to provide enough measurement access to the system parameters. In addition, the system provides very flexible sampling possibilities which can support measurements from many different parts of the cyclone, both horizontally and vertically. This flexible measurement potential provides the ability to carry out a detailed study of temperature profile and NOx distribution inside cyclone, which can be used in validating the flow pattern in the model. Most of the former studies only apply performance parameters for validation.

In phase 2, a wide range of experiments has been performed to provide a detailed study of both heat transfer and reaction inside the cyclone. The SNCR of NOx using NH_3 as reductant was chosen as a reaction for this project. All the experiments were carried out in the pilot cyclone mentioned. After safety checks and system preparation, the experiments were divided into three sub-groups. First, the cyclone is characterized before any reaction takes place (without adding ammonia). In this step, cyclone temperature profile and NOx distribution have been studied. In the next step, the reaction inside cyclone has been studied in detail, and in the final step the reaction has been studied when the cyclone is loaded with solid particles.

In phase 3, a CFD model has been developed to further map the flow pattern and provide a reliable base to discuss the mixing and residence time inside the cyclone. The model is first initiated for cold mode and validated with experimental literature study. The model properties are applied to simulate heat transfer and residence time distribution inside cyclone targeting high-temperature SNCR reduction. In the final step of CFD modeling, the system is solved, including SNCR reaction with simplified mechanisms. In the two latter steps, the model has been validated with pilot scale experiments of phase 2.

1.3 Objectives

The main aim of this project is to map the relative importance of fluid dynamics involving flow pattern and transport phenomena considering reduced chemical kinetics and to propose a methodology for process simplification for modeling.

The stepwise objectives of this project are:

- To improve the understanding of fluid dynamics and reaction kinetics inside a cyclone. For this purpose, a series of experiments supported with CFD modeling has been targeted. In the first step, the system needs to be simplified considering both reaction and fluid dynamics to be applied in CFD modeling. To perform a comprehensive experiment set, a flexible pilot is also designed and constructed. Furthermore, an extensive experimental result set is needed to validate the CFD model.
- To provide experimental background knowledge on SNCR in a cyclone reactor, an extensive experimental design has been developed considering effective parameters with a focus on fluid dynamics including temperature profile, concentration distribution, injection zone, ammonia inlet velocity, molar ratio, initial NOx and finally the effect of particles in dust-loaded cyclone. To monitor the interaction of flow pattern and reaction in cyclone, experiments have been repeated with sampling from different parts of the cyclone both vertically and horizontally. The latter has been done for the first time which led to a more detailed validation of the CFD phase.
- Application of CFD model to simulate the flow pattern in a cyclone reactor

The CFD model has been developed and validated in different scopes to provide more practical knowledge to describe the interaction of fluid dynamics inside cyclone and reaction. The CFD model simulated the cyclone reactor for SNCR reaction and predicted effective parameters such as RTD, temperature profile, flow pattern, and mixing condition reaction zone. The model has been validated with experiments and shows a very good agreement with experimental results of a detailed study.

1.4 Structure

Chapter 2 of the thesis provides the background and literature review on cyclones in general and cyclone reactors, SNCR NOx reduction importance, mechanisms and applications, CFD modeling theoretical consideration, practical approaches and applications.

Chapter 3 focuses on experimental apparatus presenting design considerations, material selection, measurement systems and experimental procedure.

Chapter 4 presents experiment design and methodology with a systematic approach. A detailed study on reaction parameters and their interaction with the

flow pattern in different zones of the cyclone is presented. This chapter ends with a discussion of results and experimental conclusion.

Chapter 5 includes CFD modeling steps, model setting, cold mode, heat transfer simulation and reaction with considering flow patterns and reaction. Results are explained in different sub-sections with a comparative discussion when needed. The chapter ends with a general conclusion about CFD modeling results with a short notice to the experimental results.

Chapter 6 contains the overall conclusion and highlights the results of experiments and CFD. It ends with suggestions for future work.

Chapter 2

Literature survey

Targeting a detailed study of a cyclone reactor, it is highly important to present a thorough literature study on different aspects involved in the main objective of the project. It would be beneficial to know what has been done that is relevant to the target and what is missing to proceed in a more focused direction. This would be even further helpful for future studies following the current Ph.D. perspective and goals.

This section includes five sub-sections: cyclone principles, application of the cyclone reactors, modeling of gas-solid cyclone reactors, selective non-catalytic reduction (SNCR), and computational fluid dynamic simulation. Each part basically makes a background study for the relevant practical study of this project and will be explained and discussed in more detail.

2.1 Cyclone Principles

In this section, cyclone principles will be discussed, specifically cyclone flow pattern and how it affects practical cyclone parameters. This is germane to know because flow pattern in a cyclone is the most important factor discriminating a cyclone from other reactors both in the concept of mixing and residence time of the reactants as well as the heat transfer. This part will be followed by cyclone

applications as a reactor and how and why it brings value to the special targets.

Basically, a cyclone as a type of centrifugal separator is a stationary mechanical device that utilizes centrifugal force to separate solid or liquid particles from carrier gas. A typical cyclone separator is shown Figure(2.1). A cyclone separator is one of the most efficient and robust dust separators. Its robustness results from a lack of moving parts and the ability to withstand harsh operating environments [1, 8]. Moreover, cyclones are well suited for high pressure and temperature applications [9–11].

In centrifugal devices, the dust-laden gas is initially brought into a swirling motion. The dust particles are slung outward to the wall and transported downward to the dust outlet by gravity and the downwardly directed gas flow near the wall. A sketch of a standard reverse-flow, cylinder-on-cone cyclone with a tangential, slot-type inlet is shown in Figure(2.1) [1].

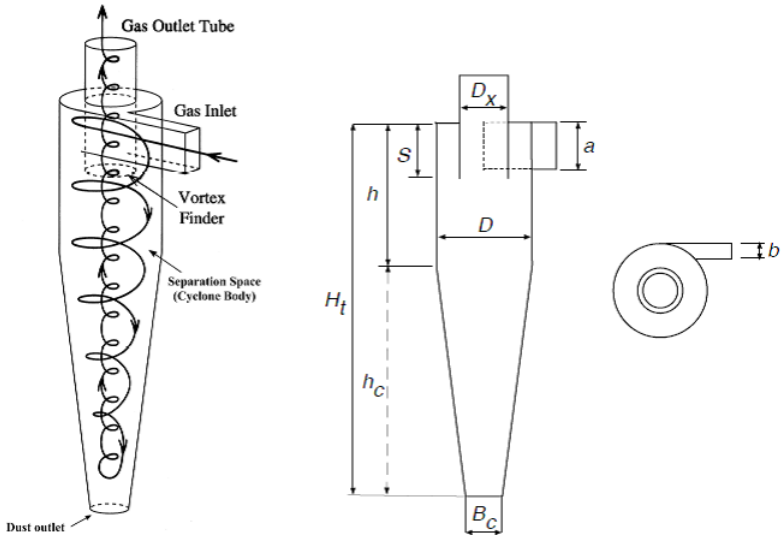

Figure 2.1: Sketches of a reverse-flow, cylinder-on-cone cyclone with a tangential inlet. The geometrical notation is indicated in the right sketch; D: Cyclone diameter, H_t: total height of the cyclone, D_x: vortex finder diameter, S: vortex finder length, a: inlet height, b: inlet width, h_c: height of the conical section, h: height of the cylindrical section, B_c: cone-tip diameter [1]

For the standard reverse-flow cyclone, the swirling motion is brought about by designing the inlet in such a manner that it forces the gas to enter the unit on a tangent to the cyclone wall. The inlet is normally of rectangular cross-section. As the gas swirls, it moves axially downwards in the outer part of the

separation space. In the conical part of the cyclone, the gas is slowly forced into the inner region of the cyclone, where the axial movement is upwardly directed [8]. This flow pattern is often referred to as a double vortex: an outer vortex with a downwardly directed axial flow and an inner one with an upwardly directed flow. The gas exits the cyclone through the so-called vortex finder, which extends downward from the center of the roof. This outlet pipe goes by many different names, with vortex tube and dip-tube being the most common, aside from the vortex finder. The particles in the inlet gas are slung outwards to the wall in the centrifugal field and are transported to the dust exit by the downwardly directed gas flow near the wall [12]. Below more details of the flow pattern in the separation space will be given.

Vortex flow

Swirling flow, or vortex flow, occurs in different types of equipment, such as cyclones, hydrocyclones and vortex burners. Two basic types of swirling flows can be distinguished:

1. Forced vortex flow, which is a swirling flow with the same tangential velocity distribution as a rotating solid body

2. Free vortex flow, which is the way a frictionless fluid would swirl.

In a real swirling flow, however, the tangential velocity distribution in a real swirling flow is intermediate between these two extremes. Now, imagine first that the swirling fluid has an infinite viscosity (behaves like a solid body). Hence, no shearing motion exists between fluid layers at different radii. In this case, the fluid elements at all radial positions are forced to have the same angular velocity Ω, which equals v_θ/r where v_θ is the tangential velocity. This is the forced vortex flow or solid-body rotation:

$$v_\theta = \Omega r \tag{2.1}$$

At the other extreme, if the swirling fluid has no viscosity, the motion of a given fluid element is not influenced by the neighboring elements at smaller and larger radii. If in such a fluid we bring an element to a smaller radius, its tangential velocity will increase, since its moment-of-momentum ($mv_\theta r$) will be conserved. Such a vortex is called a free or frictionless vortex. In such a flow, we have $v_\theta r = C$, with C a constant, so that:

$$v_\theta = \frac{C}{r} \tag{2.2}$$

This is the second basic swirl flow. A real swirling flow normally has a core of near solid-body rotation surrounded by a region of near loss-free rotation as sketched in Figure(2.2). This is called a Rankine vortex [13]. For a cyclone it is illustrated in different heights of the cyclone in Figure(2.3(a)).

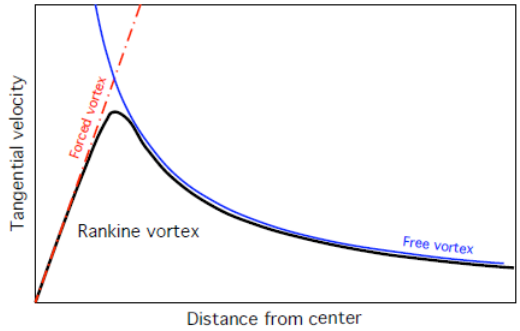

Figure 2.2: The tangential velocity distribution in a real vortex [14]

Figure(2.3) and Figure(2.4) show classical measurements and explanations, attempting to describe the three velocity components inside a cyclone separator.

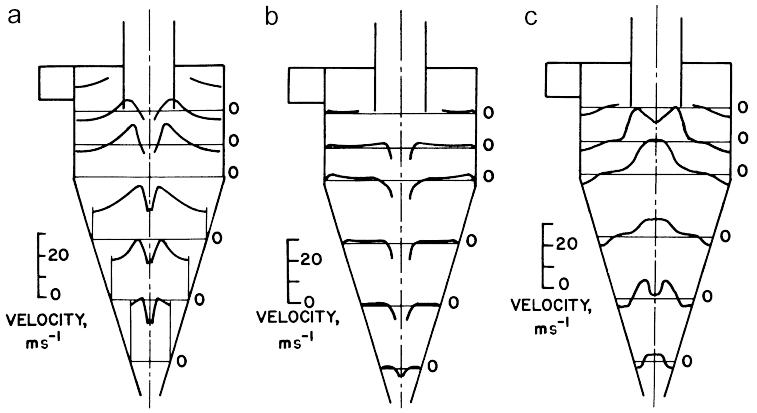

Figure 2.3: velocity profile in a cyclone: (a) tangential, (b) radial, (c) axial [8]

Although the use of the cyclone separators is common in many industrial applications, an accurate prediction tool for their behaviors is still not available. The challenge of many studies is, therefore, a detailed survey of the flow phenomena in cyclones and the design of an optimum cyclone separator (minimum

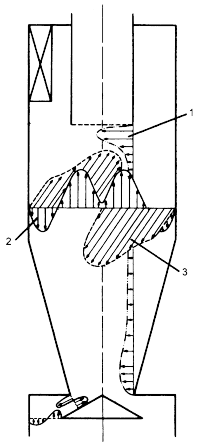

Figure 2.4: Sketch of the cyclone velocity profile: (1) radial, (2) axial, (3) tangential [15]

pressure drop and maximum collection efficiency). The cyclone performance parameters are governed by many operational parameters (e.g., the gas flow rate and temperature) and geometrical parameters. In most of the studies, the focus is only on one of the parameters at a time with some preliminary assumptions [10, 16–19].

In order to understand the practical working of the cyclones, it is necessary to master a number of topics, which span a range of different disciplines.

2.1.1 Gas flow pattern

Sketch of a standard reverse-flow cylinder on gas cyclone with a tangential entry is shown in Figure(2.1). A swirling motion is created in the separation space by the tangential injection of the gas. The gas flows downward in the outer part of the swirl and upward in the center. The downward flow in the outer part of the cyclone is critically important as it, and not gravity, is the dominant mechanism for transporting collected solids (those at the wall) out the bottom of the cyclone. In cyclones, gravity will assist but its influence is important only for cyclones operating at high solid-loaded conditions for which 'mass loading' effects are important. At the same time there is a radial flow from the outer vortex to the inner one [20].

In Figure(2.3) the radial, axial and tangential gas velocity components are sketched. The former shows the outer region of downwardly directed axial flow

and the inner one of upwardly directed flow. As mentioned, the downward velocity at the wall is the primary mechanism for particle transport out of the dust outlet. The axial velocity often shows a dip around the center line. Sometimes this is so severe that the flow there is downwardly directed. The tangential velocity profile resembles a Rankine vortex: a near swirl surrounding a core of near solid-body rotation [20].

There are limited studies about the radial velocity. It is generally inwardly directed below the lip of the vortex tube and not uniform with height. Radial velocity is generally much smaller than the tangential velocity and more difficult to measure accurately.

2.1.2 Particle flow pattern

Studying the particle flow pattern is not easy experimentally. The reason is that particles entering the separation space are subject to an inwardly directed drag and an outwardly directed centrifugal force. The separation space starts at the point where the incoming gas first experiences rotational flow and the particles carried along in this gas flow first experience a centrifugal force acting radially outwards. This point varies with inlet design and may start, for example, at the leading edge of an inlet scroll or helix upstream of the upper barrel section of the proper cyclone.

Irrespectively, the centrifugal force is proportional to the particle mass and, therefore, the cube of the particle diameter: $d_p{}^3$. The drag force, which is due to the flow of gas from the outer to the inner part of the vortex, is proportional to d_p, at least, when Stokes' law applies (Re $_P$<1) which often does in practice. The largest particles are, therefore, the easiest to separate.

In order to give an impression of the flow of a particle through a cyclone, it can be resorted to CFD simulations. Figure(2.5) shows a series of particle trajectories. The particles are injected at different radial positions along the inlet in a pre-calculated gas flow field.

Although the object is to centrifuge the particles to the wall and capture them, it is interesting to look at fine particles that some of them are not collected. An extremely fine 1.0 μm particle size with $2730 kg/m^3$ density was used to generate the particle paths shown in Figure(2.5) in a cyclone with $20cm$ diameter. The gas inlet velocity is $15m/s$ (gas at 25°C and 1 atm). On the left 10, tracks are calculated from the mean flow field; on the right 5 particles, tracks are shown where the response to the turbulent motion of the gas is taken into account. Some of the particles can be seen to exit through the vortex finder, while those injected closer to the wall reach the wall, where they are deemed to be captured

and are removed from the simulation.

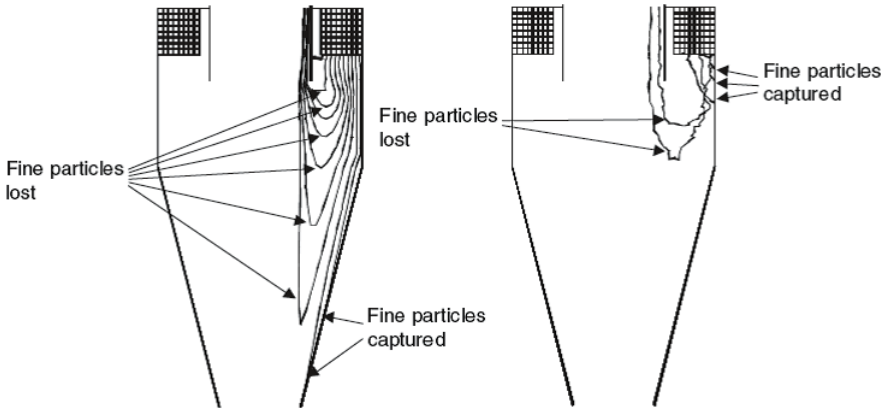

Figure 2.5: Particle tracks in a cyclone by CFD. [14]

2.2 Application of the cyclone reactors

Considering the cyclone as a gas-solid reactor, it is good to compare it with other types of gas-solid reactors.

Gas-solid reactors are usually divided into three classes according to the size of the particles and their reaction times:

- Fixed beds, rotary kilns,... , adapted to large particles ($10^{-3} - 3 \times 10^{-1}$m) and slow reactions (reaction times from $10^3 - 10^5$s)
- Fluidized bed reactors for medium sized particles ($10^{-5} - 10^{-2}$m) with reaction times (ranging from $10^2 - 10^4$s)
- Vortex and entrained flow reactors for small particles ($10^{-6} - 10^{-4}$m) and short reaction times ($5 \times 10^{-3} - 10$s)

Reactors of the first two types are used in most industrial applications and, consequently, many studies have been published. Reactions having short reaction times are more unusual and the corresponding reactors are less studied; however, more than 60% of power plants nowadays are of this type. Cyclones have potential to be reactor for this type of reactions; the most representative of vortex devices, which are extensively used for cleaning purposes. Thus a

detailed study of the application of the cyclone reactor provides a better understanding of more industrial applications. In this section, first the published applications of the cyclone reactor will be preset and then factors affecting the cyclone reactors will be discussed in general.

The first studies by Szekely [21] have shown that cyclones seem to ensure excellent heat transfer efficiencies between carrier gas, solid particles and heated walls. Moreover, residence times in cyclones are generally of the order of or lower than a few seconds. Consequently, it can be anticipated that cyclones would be well suited for carrying out fast reactions of solid particles requiring high heat fluxes. At the same time, it could be expected that solid byproducts and unreacted particles would be automatically separated from gaseous products.

One of the required conditions to achieve reaction inside the cyclones is to heat up reactant under high heat fluxes. It thus seems that the cyclone is well adapted to such a reaction, five main functions being fulfilled in the same vessel: fast heating of the particles, chemical decomposition, efficient friction of the particles against the walls which eliminates the products, further reactions of the primary products (at the walls or in the gas phase), and cleaning of the evolved gas (for example, char and mineral ashes being automatically separated at the bottom of the reactor) [22].

The potential applications of this type of reactor are now being extended to various chemical reactions such as reduction of iron [2], combustion and gasification [4, 5], coal pyrolysis [3], flash hydropyrolysis [23], flash pyrolysis [22] fast pyrolysis of biomass [24], pyrolysis of bitumen-impregnated sandstone [25], fluid catalytic cracking [6] and niobium powder production [26]. Some of the most relevant cases are briefly presented in this section.

2.2.1 Fluid Catalytic Cracking in cyclone

Usually, the Fluid Catalytic Cracking (FCC) technology in the petroleum industry uses riser reactors. Risers have various shortcomings, such as backmixing of particles due to gravity, particle clustering and radial segregation of solids, long residence time, gas and coke formation problem, etc. With the increase in the demand for light oil, people pay more attention to improving on traditional risers and even develop new types [6].

A new reactor for fast gas-solid reactions named short-contact cyclone reactor was developed on a pilot scale to improve reaction selectivity and facilitate the multi-functional purpose of the petroleum refining industry. The new reactor mainly includes two parts: reaction chamber and separation chamber. The typical structure is shown in Figure(2.6). The gas-solid catalytic reactions and

product separations could occur in the same reactor.

Their main aim was to reduce back-mixing of particles and over-cracking reactions, decrease the residence time and so on. However, the idea of the new reactor was brought up while still little work is done about this kind of reactors [6]. Although this study is not focused on the cyclone reactor itself, it is a very good example of how this type of reactor is good for special purposes.

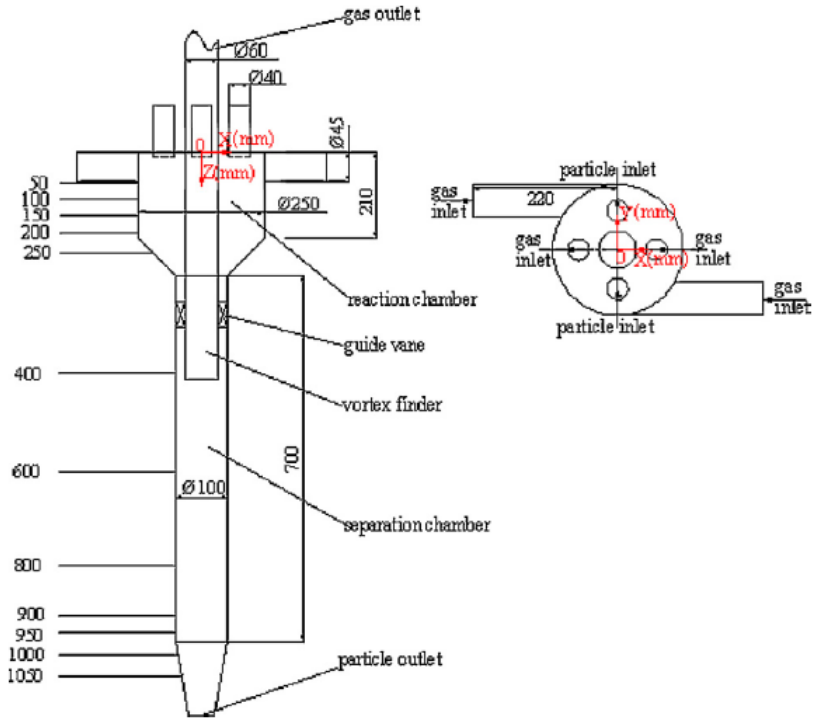

Figure 2.6: Schematic of the short-contact cyclone reactor. Left: an elevation view; right: a top view. The reactor has two gas inlets, two particle inlets, one gas outlet and one particle outlet as shown [6]

2.2.2 Fast Pyrolysis

Fast pyrolysis is a thermo-chemical process that converts biomass into gas and liquid products. The main product within the fast pyrolysis process is a fuel with a high density. This product can be transported and stored easily. This affords the possibility of decoupling the primary biomass conversion process and the prime mover regarding the time, location, and scale of the process. The fast

pyrolysis technology can have relatively low investment costs and high energy efficiencies compared with other processes, especially on a small scale [24].

Fast-pyrolysis cleaning and high temperature gas cleaning integrate in one unit. This integrated unit consists of a vortex reactor (a cyclone) with a rotating particle separator Figure(2.7) [24].

In the reactor, the biomass and the heat carrier are in direct contact, so efficient heat transfer can take place. During the transport downwards in the reactor, the biomass particles are dried, heated up and devolatilized. The average process temperature is $450-550°C$. The typical gas residence time in the reactor is 0.5 to 1 sec, so secondary cracking in the reactor is prevented. In the gas outlet, in the middle of the cyclone reactor, the fine solid particles are removed from the oil vapor by the rotational particle separator. In this separator the micron particles are captured in a bundle of channels with small diameters, rotating around a common axis. The collected particles stick to the channel walls until they are periodically removed online and the reactor is left with the main solid stream at the lower outlet of the cyclone. A scheme of the novel reactor is given Figure(2.7).

In the following study, the flash pyrolysis of wood sawdust is carried out in a cyclone reactor with steam as carrier gas between 893 and 1330K [22].

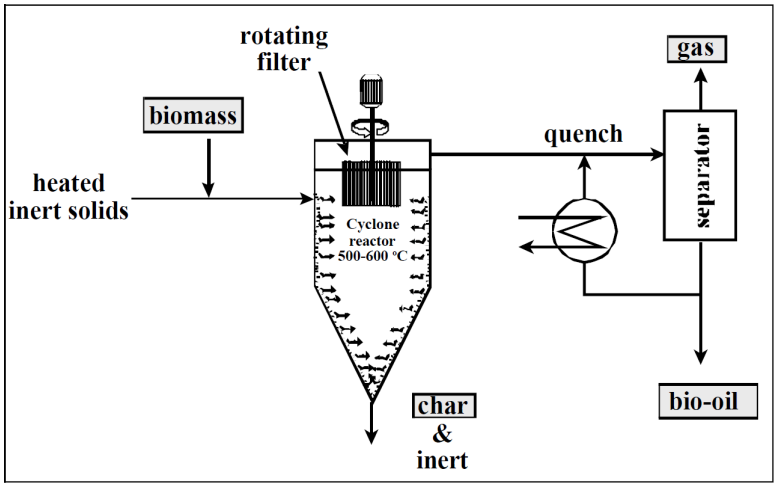

Figure 2.7: A simplified scheme of Pyrolysis reactor [24]

2.2.3 pulverized coal combustion and gasification

The experimental part of an application of a pulverized coal combustion and gasification in an atmospheric cyclone reactor published by Barnhart et al. [5]. The latter also makes an extensive comparison between the model prediction and experimental results in a complementary study [27]. The experiments were carried out in a lab-scale cyclone reactor shown in Figure(2.8)[5]. In this cyclone, air and coal enter the chamber through four equally spaced sets of tangential concentric stainless steel tubes. Coal and primary air enter through the inner tubes while secondary air enters through the outer tubes. A methane torch fires into the chamber through the top to ignite the incoming coal/air mixture. Gases leave the reactor through a throat tube which projects into the reaction chamber to prevent unreacted particles from escaping. The exhaust line is cooled by an internal cooling coil and a water jacket. The refractory sections are surrounded by four-quarter cylindrical heating for chamber preheat. A vertical axis, slagging reactor is chosen to achieve high carbon efficiency and good ash retention simultaneously. Four tangential coal/air nozzles are used to make the chamber roughly axisymmetric. A chamber radius of 7.5 cm was chosen to match industrial coal throughput rates and to allow probe insertion with minimal flow disturbance.

Experimental results include several series of coal combustion tests and a coal gasification test carried out via fuel-rich combustion without steam addition. Excellent reactor stability over a range of equivalence ratios from 0.67 to 2.4 and air flow rates from 25 to $100 kg/h$ is reported. Typical carbon efficiencies were reported 95% for fuel-lean and stoichiometric tests and 85% for gasification tests. The best gasification results were achieved at an equivalence ratio of 2.0, where the carbon, cold gas, and hot gas efficiencies were approximately 83, 45, and 70%, respectively. The corresponding product gas heating value was $2.6 MJ/m^3$. The emphasis was directed toward coal combustion and gasification via fuel-rich combustion with air at atmospheric pressure. Carbon efficiencies during coal combustion tests are excellent (90 to 100%) and are largely insensitive to changes in air flow rate and fuel/air ratio.

2.2.4 Production of niobium powder in a cyclone reactor

Production of niobium powder starts from niobium pentoxide powder and needs to be reduced within specific conditions. The reduction reaction in the cyclone has to proceed within several seconds and the number of possible reductants is limited. Using magnesium is the best option for the reduction of niobium. Additionally, its boiling point (1361K) is low enough to use it in gaseous form as a reductant in the cyclone reactor [26].

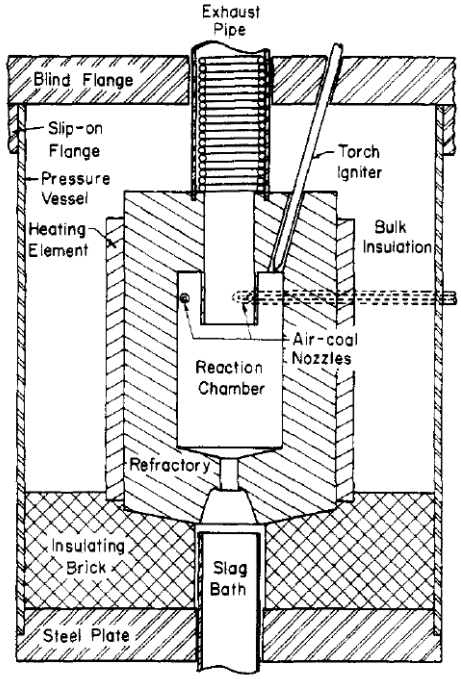

Figure 2.8: Cyclone reactor for pulverized coal combustion and gasification [5]

For that purpose, niobium pentoxide powder (optical grade) is placed into alumina dishes and heated in a hydrogen atmosphere to carry out the endothermic reaction. In a second step, niobium powder is formed by an exothermic reaction between niobium (IV) oxide and magnesium.

To execute the magnesiothermic reduction, a powder mixture of niobium (IV) oxide and magnesium is continuously dispersed in a stream of preheated argon directly before entering the cyclone reactor. Niobium and magnesium oxide powders are formed within the cyclone, separated from the gas, and collected in a product storage tank. The off-gas also contains magnesium besides argon because magnesium is used in excess over stoichiometry to achieve a complete conversion.

The obtained powder mixture of niobium, magnesium oxide, and also some magnesium is leached after deactivation by diluted hydrochloric acid to convert magnesium and magnesium oxide into water-soluble magnesium chloride [26].

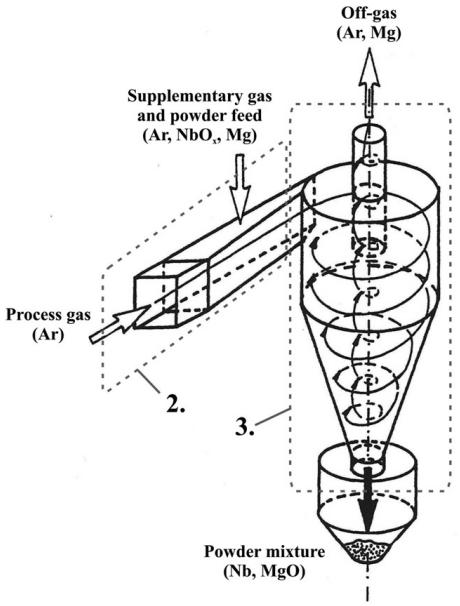

Figure 2.9: A scheme of reduction of niobium oxide [26]

2.2.5 Fine ceramic powders

Fine ceramic powders, like titania and zirconia, are advanced, high-quality inorganic materials with specific functional properties. They are massively used as pigments, catalyst sub-layers and protective coatings and, more recently, as special materials in a broad range of advanced technological applications. For massive industrial productions, vapor-phase synthesis is applied: vapor-phase precursors are fed into aerosol reactors in un-premixed conditions, where gas-to-particle conversion occurs preferably via a chemical reaction. Vapor-phase aerosol reactors intrinsically deviate from ideal behavior for un-premixing of reactants and fast chemical kinetics. Therefore, cyclone reactor could be suitable for the production of fine ceramic [28].

They applied a reactor with a typical arrangement of a reverse-flow cyclone equipment. The cyclone, as mentioned before, has a potential for technological application for process intensification by two simultaneous operating advantages: cyclone flow reduces particle recirculation towards the flame region and the cyclone arrangement segregates large particles. As a result, ceramic powders with narrow particle size distribution can be produced. This study focuses on the remodeling of an existing industrial reactor for production of fine TiO_2 according to a cyclone configuration.

As it is reported, the quality of the metal-oxide-synthesized powders is significantly affected by fluid dynamics. Therefore, an aerosol cyclone reactor has been proposed and tested. Results show that final product with a narrow particle size distribution can be obtained with this proposed cyclone reactor. To support the idea, some simulation and evaluation were also presented in the same paper which confirms the improvements by using cyclone reactor for such systems.

As a general discussion when used as a gas-solid reactor, this type of device can enhance the conversion of the reactants by increasing the residence time of the solid reactants due to swirling motion. Calculation of the performance parameters of the cyclone reactors generally needs reliable information about the flow pattern, the heat and mass transfer efficiencies, and thermodynamics and kinetics of the chemical reactions to be carried out in the process. In addition to the common cyclone parameters, reaction parameters must also be considered in the cyclone reaction chamber.

In the next section, modeling studies on gas-solid cyclone reactors will be presented briefly. Also, the technical review of the cyclones and cyclone reactors leads to a general overview of both practical and modeling tools, and how each proceeds within the scientific and industrial approaches will be reviewed.

2.3 Modeling of gas-solid cyclone reactors

Cyclone geometry, particle properties and operational conditions are used as inputs to make a good approximation for operational cyclone parameters. The basis of the available algebraic models is approximations of the velocity field within the cyclones. The most common models for describing the velocity field have been developed by Barth [29], Alexander [30] and Muschelknautz [31]. Based on the velocity field, expressions and methods for determining the cut-size diameter have been suggested by several authors, including Barth [29], Muschelknautz [31], Lapple [32,33] and Leiht [34]. Here instead of the common modeling of the cyclone, models developed for the cyclone reactors are reviewed.

First, analytical and experimental modeling related to the hydrodynamics of the cyclones is presented. Then, a chemical reaction in cyclone reactors is reviewed as phenomenological models. The aim of this part is to find a way for the simplification of very complex phenomena inside the cyclone reactors. To provide a comprehensive background for the state of the art of the cyclone reactors, both analytical and numerical studies are discussed here. It is necessary to have a brief knowledge of different approaches and models even though the focus is on the computational fluid dynamic modeling in this Ph.D. project.

2.3.1 Analytical modeling of the cyclone reactors

There are fewer studies on modeling of the cyclone reactors because of the large number of unknown processes involved such as hydrodynamics, transfer resistances and chemical reaction. In this part, the previous experimental and analytical experience will be reviewed.

The first four models developed for combustion of pulverized coal in a cyclone reactor are cyclone coal combustion, cyclone char combustor, cyclone gasifier and the macroscopic model of the cyclone reactor.

A cyclone coal combustion model is developed based on fluid dynamics and particle-gas interactions. Simple approximations are used for pyrolysis and char particle combustion. However, a sophisticated fluid mechanic treatment includes a four-region model of the reaction chamber in which the basic conversion equations are simplified for each region by appropriate assumptions. The wall-adjacent region is found to be by far the most important since particle loading and chemical reactions are concentrated in this zone. Important output parameters from the model include carbon conversion efficiency, ash retention, pressure drop, and radiative and convective heat loss. This investigation reported good agreement with limited experimental data from a cyclone operated by the Pittsburg Energy Research Center [27].

Following the coal combustion, a cyclone char combustor model is developed with direct analysis of the governing mass, momentum, and energy equations. The equations are non-dimensionalized, and an order of magnitude analysis is performed to determine the significant dimensionless parameters with an eye toward simplifying scale-up of laboratory cyclone reactors. Among the dimensionless groups found to be important are the swirl number, particle loading ratio, the Biot modulus, and a reaction time/residence time ratio. This study suggests a useful correlation procedure, but the absence of any gasification chemistry or predictive potential limits the applicability of the model [27].

A parametric analysis of a cyclone gasifier by developing broad assumptions is carried out. This model gives closed form solutions to the continuity, momentum, and species conservation equations. In this model, the energy equation is eliminated in favor of an estimated reactor temperature of $2200K$. Particles are assumed to reside only in the wall-adjacent region, making a detailed description of the bulk fluid flow unnecessary. Parameters that are systematically varied include the gasification rate coefficients, swirl number, and coal mass fraction pyrolyzed. Swirl number proved to be of great importance through its effect on mass transfer rates since the gasification reactions were presumed to be diffusion-controlled. A commonly cited virtue of swirl burners is long particle residence time; however, the authors point out that increasing residence time is

beneficial only if the mass transfer rate is sufficient to keep gasification products swept away from the particle surface [27].

After these studies, John S. Barnhart [27] developed a macroscopic and isothermal model of Coal Combustion and Gasification via fuel-rich combustion for a cyclone reactor. The cyclone is represented by three zones as shown in Figure(2.10) with some assumptions;

- The pyrolysis zone occupies the truncated annulus between the exit throat tube and the chamber wall
- The perfectly stirred reactor (PSR) occupies the lower portion of the same annular region
- The plug flow reactor (PFR) zone in an evenly distributed manner over that portion of its length not enclosed by the throat tube

The PFR lies along the axis of the cyclone, has a diameter equal to the outside diameter of the throat tube, and extends from the bottom of the cyclone to the base of the exit cooling coil. The balance of this section consists of a zone-by-zone description of the cyclone model.

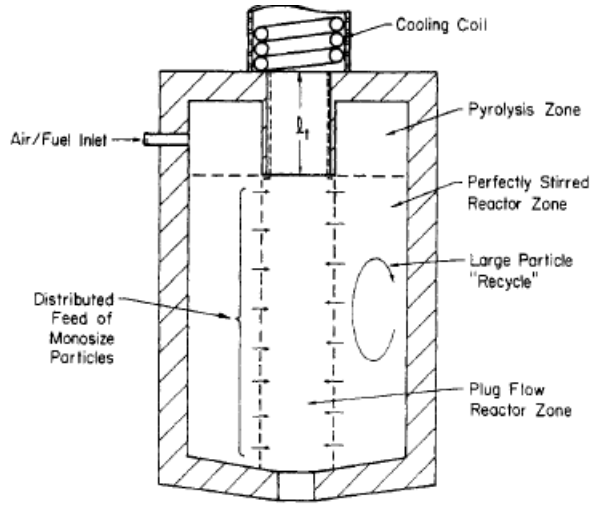

Figure 2.10: Hypothesized cyclone reaction zones [27]

The model predicts carbon conversion efficiency, product gas composition, and selected gasification parameters (product gas yield, combustible product gas yield, cold and hot gas efficiency, and heating value) for fuel-rich cases.

Modeling of fuel-rich gasification would be improved by the inclusion of mechanisms for char oxidation by steam and carbon dioxide. Further modifications to the model are prompted by more detailed exhaust data and internal temperature and composition profiles, particularly from industrial-scale reactors.

2.3.2 Phenomenological model

A phenomenological model is used to analyze the behavior of the internal aerodynamic processes and particulate motion occurring in non-slagging coal-fired cyclone combustors by Morgan [35]. A phenomenological model is an aerodynamic flow model incorporating the effects of boundary layer flows, momentum coupling between the flow and particles and a model of coal combustion including the effect of particle fragmentation. Loss of particles into the exhaust nozzle and collection of material in the collection pockets is modeled by means of balance equations including centrifugal force field effects, radial drift velocity, and turbulence level and particle concentration across the unit; it originates from work directed at predicting cyclone dust separator performance. For analysis purposes the combustor is divided into five regions:

1. A thin outer boundary layer region in which most of the combustion occurs, region 1. Here the model calculates a mass average residence time for each discretized coal particle size. This is then averaged over the distribution function to give an average time spent by all particles in this region, thus allowing a total particulate mass loading in region 1 to be evaluated and a recovery factor subsequently calculated. Most burning/ash material passes directly into the boundary layer regions 2a and 2b. An integral momentum equation is solved to give the thickness of this crucial outer layer as well as values of the wall drag coefficient. Important inputs to this equation are both the wall roughness and the physical scale of the combustor; both parameters crucially affect system performance via this parameter.

2. A top boundary layer region in which coal and ash particles are convected towards the exhaust nozzle, region 2a. Fine particles escape into the exhaust and larger materials are recycled through regions 4 and 3 back to region 1.

3. A bottom boundary layer region in which coal and ash particles are convected towards the central ash collector, region 2b. Larger particles pass directly into the central collector whilst most of the remaining fine particles escape directly into the exhaust or are recycled to region 1.

4. A region encompassing much of the main body of the system, region 3.

Here centrifugal forces dominate, particulate loading is small, whilst larger recirculating coal particles from regions 2a and 2b are flung back into region 1. Only very fine ash can be suspended in this region.

5. A central region of flow extending downwards from the outlet region, region 4. This is essentially a plug flow region under combustion conditions. A reverse flow/recirculation zone may be formed in the end of the exhaust nozzle as well as substantial tangential velocity gradients, but these have little influence on region 4 inside the cyclone combustor.

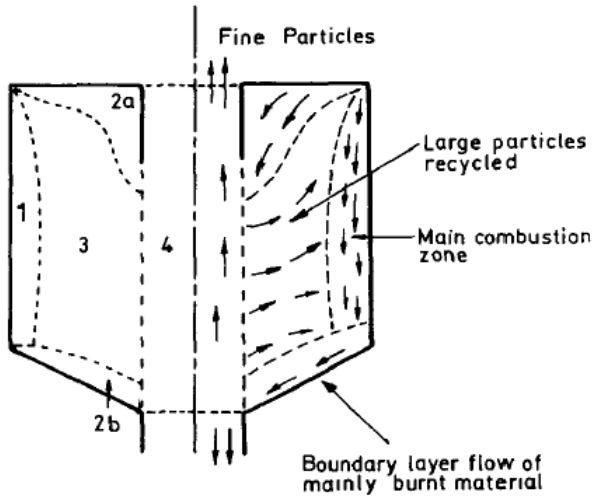

Figure 2.11: Analysis Zones and Particle Flows [35]

A non-slagging cyclone combustor operates normally fuel-rich at a mixture ratio of about 0.7 to maintain cyclone chamber gas temperatures below 1300°C and wall temperatures at about 1100°C. With crushed coal of size range $\bar{d}_m \cong 200 - 400\ \mu\text{m}\ 90\% < 1mm$, having a high ash fusion temperature, good fuel burnout and retention of particles larger than 30μm in the cyclone chamber has been demonstrated. The long residence times of material in the outer regions of the cyclone chamber cause a large slip velocity between that of the inlet and the main vortex in the cyclone chamber and this factor affects the design of the tangential inlet.

In this study, burnout of the gasified products of combustion is achieved in a secondary combustor, and Low NOx emissions derive from the low operating temperatures of the primary cyclone chamber.

In this section, modeling aspects and assumptions are briefly discussed considering a few papers which study the modeling of the cyclone reactors mostly for

combustion purposes. However, the application of the cyclone reactors in the former section shows more industrial potentials and tendencies for using cyclone reactors. This altogether encourages the demand for more detailed studies on cyclone reactor and its potentials and advantages that could be further applied to gain more knowledge either in experimental investigations or modeling studies. The general idea of using cyclone reactors can be definitely developed when the flow pattern behavior and kinetic effects of reactant residence time will be clarified with a more practical approach. This Ph.D. project follows this objective and hence needs to propose a specific reaction which is doable in cyclone reactor and can be applied further in the industries based on the most recent demands.

With increasing demand for NOx emission control, in the next section NOx emission and De-NOx methods will be reviewed. Then, background study on selective non-catalytic reduction (SNCR) as a selected reaction for this Ph.D. study will be presented.

2.4 Selective Non-Catalytic Reduction (SNCR):

In this section, general NOx emission sources will be reviewed, and the general De-NOx techniques will be briefly discussed as an introductory part to selective non-catalytic reduction (SNCR) method that is a core part of this study. The SNCR method will be described in more detail, and the effect of parameters on NOx reduction will be discussed thoroughly.

2.4.1 NOx Emission and De-NOx methods

There are a number of oxides of nitrogen, including nitrous oxide, N_2O, nitric oxide, NO, nitrogen dioxide, NO_2, nitrogen trioxide, N_2O_3, and nitrogen pentoxide, N_2O_5, that are referred to collectively as NOx. The three oxides of nitrogen that are of primary concern to air pollution are NO, NO_2 and N_2O. NO is a colorless gas that is a precursor to NO_2 and is an active compound in photochemical reactions that produce smog. NO_2 is a reddish-brown gas that gives color to smog and can contribute to opacity in flue gas plumes from stacks.

NO_2 is a criteria pollutant with a National Ambient Air Quality Standard of $100\mu g/m^3$, or 0.053 ppm, annual average [36]. It is also a precursor to nitric acid and HNO_3 in the atmosphere and is a major contributor to acid rain.

By far the largest source of NOx is combustion, although there are other indus-

trial sources such as nitric acid manufacturing. Figure(2.12) shows the relative contribution from NOx emission sources. A large amount of NOx energy production (power plants) and energy use in industry (e.g., cement industry) are evident, and the very large contribution from motor vehicles and other forms of transportation, including ships, airplanes, and trains, is pronounced [37].

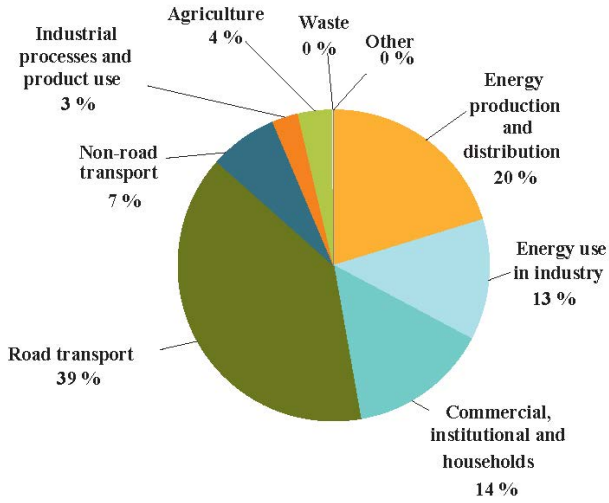

Figure 2.12: NOx-emission source [37]

The formation of NOx from combustion is determined by the interaction of chemical and physical processes occurring within the combustor. The three principle NOx forms are: (1) thermal NOx, (2) prompt NOx, and (3) fuel NOx. Understanding these mechanisms enables to utilize control methods in combustion for NOx emissions due to modification of combustion.

Thermal NOx: Thermal NOx results from the oxidation of atmospheric nitrogen in the high temperature of a combustion system. At high temperature, oxygen dissociates or reacts with free radicals to form free oxygen atoms (R1), then these attack nitrogen molecules to start a chain reaction forming NO. This reaction mechanism, the overall reactions, was first proposed by Zeldovich [38]; hence it is called the Zeldovich mechanism as seen below:

$$O_2 \rightleftharpoons 2O \tag{R1}$$

$$N_2 + O \rightleftharpoons NO + N \tag{R2}$$

$$N + O_2 \rightleftharpoons NO + O \tag{R3}$$

So the final reaction that produces NO is (R4):

$$N_2 + O_2 \rightleftharpoons 2NO \tag{R4}$$

The overall reaction that produces NO_2 is (R5):

$$NO + 1/2O_2 \rightleftharpoons NO_2 \tag{R5}$$

The reaction rate is a strong function of temperature. As an example, by decreasing the temperature from 1982°C to 1760°C, the time required to produce $500ppm$ NO increases from $0.1s$ to $1s$ [39].

Fuel NOx: Some fuels contain nitrogen, e.g., organically bound nitrogen in hydrocarbon compounds. Nitrogen in the fuel reacts with oxygen. Carbon-nitrogen bonds are broken more easily than diatomic nitrogen bonds, so fuel-NOx formation rates can be higher than thermal-NOx (not at very high temperatures) in fuels with considerable nitrogen content. Combustion control techniques that aim at reducing thermal-NOx formation by reducing flame temperature may not be effective for fuels that have high nitrogen content [40].

Prompt NOx: Prompt NOx is the third source of NOx emission attributed to the reaction of atmospheric nitrogen, N_2, with free radicals such as C, CH, and CH_2 fragments derived from fuel. Occurring in the earliest stage of combustion, this results in the formation of fixed species of nitrogen such as NH (nitrogen monohydride), HCN (hydrogen cyanide), H_2CN (dihydrogen cyanide) and CN- (cyano radical) which can oxidize to NO.

De-NOx techniques: There are various ways to reduce NOx emissions: temperature reduction, creation of a combustion environment that restrains NOx formation and end-of-pipe (post-combustion) treatment for removing NOx prior to releasing it into the atmosphere. The two broad categories for the control of NOx emissions are combustion control and flue gas treatment. Figure(2.13) [41] summarizes the different NOx controlling techniques.

A variety of combustion control techniques are used to limit the formation of NOx. Some reduce the peak flame temperature, some reduce the oxygen concentration in the primary flame zone, and one reburn. More details can be found in [42–45].

Although a significant reduction of NOx can be achieved by means of combustion modifications, generally up to 50% of the sum of different measures, this is often insufficient to comply with the emission standards and/or cannot be applied in existing combustors. Additional treatment is required and could be achieved by the use of end-of-pipe flue gas treatment technologies. Figure(2.13) illustrated all different flue gas treatment methods among which two methods, Pulsed Corona Discharge and Electron Beam Flue Gas Treatment (EBFGT) are basically different from the rest. These two methods apply at high-efficiency electric field to generate oxidants [46–48].

The wet systems are based on absorption of NOx to liquid solutions with low efficiency [49–51].

In the series of Selective Catalytic Reduction (SCR), Non-selective Catalytic Reduction (NSCR) (3-way catalyst) and Selective Non-Catalytic Reduction (SNCR), the first two are based on the reduction of NOx by reducing agents within heterogeneous catalytic bed in the defined temperature range. More details can be found in [52–61]. SNCR, which is under focus in this study, is NOx control of flue gas before emission. The capital cost of SNCR is low compared with SCR and NSCR systems since there is no catalyst and also low compared to pulsed corona discharge and EBFGT because of the energy consumption required to achieve adequate reduction [46].

In the following section more details of the SNCR process will be described.

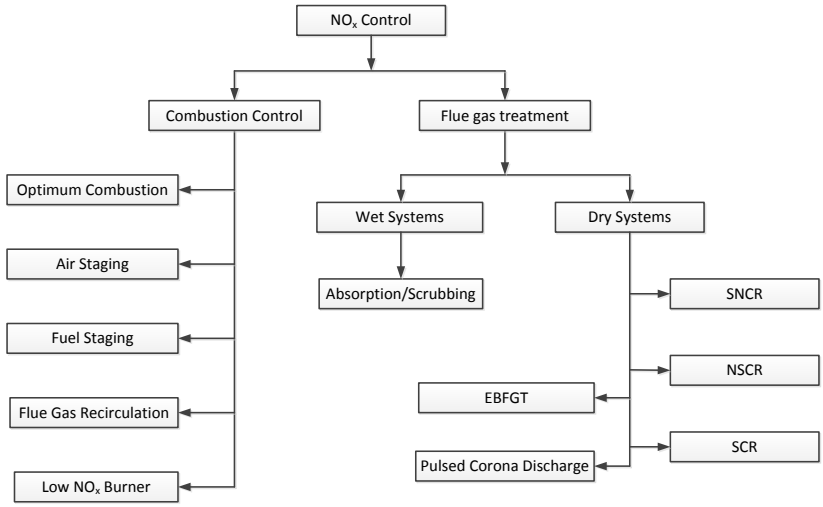

Figure 2.13: De-NOx techniques [41]

2.4.2 Reducing agent in SNCR

SNCR is a simple process, referred to the thermal De-NOx method, and involves the reduction of NOx to N_2in the presence of oxygen by reaction with nitrogen agents at 750°C-1100°C, the higher temperature being needed for urea. Lyon [62] developed the SNCR process and applied it in 1974 for the first time. In most full-scale applications, the reagents of choice are either NH_3 or urea. In certain laboratory and pilot scale experiments cyanuric acid has also been investigated as a potential reagent. Caton et al. [63] made a summary of the possible major chemical pathways for the removal of NOx using three agents: ammonia, urea, and cyanuric acid Figure(2.14). As shown, from left to right, the first step is the decomposition of the chemical agent.

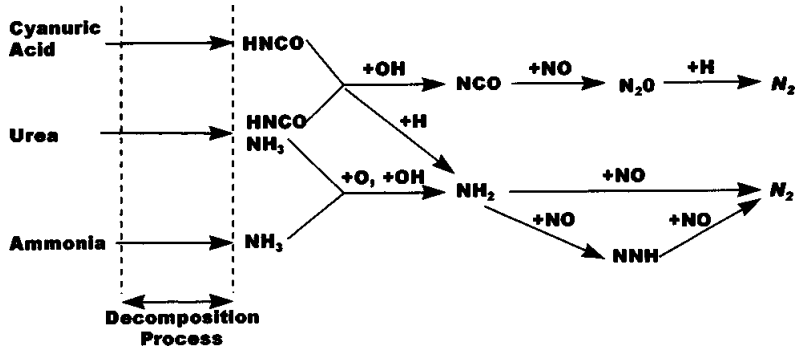

Figure 2.14: Schematic figure of the possible chemical pathways for the reduction of nitric oxide (NO) to molecular nitrogen N_2 using cyanuric acid, urea, or ammonia [63]

The chemical pathway for each agent is presented briefly.

2.4.2.1 Ammonia gas

The most used reducing agent for the reduction of NOx is ammonia. The ammonia gas reacts homogeneously with NO to form atmospheric nitrogen according to the simplified scheme seen in Figure(2.15). Because of the importance of temperature on this process, the details will be described in the temperature window section for different temperatures.

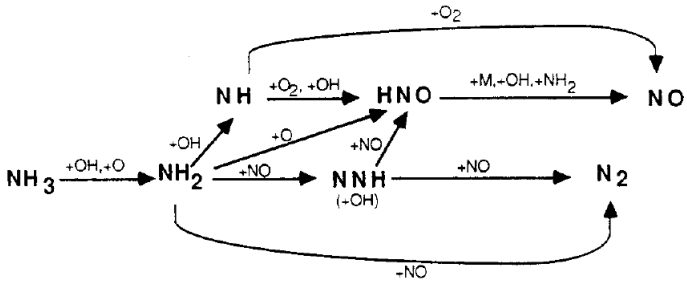

Figure 2.15: Reaction path diagram for the NOx reduction by Ammonia [64]

2.4.2.2 Urea

Urea behaves differently compared to ammonia. After injection of urea in the flue gas, aqueous urea solution is heated to the boiling point of water at which the water is evaporated [65] (same mechanism for SCR and SNCR). When all the water has evaporated the urea undergoes thermal breakdown, producing ammonia according to reaction path(R6-R8) where the (R7) is evaporated.

$$CO(NH_2)_2(aq) \rightarrow CO(NH_2)_2(l) + H_2O \tag{R6}$$

$$CO(NH_2)_2(l) \rightarrow CO(NH_2)_2(g) \tag{R7}$$

$$CO(NH_2)_2(g) \rightarrow (NH_3)(g) + HNCO(g) \tag{R8}$$

The rate of evaporation (R7) can be determined from the Equation(2.3) [65]:

$$r = 1 \times 10^{12} \times e^{-V/RT_d} \qquad [kg/s] \tag{2.3}$$

where V is the heat of evaporation and T_d is the temperature of the droplet. The heat of evaporation has been determined to be $87.4 kJ/mol$ [65]. After decomposition of urea, the product (ammonia) will enter into the ammonia reaction path shown in Figure (2.14).

According to Miller and Bowman [64], 45% of the formed urea will decompose to isocyanic acid. This will act to reduce the NOx similar to cyanuric acid.

2.4.2.3 Cyanuric acid

Cyanuric acid ($C_3H_3N_3O_3$) decomposes thermally to isocyanic acid and small amounts of ammonia. The isocyanic acid enters into the pathway as stated in Figure(2.14).

2.4.3 Effective parameters on SNCR

The SNCR process efficiency relies on temperature, reagent/flue gas mixing, reagent/NOx ratio and oxygen content [66]. SNCR systems reduce NOx emissions by 30–90% but the performance is highly variable for different applications.

In this part, effective parameters on SNCR of NOx, mechanism of SNCR and CFD modeling-related studies will be reviewed.

2.4.3.1 The temperature window and Mechanisms of SNCR

The temperature window is the range of temperatures in which the reduction of NOx takes place. This interval is relatively narrow (750°C- 1100°C) below 750°C; the reaction is too slow to give any reduction, and most of the injected NH_3 remains unreacted. At higher temperatures (higher than 1200°C) NH_3 tends to oxidize to form NO [67]. Figure(2.16) shows the experimental results of temperature window for SNCR with ammonia [64]. The optimum temperature is approx. 1230K (950°C) for this system. Generally, the optimum reduction temperatures from different observations are in agreement within 50°C, varying roughly between 935 and 985°C [67–71].

The temperature range depends on some parameters such as flue gas composition (mainly CO and oxygen in low concentration), inlet gas velocity and system geometry, which influences the mixing between the reagent and the NOx. Therefore, the possibility of NOx removal varies from one system to the other. Table (2.1) shows the temperature ranges and optimum temperatures reported in various studies [66, 68, 69, 71–81].

Because of the importance and effect of temperature in the kinetic mechanism of reaction, a lot of studies have been done to show the effect of temperature on $NH_3/NO/O_2$ on the basis of a kinetic mechanism of chain reactions [64, 70, 72,

Table 2.1: NH_3-SNCR studied

Researcher	Year	Temperature range (°C)	Optimum Temperature (°C)	NO_{inlet} (ppm)	Max. reduction (%)	O_2 (%)	R= NH_3/NO_{inlet}	Time (Sec)	Reference	System
Lyon	1975	925-1050	982	1020	> 90	0.5-2.2	1.5	0.075	[66]	Laboratory Plug Flow reactor
Muzio et al.	1977	705- 1100	970	300	78	2-4	1	0.5	[68]	Plug Flow Combustion 58.5 kW
Muzio et al.	1979	815-1100	928	500	65	5	1		[72]	Laboratory Scale study of coal-derived combustion
Banna et al.	1981		847	1450	90		2		[73]	Lean combustion
Lucas et al.	1982	830-1025	950	510	96			0.04	[69]	Lean-burning oil-fired laboratery combustion tunnel
Lodder et al.	1985	827-1077	1000	345	75	1	1.5		[74]	Fired Boiler 1MW
Kimball-Linne and Hanson	1986	777–1177	1010						[71]	flow reactor-plug flow
Hulgaard et al.	1990	750-1100	950	450	70	4	1.3		[75]	Pilot-scale of pulverized coal combuster
Iron et al.	1991	940-1040	985	225	40	3	1		[76]	0.15 MW linear furnace and 6 MW scale modelof a power stationfurnace
Leckner et al.	1991	600-1100	850	50-200		5-7	2-6	0.5-2	[77]	application of SNCR in CFB
Caton et al.	1995	900-1100	827-877	330	77-98	1-15	1.5		[78]	Laminar Flow, Electrically Heated
Østberg et al.	1996	727-1127	880-1070	500-600	80	1-4	2-3	0.012	[79]	Bench scale reactor using flue gas
Alutza et al.	1997	450-1000	627-777	300	20-70	4-21	1	-	[80]	Lab scale hybrid reburning/SNCR
Liang et al.	2013	700-1150	850-1000	400-500	20-75	1-6	1.2	0.01-0.12	[81]	Lab scale laminar flow

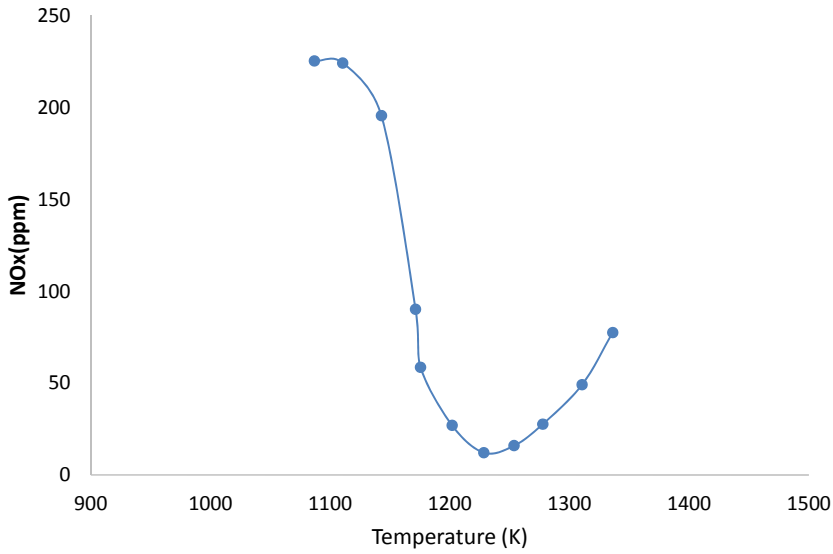

Figure 2.16: Temperature window for SNCR with ammonia. Initial condition: NO_i=225ppm, NH_3=450ppm, O_2=1.23% [64]

82–87]. Generally, NOx removal by SNCR is illustrated in Figure (2.15) which is explained below based on the studies mentioned.

The initial reaction in NO reduction is reaction of NH_3 with OH radicals to give amide NH_2 (R9):

$$NH_3 + OH \rightleftharpoons NH_2 + H_2O \tag{R9}$$

Amide NH_2 also can be formed by reaction of NH_3 with oxygen atom O (R10):

$$NH_3 + O \rightleftharpoons NH_2 + OH \tag{R10}$$

The amide radical is highly selective towards NO and causes the primary reduction of NO at optimum temperatures even in an oxidizing environment.

$$NH_2 + NO \rightleftharpoons N_2 + H_2O \tag{R11}$$

$$NH_2 + NO \rightleftharpoons NNH + OH \tag{R12}$$

Reactions (R11) and (R12) are dependent on concentration of NH_2 inside the reactor which is formed in reactions (R9) and (R10) which in turn depend upon OH and O concentrations. This indicates that the concentration of O and OH for overall reaction is important to continue the NH_3 to NH_2 conversion. They must be regenerated to self-sustain the reaction. This regeneration is described by the sequence reactions (R13-R16):

$$NNH + NO \rightleftharpoons N_2 + HNO \tag{R13}$$

$$HNO + M \rightleftharpoons NO + H + M \tag{R14}$$

Here, M is the third body which could be any inert molecules and helps the reaction to take place.

$$H + O_2 \rightleftharpoons OH + O \tag{R15}$$

The O atom either continues Reaction(R16) or, in the presence of water, it reacts:

$$O + H_2O \rightleftharpoons OH + OH \tag{R16}$$

Thus, there is a net gain of chain carriers per cycle, and as long as branching sequence occurs at least a quarter of the time, the overall reaction would be self-sustaining [64].

Reactions below 750°C: The reactions (R15) and (R16) are strongly dependent on temperature. At the temperature lower than 750°C, these two reactions

are very slow, thus OH concentration is not enough to convert NH_3 to NH_2 reaction (R9); thereby chain termination reactions compete with the branching sequence, making limited NO reduction. The chain terminating reactions are reactions (R11), (R17) and (R18):

$$NH_2 + HNO \rightleftharpoons NO + NH_3 \tag{R17}$$

$$OH + HNO \rightleftharpoons H_2O + NO \tag{R18}$$

These are all undesirable to NO reduction because they consume NH_2 and OH radicals without producing any further radicals; whereas for any substantial reduction to occur, enough OH and O radicals are required to convert NH_3 to NH_2. Thus below 750°C, the rates of reactions (R9) and (R10) limit the overall process.

Reactions in range 750°C –1000°C: The reaction sequences (R9-R11) and the reactions (R9), (R10) and (R12) onwards are dominant over the sequence (R9), (R10) and (R19) even up to temperatures below 1000°C. This is because in the range 750°C –1000°C, the rate of reaction of (R12) is greater, compared to those of NH_2 oxidation reactions.

$$NH_2 + OH \rightleftharpoons NH + H_2O \tag{R19}$$

$$NH_2 + NH_2 \rightleftharpoons NH_3 + NH \tag{R20}$$

In the temperature range 750°C–1000°C, the mix of branching and terminating is just right to cause the growth in chain carrier concentration. With the increase in temperature above 750°C, the reaction path leading to the chain branching reaction (R14) becomes more important than the one leading to a termination reaction such as (R18). This can be explained by greater activation energy of (R14) than (R18). Then H-radicals from the former reactions may react with either molecules of O_2 or water causing more chain branching as follows:

$$H + H_2O \rightleftharpoons OH + H_2 \tag{R21}$$

or reactions (R15)and (R16). The branching can be observed by the number of OH radicals formed per OH radical consumed in each cycle.

Due to these branching sequences in (R9, R12, R13, R14, R15 and R21), one OH consumed and two OH produced and in (R9, R12-R16), one OH consumed and four OH produced, enough radicals are produced to drive reactions (R9) and (R12), and significant NO reduction is thus achieved within the optimum temperature range.

Reactions above 1000°C: When the temperature is further increased beyond 1000°C, the OH radical concentrations start building up due to the branching sequence mentioned above. An excessive increase in OH concentration initiates an NH-forming sequence and reaction (R19) which may start competing with reaction (R9). Therefore, the NH radical concentration starts building up and NO formation via sequence (R9, R10, R14, R18, R19, R22-R24) starts competing with the NO reduction sequence. Once NH is formed, the high-temperature oxidation reaction sequence leads directly to NO formation:

$$NH + O_2 \rightleftharpoons HNO + O \tag{R22}$$

$$NH + OH \rightleftharpoons HNO + H \tag{R23}$$

followed by:

$$NH + O_2 \rightleftharpoons OH + NO \tag{R24}$$

$$HNO + OH \rightleftharpoons H_2O + NO \tag{R25}$$

At a temperature around 1230°C, the NO destroyed through the NO reduction sequence would just be balanced by that formed through oxidation sequence. At a sufficiently high temperature, the oxidation sequences become significantly dominant, resulting in an increase in NO concentration.

2.4.3.2 Reaction time

Reduction of NOx is a fast reaction; therefore, most experiments in the literature for SNCR processes have been done in plug flow reactors which are often measured as residence time.

The time required to complete NOx reduction by the SNCR method is reported to range from 40 to 50ms in plug flow reactors. Muzio et al. [68] reports that during his investigation all the reaction occurred within 200ms from the point where the NH_3 is injected. In a study by Lyon [66], 75ms is observed in the temperature 982°C, and Kimball-Linne and Hanson [71] report a reaction time of 80ms at the optimum temperature. Also, Lucas and Brown [69] report 40ms for their study.

The complete reaction time significantly depends on temperature and flow pattern and it is different from one reactor to another. But it seems that a consideration of the residence time of about 100ms at the optimum temperature should be reasonable for a new reactor design.

2.4.3.3 Effect of Oxygen on SNCR

For initiating the SNCR, the presence of oxygen is required. It is found that without oxygen the NO removal is impossible [66]. Various investigators have confirmed that the presence of oxygen is essential for the process. Literature reported different oxygen levels in their investigations,Table 2.1.

It is reported that increasing the excess O_2 level from 2% to 4% has no significant effect on the magnitude of NO reduction in higher temperatures. Moreover, it is found that at the higher excess oxygen levels, the NH_3 is more effective in removing NO at a temperature around 870°C [68] and is independent of oxygen concentration.

A study on the effect of O_2 content of the flue gas at two different temperatures shows that at 1000°C, the reduction is effectively independent of O_2 concentration, but at a lower temperature (908°C) reduction increases monotonically with O_2 concentration [76]. The result is illustrated in Figure(2.17). They also reported that, over the range of O_2 contents which are likely to be encountered on industrial pulverized fuel boilers, the NOx removal efficiency is not a strong function of O_2 concentration.

However, at a lower reactor temperature and very high oxygen (>10%) concentration, the NO reduction is decreased. For example, for 1% oxygen, 98% NO removal is achieved, for 15% oxygen only 77% NO removal is achieved [78].

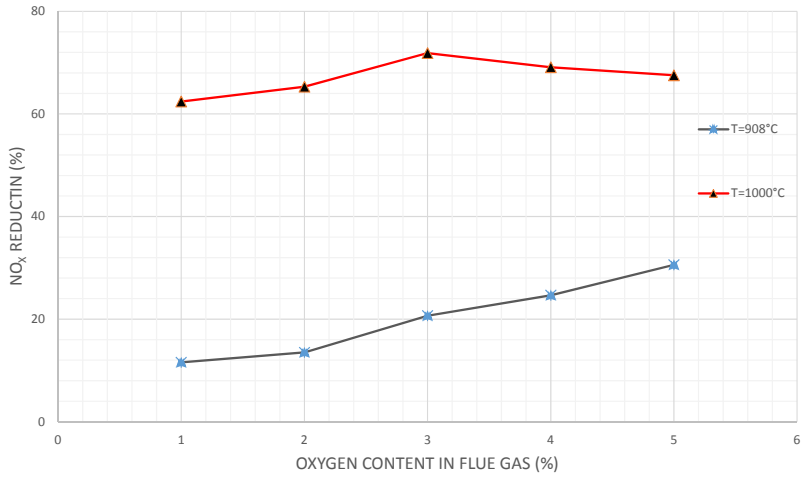

Figure 2.17: Effect of Oxygen Content on SNCR on 908°C and 1000°C at NH_3/NOx=1 [76]

This is mostly because the additional oxygen increases the oxidation reactions. The higher oxygen cases, however, result in less (or no) ammonia present in the reacted gases. The additional O_2 minimizes any NH_3 slip, but emission of nitrous oxide may increase.

As a mechanism approach, it is found that with the presence of O_2, chain branching may occur by subsequent reactions (R9, R10 and R15), and a self-sustaining chain reaction could occur [66].

It is proposed that products of NH_2+NO reaction is N_2H+OH (R12) and N_2+H_2O (R11) instead of N_2+H+OH. There are two advantages of excess O_2. First: there would be more equilibrium OH present initially in the combustion products. Second: the reaction sequence (R15) and (R16) becomes dominant over (R21), the former resulting in more OH. Even if there is no initial water, the O_2 atom produced by (R15) reacts directly with NH_3 via (R10) producing both NH_2 and OH. In the absence of O_2, reaction (R15) would not occur, and hydrogen atoms would react only with NH_3 at a rate too slow to result in NO removal in the time scales of interest [83].

There are differences at final NOx reduction between Figure(2.16) and Figure (2.17) at temperatures 908°C and 1000°C for two experiences. It seems that, because of ammonia concentration in the flue gas, in Figure(2.16) the molar ratio of ammonia to initial NOx is 2 whereas in Figure(2.17) it is 1. It means we cannot compare these two studies.

2.4.3.4 Effect of molar ratio NH_3/NOx

The ratio moles of injected NH_3 to the moles of initial NOx in the gas flow are called molar ratio. The effect of the molar ratio in reduction performance has been investigated by a number of researchers. The results obtained by Muzio et al. [68] are illustrated in Figure(2.18) which is obtained from a combustion tunnel. The largest NO reduction occurred at molar ratio 1.6 in this study. Another investigation on coal-fired boilers shows that a 65% reduction obtains at NH_3 /NO =1 [72].

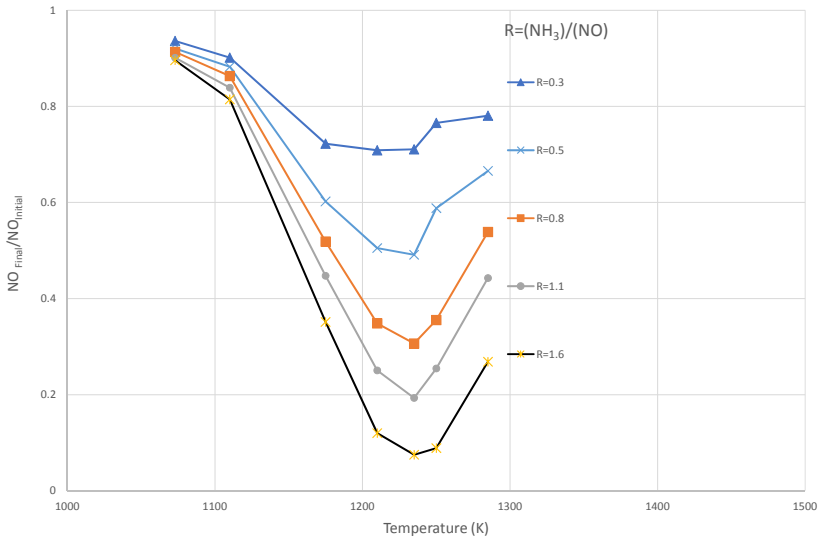

Figure 2.18: Effect of NH_3/NO molar ratio on efficiency in different temperatures with initial NO 300*ppm* and Oxygen content 4% [68]

Also, the SNCR by NH_3 studied in a lean-burning oil-fired combustion tunnel as a function of molar ratio, temperature, concentration of NH_3 added and the source of NO by Lucas and Brown [69]. They found that at a fixed equivalence ratio, the optimal reduction temperature increases with increasing molar ratio. The range of optimal reduction temperature varied from approx. 875°C to values in excess of approx. 975°C.

Another investigation on the SNCR of NOx by NH_3 as a function of the molar ratio in the flue gas containing 1% $O_2$by Lodder and Lefers [74] shows that NOx reduction increases with increasing molar ratio and, for molar ratio greater than 2.0, ammonia slip (unreacted NH_3) become important.

2.4.3.5 Effect of initial NOx concentration

Muzio et al. [68] have reported that the effectiveness of the selective reduction of NOx is reduced at a low initial concentration. They found that with initial NOx levels less than 400*ppm*, the injected NH_3 becomes less effective as a reducing agent at a given molar ratio. However, when the initial NOx is greater than 400*ppm*, there is little effect of initial NOx concentration on NOx reduction. In Figure(2.19) the results are illustrated. This reduction in the effectiveness of SNCR at low initial NOx concentration prevents the attainment of very low (below 100ppm) NOx.

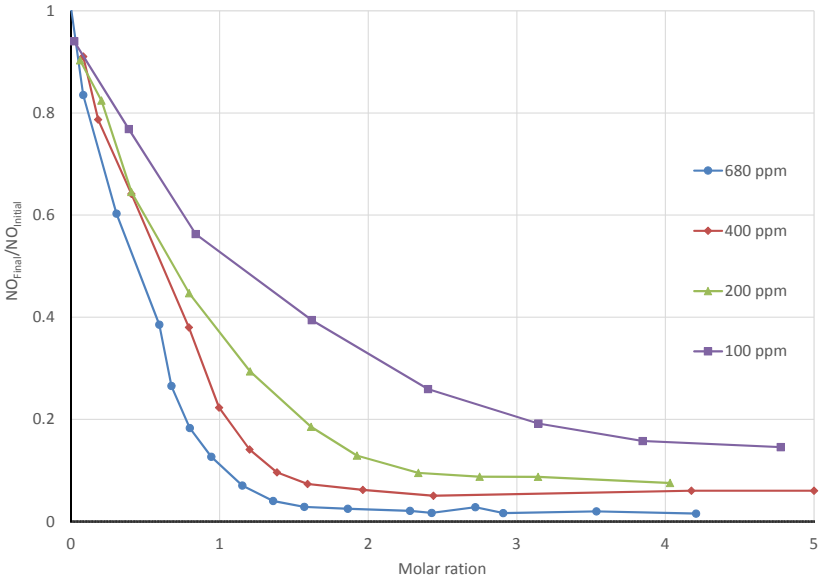

Figure 2.19: Effect of initial NO concentration on NH_3 SNCR performance at 963°C and 2% O_2 [68].

These results are confirmed by another study in a coal ash deposition [76], which shows that by decreasing the initial NOx from 250ppm to 175ppm, NOx conversion is decreased from 38% to 31%.

2.4.3.6 Mixing

Most experimental studies in the literature are done in plug flow reactors to assume an infinite rate of mixing. Diffusion time of NH_3 at 1027°C from a point equidistant from the centerline and wall was estimated by Dean et al. [84]

0.00013 s in a tube with 0.2 cm i.d. and 0.0032 s in a tube with 1.0 cm i.d. In both, diffusion time is much shorter than the reaction time for SNCR to support the plug flow assumption.

The effect of mixing on the SNCR process is studied by Banna and Branch [73], Branch et al.[88], Østberg et al. [79], Røjel et al.[89], Oliva et al. [90] and [81], but the results appear to be contradictory. Branch et al.[73] observed that under non-premixed conditions the temperature window for NO reduction widens, indicating that incomplete mixing may extend the temperature range in which NO removal is effective to a higher temperature. In contrast, Østberg et al. [79] found from bench-scale experiments that delayed mixing tends to narrow the temperature window. Røjel's results [89] show that finite rate mixing affects the SNCR process's efficiency at high temperatures where it may cause a narrowing or a widening of the temperature window, depending on the NO concentration.

In systems with higher NO levels, finite rate mixing may have an adverse effect on the SNCR process.

2.4.3.7 Effect of CO

The SNCR process will inhibit the oxidation of CO to CO_2. Thus, if CO is present at the point of injection, its oxidation could be inhibited and it could be emitted to the atmosphere [72]. Different investigations [73, 91] confirm the concurrent inhibition of CO by NH_3. In addition, it is observed that additional CO causes NO reduction curves to shift towards a lower temperature [74]. The presence of CO enhances the reaction of NH_3 with NO and O_2 but decreases selectivity, i.e., causing more NH_3 to react with O_2 to form NO rather (in lower temperature) than to react with NO to reduce it [86]. The oxidation of CO could be carried out at a higher temperature and higher initial CO as (R26):

$$CO + OH \rightleftharpoons CO_2 + H \tag{R26}$$

In case CO can start the oxidation, much larger concentrations of OH and O will be produced because the H atom obtained from reaction (R26) may start the sequence followed by (R15) and (R16) which accelerates the NH_3-NO-O_2 reaction.

2.4.4 Reduced Mechanism for SNCR

A reduced chemical kinetic mechanism for the prediction of SNCR chemistry has been developed by Duo et al. [87], which describes the kinetics of the reactions by a simple model assuming first-order oxidation of NH_3 to NO and second-order reduction of NO to N_2. For the purpose of developing a simple and quantitative description of the rate of reactions occurring in the thermal De-NOx process, the kinetics of the homogeneous reaction between NO and NH_3, with excess of O_2, is studied in an isothermal plug flow reactor. In this study it is observed that with increasing residence time, the optimum temperature is decreased and the degree of reduction of NO is also increased. However, it is sensitive to residence time only at very short residence times at higher temperatures. This study also shows that the degree of conversion of NH_3 increases with both temperature and residence time. Simplified Reaction Mechanism for the SNCR Process is a single initiation step followed by two parallel reaction pathways, one leading to reduction Reaction(R29) and the other to formation (oxidation of ammonia) reaction(R30).

$$NO + NH_3 + \frac{1}{4}O_2 \rightarrow N_2 + \frac{3}{2}H_2O \tag{R27}$$

$$NH_3 + \frac{5}{4}O_2 \rightarrow NO + \frac{3}{2}H_2O \tag{R28}$$

The simple model proposed describes the reaction rates as:

$$R_{NO} = -k_r\,[NO]\,[NH_3] + k_{ox}\,[NH_3] \tag{2.4}$$

$$R_{NH_3} = -k_r\,[NO]\,[NH_3] - k_{ox}\,[NH_3] \tag{2.5}$$

The rate constants for Eq(2.4) and Eq(2.5) are:

$$\mathrm{k}_r = (2.21 \pm 0.33) \times 10^{14} \exp\left[\frac{-(38160 \pm 170)}{T}\right],\ \frac{1}{s}$$

$$\mathrm{k}_{ox} = (2.45 \pm 0.49) \times 10^{14} \exp\left[\frac{-(29400 \pm 250)}{T}\right],\ \frac{m^3}{mol.s}$$

Results of this study verify that the kinetic model can give a satisfactory prediction of the experimental results under different conditions.

The application of this simple model further developed to describe the influence of the major parameters that can be varied in the De-NOx process (injection

temperature, temperature gradient, residence time, amount of injected NH_3 and amount of injected additive) [92]. In this study the model predictions are compared to experiments carried out in a fluidized bed boiler and in a pilot plant using flue gas withdrawn from a coal-fired utility boiler, and it is compared with the kinetic model of Miller and Bowman [64]. Results show with ideal mixing between the injected NH_3 (as in the cyclone of the fluidized bed boiler), a good agreement between the model predictions and the experiment is obtained. This empirical model gives a better description of the result for a fluidized bed boiler than Miller and Bowman's kinetic model [64].

This mechanism also allows for more investigation on the influence of mixing on SNCR [79]. In this study, an experimental and theoretical investigation of mixing in the SNCR process is performed. The experiments are carried out in a bench scale reactor using the flue gas from a natural gas burner as the main gas and injection of a jet of NH_3 mixed with the carrier gas in cross flow. The results show a dependency on the carrier gas flow at temperatures above the optimum temperature for NOx reduction. It also reported no dependency on the variation of the O_2 concentration in the carrier gas from 0 to 21 vol%. It is further concluded that an increasing momentum ratio of the jet to the main gas improves the NO reduction up to a limiting value of the momentum ratio of approximately 20, with no further improvements observed above this value. Chemical kinetic modeling of the initiating reactions involving NH_3 shows that the reaction with OH radicals is the primary initiating reaction. It is also shown that process performance is influenced by the O_2 concentration in the flue gas. The experimental results apply to verify the droplet diffusion model proposed by Østberg and Dam-Johansen in a former study [93].

Another reduced chemical kinetic mechanism for the prediction of SNCR chemistry is proposed by Brouwer et al. [94] to describe the reduction of NOx by injection of ammonia or urea with the use of limited computational efforts. The model was developed by the reduction of a Detailed Chemical Kinetic Model (DCKM) developed by Miller and Bowman [64]. This DCKM consists of 213 reactions.

It is identified that the principle NO reduction pathway occurs by reaction with NH_2 forming N_2 for ammonia and by reaction with HCO forming N_2O as intermediate for the cyanuric acid. When using urea both pathways are important. This knowledge is used to develop the reduced mechanism. The mechanism assumes instantaneous breakdown of the reactants into ammonia and isocyanic acid (HNOC). Urea breaks down into both ammonia and HNCO in the ratio 1.1 moles of NH_3 to 0.9 moles of HNCO because HNCO subsequently reacts along the ammonia pathway [94]. The reaction pathway for the reduction of NO with ammonia, cyanuric acid and urea is schematically shown in Figure(2.20).

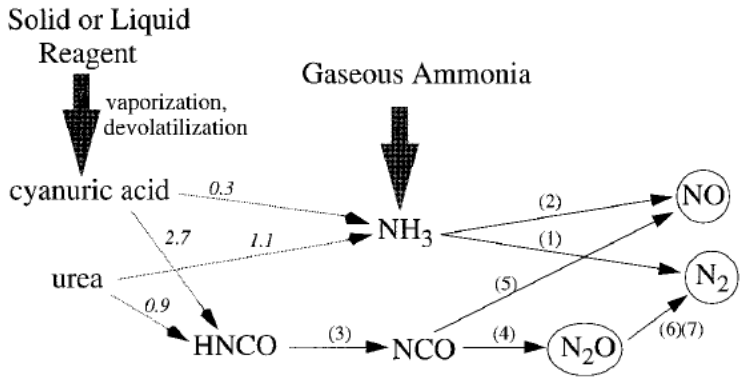

Figure 2.20: Schematic of the reduced SNCR model (numbers in parentheses correspond to reaction numbers in Table(2.2)) [94]

The reduced mechanism consists of 6 species and 7 irreversible finite-rate reactions. The reaction mechanism can be seen in Table(2.2).

Table 2.2: Reduced model for SNCR of NOx using ammonia, urea or cyanuric acid [94]

Reaction	A	b	E_a
1. $NH_3 + NO \rightarrow N_2 + H_2O + H$	$4.24E+08$	5.30	83,600
2. $NH_3 + O_2 \rightarrow NO + H_2O + H$	$3.500E+05$	7.65	125,300
3. $HNCO + M \rightarrow H + NCO + M$	$2.400E+14$	0.85	68,000
4. $NCO + NO \rightarrow N_2O + CO$	$1.000E+13$	0.00	−390
5. $NCO + OH \rightarrow NO + CO + H$	$1.000E+13$	0.00	0
6. $N_2O + OH \rightarrow N_2 + O_2 + H$	$2.000E+12$	0.00	10,000
7. $N_2O + M \rightarrow N_2 + O + M$	$6.900E+23$	−2.50	64,760

Units are A = cm–mol–s–K; E_a = cal/mol.

The first two reactions describe the ammonia chemistry. Reaction1 is the degradation of NO at a lower temperature. Reaction2 is the formation of NO from NH_3 and O_2 at high temperatures. Reaction3 through Reaction7 describe the isocyanic acid chemistry. Reaction3 is the degradation of HNCO into NCO. HCO can subsequently react with OH and form NO through Reaction5. The desired reaction in the HNCO pathway is Reaction4 where NCO reacts with NO to form N_2O. The N_2O formed through Reaction4 reacts with OH or a third body to form N_2 through Reaction6 and Reaction7.

The SNCR process is limited to a narrow temperature window and oxygen level, and the global reaction mechanism works well for this process, as indicated in Figure(2.21).

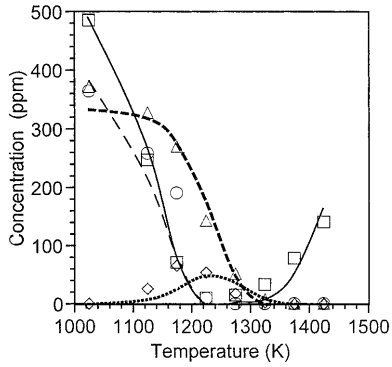

Figure 2.21: Comparision of the reduced SNCR model to fully detailed chemical kinetics prediction for homogeneous, isothermal conditions at various temperatures. Symbols are fully detailed chemistry ($\square = NO$, $\bigcirc = NH_3$, $\triangle = HNCO$, $\diamond = N_2O$), and lines are reduced chemistry (— =NO, — — $= NH_3$, - - - - $= HNCO$, $\cdots = N_2O$) [94]

It is seen that the reduced model describes the ammonia, urea, cyanuric acid and NO chemistry very well in the limited temperature window. Furthermore, it is seen that a minimum in NO concentration is obtained in the temperature range from approximately 1200K to 1300K. The model is evaluated by Brouwer and Heap [94] for the three reduction agents by comparison with experimental results found in the literature. In Figure(2.22), the reduced mechanism using ammonia as reducing agent is compared with the full mechanism and experimental data obtained by Lyon [67]. The initial conditions for this comparison is 225ppm NO, 450ppm NH_3 and 1.23% O_2. It is seen that the reduced model predicts the reduction and the temperature dependence just as good as the DCKM.

In Figure(2.23), the reduced model for NO reduction using cyanuric acid with and without CO is compared with the DCKM and experimental data presented by Caton and Siebers [95].

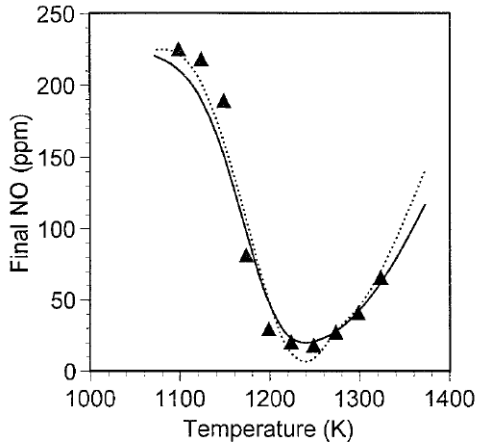

Figure 2.22: Comparison of the reduced SNCR chemistry with full chemistry set and the data of Lyon for homogeneous conditions ($\cdots$ = $fullchemistry$, — =Reduced model, ▲ = $Data from Lyon$) [94]

2.5 Computational fluid dynamics (CFD) simulations

CFD is a powerful tool for process design, optimization, analysis, and pollution control and can be applied for different purposes. For example, numerical modeling of a highly swirl 2-phase flow provides a valuable tool that can be used for the investigation and better understanding of chemical reactions, particle behavior and pollutant emissions in cyclone reactors.

In CFD modeling, the equations governing the flow of the gas, the Navier-Stokes equations, are written in a finite difference form and solved with the aid of a computer on a grid of points spanning the body of equipment. The particles can either be treated as a sort of second fluid in the cyclone or as individual particles, which can be tracked in the precalculated gas-flow field.

Flow in the inner space of a cyclone has several characteristics that make its numerical simulation difficult. Obviously, intense swirl, shear, confined and unstable flow structures will not be easy to simulate. Three features of flow inside the cyclones, the high curvature of the average streamlines, high swirl intensity and radial shear, adverse pressure gradients and recirculation zones make turbulence inside cyclones highly anisotropic. It means that most models based on first order turbulence closure, for example, the $k - \varepsilon$ model and its

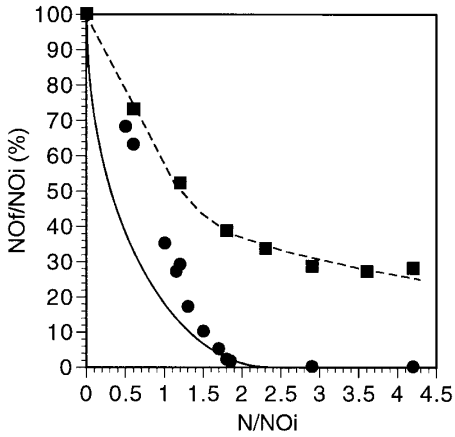

Figure 2.23: Comparison of the reduced SNCR model to the data of Caton and Siebers for homogeneous conditions with and without CO. Symbols are data(■ = *withCO*, • = *withoutCO*) and lines are the results from mixing and reduced chemistry model(- - - - =with CO,—=without CO).[94]

variations, are very weak at capturing the real flow. The studies have shown that at least second-order closure, for example, a Reynolds Stresses Transport Model (RSTM), is needed to capture anisotropy and achieve a realistic simulation of the cyclone flow [96–98].

2.5.1 CFD studies on gas flow

Choosing the turbulence model is the most critical aspect of CFD simulation of the cyclone. The first CFD simulation of the cyclone flow was performed by Boysan [99] in 1982 by using the finite-element method. The results show that the standard $k-\varepsilon$ turbulence model is not able to accurately simulate this kind of flow. In a second study, good agreement between experimental data and simulation of overall pressure drop and the radial velocity profile were found by using the RSTM model [100].

A comprehensive study was also done on several turbulence models by Hoekstra [101] in 1999. The relative performance of the $k-\varepsilon$ model, a variation RNG-$k-\varepsilon$ model (ReNormalization Group), the differential RSTM known as the LRRG model (modification of Launder, Reece and Rodi implementation of differential RSTM by Gibson) is evaluated [101]. Simulations were also compared with velocity measurements carried out by means of LDA (Laser Doppler

Anemometry). In this study, tests are performed with three different vortex finder diameters which produced three different swirl numbers. For a case with swirl number (ratio of the angular momentum to the axial momentum) 2.2, the comparison of tangential velocity is illustrated in (Figure 2.24). For all runs, the $k-\varepsilon$ model predicted only the inner vortex structure clearly (solid-body rotation), a logical result given its foundations, albeit contrary to experiment. The RNG $k-\varepsilon$ model shows significant improvement, while the RSM exhibited the best behavior.

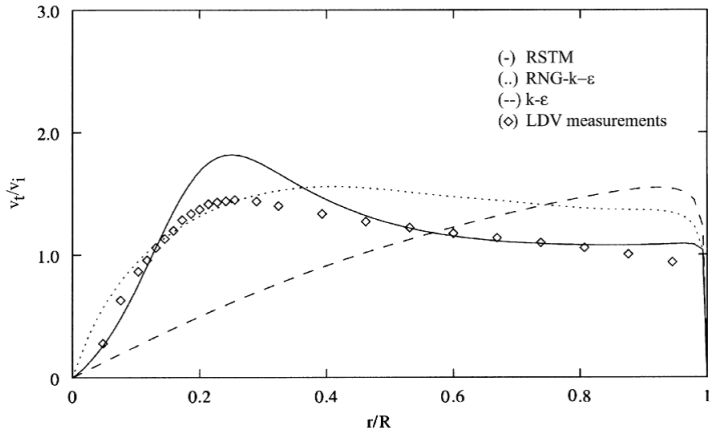

Figure 2.24: Comparison of tangential velocity profiles. V_{in}=6.2 m/s, Swirl number =2.2 [101]

The same observations are also found in comparing the same models by Pant et al. in 2002 [102, 103].

In another comparative study, the effect of temperature and inlet velocity on the cyclone pressure drop is done [16]. The simulation results by using the RNG-$k-\varepsilon$ model and the RSTM are compared with four different empirical models and experimental data. Investigation on the effect of inlet velocity on pressure drop showed that the RSM had the closest agreement with the experimental results.

The superiority of the RSM over other models has been established by other literature accordingly [17, 18, 104–112]. These investigations of various characteristics of the cyclone separator flow field, such as velocity profiles, pressure drop, effect of particle size and mass loading on separation efficiency, and effect of pressure and temperature on cyclone performance, have shown the ability of the RSM for realistic prediction of the flow field inside cyclone separators.

Different RSMs models are available, for example, Launder-Reece-Rodi (LRR)

and Speziale-Sarkar-Gatski (SSG). Among these RSM models, it is still not clear which is the most suitable form of the RSM for cyclone separator simulations as both algebraic (used in CFD modeling) and differential RSMs have been employed. Between these two, the differential form of the RSM is more accurate. Within the differential RSMs, the difference between a basic and an advanced differential RSM is also of relevance. An example is a comparison study on the predictions of various turbulence models with LDA measurements for the tangential velocity profile in an industrial hydrocyclone [113]. In this study, turbulence models including two differential RSM implementations, the basic LRR implementation and the advanced SSG implementation along with the standard $k-\varepsilon$ and a $k-\varepsilon$ model modified to account for the streamline curvature were tested. They found the flow field to be highly sensitive to the model choice, whereas the pressure distribution predictions are relatively robust [113]. The typical Rankine profile is obtained only by means of the RSMs. The SSG model produced more acceptable results compared to the LRR model in the lower part of the cyclone [113].

Despite a number of advances, the ability of unsteady RANS (Reynolds Average Navier Sotkes) simulations with advanced RSM to accurately predict complex flow structures is still not fully established. Only relatively stable and ordered flows have been simulated. In order to fully establish their viability for cyclone separator simulations, these models should be tested for conditions of highly incoherent and variable PVC (Processing Vortex Core). Meanwhile, LES (Large Eddy Simulation) simulation of swirling and cyclone flows is presently becoming a new standard [114].

Derksen [115] is among the first to simulate the PVC phenomenon by means of LES simulations. The capabilities of LES to simulate the turbulent flow in a cyclone separator are reported in several studies [112, 114, 116–120]. Another simulation is reported by Derksen [115], which is limited to small-scale cyclones at a moderate inlet Reynolds number. With increasing computational power, simulation of industrial scale equipment (with Re = 280000) is also reported [19, 120].

Targeting cyclone simulation, the DNS (Direct Numerical Simulation) fully resolved Navier Stokes equations. All of the relevant scales of turbulent motion are captured in the direct numerical simulation. This approach is extremely expensive even for simple problems in modern computing machines. There is no study of the cyclone simulation with this model.

The LES approach seems to offer a very realistic simulation. However, due to the scale and complexity of today's industrial cyclone separator simulations, the unsteady RANS approach with higher-order turbulence closures is the only practical approach that offers affordable realistic predictions of flow inside the

cyclone. It is only a matter of time before resolved simulations using LES will become the preferred alternative.

In conclusion, as mentioned, the choice of the turbulence model is the most critical aspect of CFD simulation of the cyclone. An appropriate turbulence model should be selected to resolve these flow features. The models based on first order turbulence closure have a limited ability for capturing the real flow [121]. Generally, at least a second-order closure is needed to capture the anisotropy and achieve realistic simulations [121]. Of the three available approaches to capture the turbulent characteristics, namely RANS, LES and DNS, RANS approach is the oldest approach to turbulence modeling. In the unsteady RANS, an effect averaged version of the governing equations that also includes transient terms is solved. In the LES approach, the smaller eddies are filtered and are modeled using a sub-grid scale model, while the larger energy carrying eddies are simulated. The DNS solves fully resolved Navier Stokes equations. All of the relevant scales of turbulent motion are captured in a direct numerical simulation. This approach is extremely expensive even for simple problems on modern computing machines. Until sufficient computational power is available, the DNS will be feasible only for model problems, leaving the simulation of industrial problems to LES and RANS approaches. LES approach of full-size equipment is a realistic simulation with some minor details.

In the following sections, relevant details about CFD basics will be discussed together with gradual outcomes of the literature.

2.5.2 CFD studies on two-phase flow in cyclones

Two-phase flows can be classified according to the importance of the interaction mechanisms [122], [123]. Figure(2.25) [123] shows an elementary and practical sketch. In CFD modeling of the cyclone, two different regimes are distinguished, depending on the existence of mutual, significant interaction between particles: dilute and dense two-phase flow. Two regime is divided based on volume fraction of particles in fluid ($\phi \approx 10^{-3}$), which translates generically as an inter-particle spacing $L/d_p \approx 8$ (L is the average distance between two particles and d_p is the average diameter of of particles). In the dilute regime, all the influence of particles on the gas can be neglected for $\phi < 10^{-6}$ ($L/d_p > 80$), which is known as one-way coupling; for higher volume fractions, it needs to be accounted for two-way coupling.

Aside from obvious issues of volume and continuity, the generic flow feature most affected is turbulence. In the dense regime ($\phi > 10^{-3}$, $L/d_p < 8$), interparticle interactions become of importance, with physical collisions and indirect influence through the nearby flow field. The collisions can lead to coalescence and break-

up, which must be considered too. This regime is called a frequent four-way coupling which is suitable for the fluidized bed. Where:

ϕ: volume fraction of particles, $\phi = \frac{MV_p}{V}$
M: number of particles
V_p: volume of a single particle
V: volume occupied by particles and fluid
d_p: diameter of particle
L: Distance between the center of particles

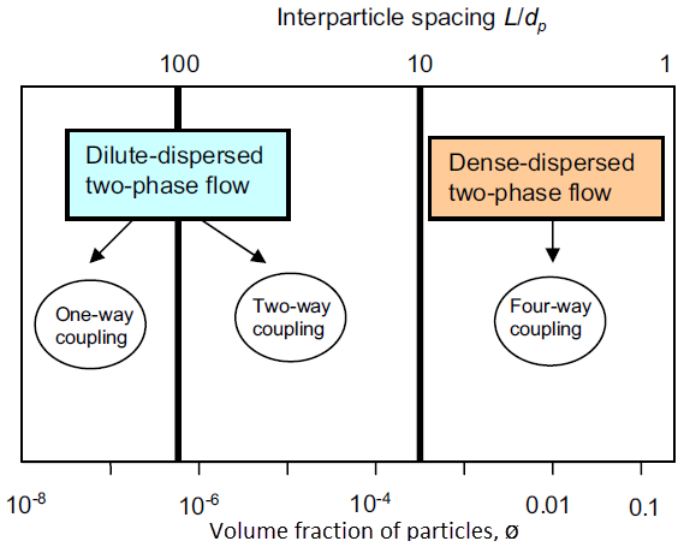

Figure 2.25: Map of regimes of interaction between particles and turbulence [123]

Considering the framework mentioned, numerical models have developed in two parallel paths, either by a Lagrangian or by an equivalent Eulerian formulation. In the Lagrangian model, particle trajectories are obtained by integrating the particle equation of motion. In the Eulerian approach, conservation equations are written for the mass, momentum and energy of the particle cloud as a continuum and integrated to predict volume averaged properties through the field.

The suitable choice is often problem-specific. Generally, Lagrangian methods are more suited to dilute flows, free of numerical diffusion, less influenced by other errors and more stable for large particle velocity gradients. Also, the treatment of realistic poly-dispersed particle systems is straightforward. However, for

highly loaded flows, limitations related to computer storage, calculation times and convergence arise [124]. In those cases, the Eulerian approach becomes more adequate. Moreover, the Eulerian approach seems also to be the right framework for modeling particles' mutual interaction [125], although Lagrangian methods have also been applied [123] and [126].

Eulerian–Lagrangian models of the cyclone

The Eulerian–Lagrangian approach is generally more suitable for cyclone separator simulation over the Eulerian–Eulerian approach. In the Eulerian–Lagrangian approach, the gas is treated as a continuum while the solid phase is resolved by tracking individual solid particles (Lagrangian tracking) through the flow field. Lagrangian tracking essentially applied Newton's second law of motion to a particle to determine its position. For cyclone, only the drag and gravity forces are of significance due to the large gas-particle density ratio. Of these, drag force, due to the relative slip between the particle and gas, is the dominating force and is typically modeled using an empirical correlation like the Morsi Alexander model [127].

Depending on the volume fraction in the cyclone, either one-way or two-way coupling is applied to account for the interactions between the two phases. For dilute flows, the gas-phase flow is not influenced by the solid flow and Lagrangian tracking decoupled from the gas flow calculation is sufficient. One advantage is that the Lagrangian tracking can be performed as a post-processing step calculation using the converged and time-averaged single phase simulation. Furthermore, the time-averaged gas flow field smoothes out all the turbulent fluctuations. Only particles of large size will behave as exclusively influenced by the time-averaged gas flow, while very small particles will tend to fluctuate following turbulent fluctuations of the gas velocity (turbulent diffusion). There will be a complete range of intermediate behaviors between these two extremes. Turbulence fluctuations are random functions of space and time.

The Stochastic Lagrangian model has been used successfully by many researchers, including Yuu [128], Boysan [99], Hoekstra [101], Sommerfeld [103], Wang [129], DeSouza [119] and Mikulcic [120]. The one-way coupling approach assumes the negligible effect of particles on the gas flow. As a result of the collection process, high local solid concentration is observed in the near wall regions. These regions are not effectively modeled using a one-way coupling. Hence in most of the Lagrangian tracking results, the computational simulations show larger cut-sizes than those observed experimentally.

The effectiveness of the LES to accurately predict the gas-flow field in cyclone separators has been established [118]. Subsequently, the Lagrangian tracking

has been applied to calculate the particle flow in the LES simulations.

Depending on the particle size distribution, agglomeration may also become an important factor in predicting the cyclone efficiency. Particle sizes ranging from 1 to 10 μm tend to agglomerate due to the turbulent flow. For this range of particle size, the turbulence induced motion is more dominant compared to gravitational motions. Van der Waal forces are considered strong enough between the particles to result in particle agglomeration and bigger size particles. Sommerfeld [103] observes that the separation efficiency increased considerably for smaller particles in an agglomerating regime.

At higher solid concentrations, the interactions between the two phases become significant and a two-way coupling for the momentum between the particulate and fluid phases needs to be considered. Traditionally, the particle-source-in cell (PSIC) model is used for this purpose [130]. In this model, the flow field is calculated first without the particle-phase source terms until a converged solution is achieved. A large number of parcels (i.e., discrete particles representing large groups with the same properties) are then tracked through the flow field. The source terms are then obtained from these tracks for a second Eulerian calculation of the gas flow. The procedure is repeated iteratively until convergence is achieved. The accuracy of this method depends on the number of parcels. Typically, a minimum of 10000 to 20000 parcels are used. Derksen [131] studied the effect of mass loading on the gas flow and solid particle motion in a Stairmand high-efficiency cyclone separator using a two-way coupled Eulerian–Lagrangian simulation. They observed that compared to one-way coupling the two-way coupled simulation yield higher overall efficiencies.

The standard Lagrangian approach neglects the particle-particle interactions. However, at a higher solid concentration, these interactions must be included. The discrete element method (DEM) solves the force balance on individual particles and takes into consideration both the particle-particle and particle-gas interactions and has been used to simulate the motion of particles for highly dense flows [132]. This approach gives information about the position and velocities of individual particles.

Eulerian–Eulerian models of the cyclone

In Eulerian particle modeling, the particles are considered as a continuous fluid, just like the gas. This 'fluid' interpenetrates with the gas in the cyclone and interacts with it in accordance with the known laws of interaction, for instance, Stokes' law. Transport equations, which are coupled through the interaction terms, are solved for both fluid and particle phases.

Eulerian–Eulerian schemes have been used in many practical multiphase flow simulations, for instance, and typically, in fluidized-bed applications to which they are particularly suited. However, Eulerian models cannot treat different particle sizes directly while considering every size class as a distinct phase, which is evidently a serious drawback for practical problems.

Eulerian–Eulerian mostly used for cyclones, hydrocyclone and Dense Medium with high volume fractions of solids [133–137]. In [138] a mixed $k-\varepsilon$ /algebraic RSTM, a stationary gas flow model is used along with a simple Eulerian model of a diluted gas-solid flow. The most important is the reduction in swirl leading to a reduction of pressure drop. Further in [106], the Eulerian–Eulerian model is used for the dense regime. Results on collection efficiency, as compared with dedicated experiments, are not conclusive or even deviant. However, interestingly, the attenuation of both swirl and turbulence with mass loading is clearly noticed.

As it is obvious, CFD modeling of the cyclone continues progressively and has the potential for more theoretical and practical studies. Closer to the target of the present Ph.D. study, not many CFD studies have been developed. In the next section, outcomes of CFD studies of the cyclone reactors will be discussed to provide a narrow down direction to what is targeted for the present project.

2.5.3 CFD studies on cyclone reactors

CFD simulations of the fluid and particle flows in cyclone reactors have a potential to provide a good understanding of the flow and reaction patterns within the cyclones. In this case, the system to be used for the simulations is very complicated and needs to be simplified. This would further provide a better understanding and knowledge of design, scale up and optimization studies. The main aim of this section is to map the relative importance of fluid dynamics and chemical reactions in different high temperature gas-solid processes which are studied until now.

Experiments and numerical simulation of sawdust gasification air cyclone gasifier

In this work, experimental and numerical simulation of sawdust gasification in an air cyclone gasifier is investigated to produce a high-quality fuel gas with less tar by Sun [139]. Numerical simulations are made based on commercial CFD code Fluent, with the help of UDF (user defined function) to consider the gasification reaction rate. The main assumption for simulation that he considered is:

- The biomass can be represented as spherical particles and the particle diameter remained constant during the gasification, based on the volumetric model.
- The fuel was composed of C, H, and O. The gas-phase species included in the model were CO, CO_2, H_2O, O_2, H_2, CH_4 and C_2H_4
- Sawdust pyrolysis was simply described as a one-step global reaction:

  $Sawdust \rightarrow char + volatiles, volatiles \rightarrow a \times gas + b \times tar$

In this study, the combustion of volatiles and char was described by eight reactions with known kinetic rates of reaction.

A three-dimensional model of a cyclone gasifier is developed. The mesh with approximately 84,600 cells is designed for a cyclone with diameter 200 mm and 2280 mm height. To model the turbulence in the reacting flow model, the realizable $k - \varepsilon$ model is used. The stochastic tracking model is applied to analyze the gas-solid flow field. The model predicts the trajectory of a discrete-phase particle by integrating the force balance on the particle, which is written in a Lagrangian reference frame. Species transport model is used to model the reactions in the cyclone gasifier.

The chemistry-turbulence interaction model is Finite-Rate/Eddy-Dissipation which computed both the Arrhenius rate and the mixing rate and used the minimum of the two. The simple P-1 radiation model is used in this study. The radiation model is defined based on the expansion of the radiation intensity into an orthogonal series of spherical harmonics. The finite volume method is used to discretize the governing equations and the equations are solved by a SIMPLE algorithm. The CFD model of the process is validated with experimental data. This developed CFD model provides a good reference for the gasifier to predict operational parameters such as gas temperatures, gas concentration produced, and heat value produced [139].

Simulation study on production of fine ceramic powders in a cyclone reactor

Another cyclone reactor CFD modeling is done by Maurizio Masi [28] to produce fine ceramic powders in a cyclone reactor. In this case, it is reported that the quality of fine metal-oxide powders synthesized in the vapor-phase aerosol reactor is significantly affected by fluid dynamics. Under turbulent regimes, depending on nozzles and reactor configuration, backflows may arise with consequent re-circulation of as-synthesized particles in the flame region. Masi proposed an

innovative cyclone aerosol reactor configuration, which can reduce re-circulation of particles and, simultaneously, provide a segregation of the largest particles. As a result, a final product with a narrower particle size distribution can be obtained. To evaluate this innovative configuration, an existing industrial aerosol reactor was remodeled according to cyclone geometry and simulated.

Several studies are presented for SNCR in different types of reactors due to the importance of NOx emission control [140–149] mostly in experimental and pilot scale. There are also some industrial SNCR application studies which apply common reactors for SNCR [150–152].

The application of the cyclone reactor for SNCR is only mentioned in [153] for an industrial optimization purpose and also recently in [154]. Both studies include CFD modeling of SNCR but are mostly focused on SNCR efficiency following optimization purposes.

However, a comprehensive study of the cyclone flow and its effect on reaction parameters is not yet available. With considering flow dynamics and reaction together, further development studies are needed to support the potential of the cyclone reactors to provide better reaction conditions.

2.6 Conclusion and perspective of project

In this literature survey the principles of the cyclones and their applications are discussed. The idea of applying cyclone as a reactor is to apply cyclonic flow to achieve more efficient reaction inside the cyclone with providing better reagent mixing and higher residence time for the chemical spices to react. It is further developed by considering cyclone heat transfer properties based on the swirl flow which could be an advantage for high temperature reactions.

Therefore, when describing a cyclone as a reactor, it is very important to know principles about flow patterns that subsequently control some reaction parameters such as residence time, mixing conditions and temperature.

To provide a better understanding of such behavior and regarding the demands and more recent applications of the SNCR reaction in different industries, SNCR is selected for the present investigation. The reaction is classified as a high-temperature fast reaction and is hence a good choice to investigate chemical reaction parameters as well as temperature effects when cyclonic flow plays a unique role inside the cyclone reactor.

With regard to the complexity of flow in the cyclone when adding reaction

parameters, a proper modeling tool could be beneficial to simulate the system. To simplify this model and avoid unnecessary complexity, a reduced reaction mechanism is preferred. The relevant principle models, including CFD models and selected case studies, has been presented in this review and supported by a detailed and well-known reduced reaction mechanism that has been applied widely in different case studies.

This review provides background knowledge for a CFD-based SNCR inside a cyclone reactor. The suggested method based on the review is to use a CFD code with a reduced mechanism, which may even consist of a two-step reaction for NH_3-SNCR and results then will be computed and confirmed/optimized and finally validated by pilot scale experiments in a setup that is specifically designed and manufactured for this purpose.

Adding to the main purpose of characterization of the cyclone reactor considering the environmental legislation and the necessity of additional controls on NOx emission in the industries, the results of this study could be of interest in industries such as CFB boilers in power plants, cement and other chemical/mining industries for applying a simple, available cyclone reactor for NOx emission control. This leads to avoiding extra work/cost for adding a specific SNCR unit to the plant.

In all the industries mentioned, in real case, solid particles are present inside the cyclone. These particles may have an effect on chemical reaction or reaction-flow interaction which is important to investigate. To the author's knowledge, no particular study on particle-reaction-flow interaction has been published before, not only in cyclones but even in general combustion technological investigations.

Part of our design purpose is to provide a cyclone reactor with a potential to study on the effect of particles. Some experiments will be also provided to check the functionary of cyclone in presence of particles, however further detail study experiments with particles is not in the scope of this project.

Altogether, with the basic simulation and modeling of the SNCR in the cyclone reactor, will provide a good background to be applied in detailed kinetic simulations, research purposes, industries, and scale-up targets.

Chapter 3

Experimental apparatus

Introduction

To provide a suitable apparatus to study fluid dynamics and reactions inside a cyclone reactor at high temperature, a pilot scale set-up is needed. Therefore, an apparatus was designed and constructed to study SNCR as a fast reaction in a cyclone reactor. The basic design parameters are listed in Table(3.1). The flue gas is produced by a max $27kW$ swirl burner fired with natural gas and compressed air. Combustion takes place in a combuster and enters into the cyclone by a connector tube. This system, combustor, provides internal heating and proper temperature, also applying to produce initial NOx.

Based on the fact that the system is working in high temperatures and heating by natural gas combustion, the sandwich three layer plan is used for manufacturing the combustion chamber and cyclone reactor as well as connecting tube between chamber and cyclone. The three-sandwich plan is composed of two layers refractory material (high-density refractory cement/ high-temperature resistance and low-density refractory material/good isolation) and steel shell.

Three important parameters in SNCR are temperature, mixing and residence time of reactant, which could be studied. More specifically, the system is designed to provide the ability to inject ammonia in different positions as well as the possibility of taking samples from different zones.

The flue gas with a specified NOx concentration is added to the cyclone rector to study the reduction by ammonia. The reaction is homogeneous in the gas phase and particles will be used to understand the effect of the appearance of particles on the temperature profile, flow pattern and mixing, and consequently the effect on SNCR process.

Besides, to provide proper temperature conditions when the particle is loaded, it is important to heat up particles before reaching the cyclone reactor. For this purpose, the swirl burner has been selected for the system, which enables particle loading through the swirl burner.

The apparatus consists of fuel dosing (natural gas and air), swirl burner, combustor, particle loading system, cyclone reactor, control system, gas sampling system and data acquisition system, as shown in Figure(3.1) and will be explained in detail in this chapter.

Table 3.1: Considerations for design of the cyclone reactor at high temperature for SNCR process

Power	0.2-27 kW
Fuel/flow rate	Natural gas/0.25 -41Nl/min
Air flow rate	50-510 Nl/min
Combustor diameter	200 mm
Inlet velocity of the cyclone at high temperature	12-25 m/s
Max. Temperature	1400 °C
Pressure in combustor	-20 Pa
Particle loading	0.13-136.5 kg/h

3.1 Fuel dosing system

The fuel-dosing system includes natural gas and air feeding. The natural gas is supplied from the national grid with the listed composition in Table(3.2). The flow rate of the natural gas to the burner is controlled by a ball valve (V-14 in Figure(3.1)) and a pressure regulator (PREG-11 in Figure(3.1)). The maximum flow rate of the natural gas is normally $41Nl/min$, equivalent to a power of $27kW$. Ammonia can be added to the natural gas before the burner to simulate nitrogen-rich fuels.

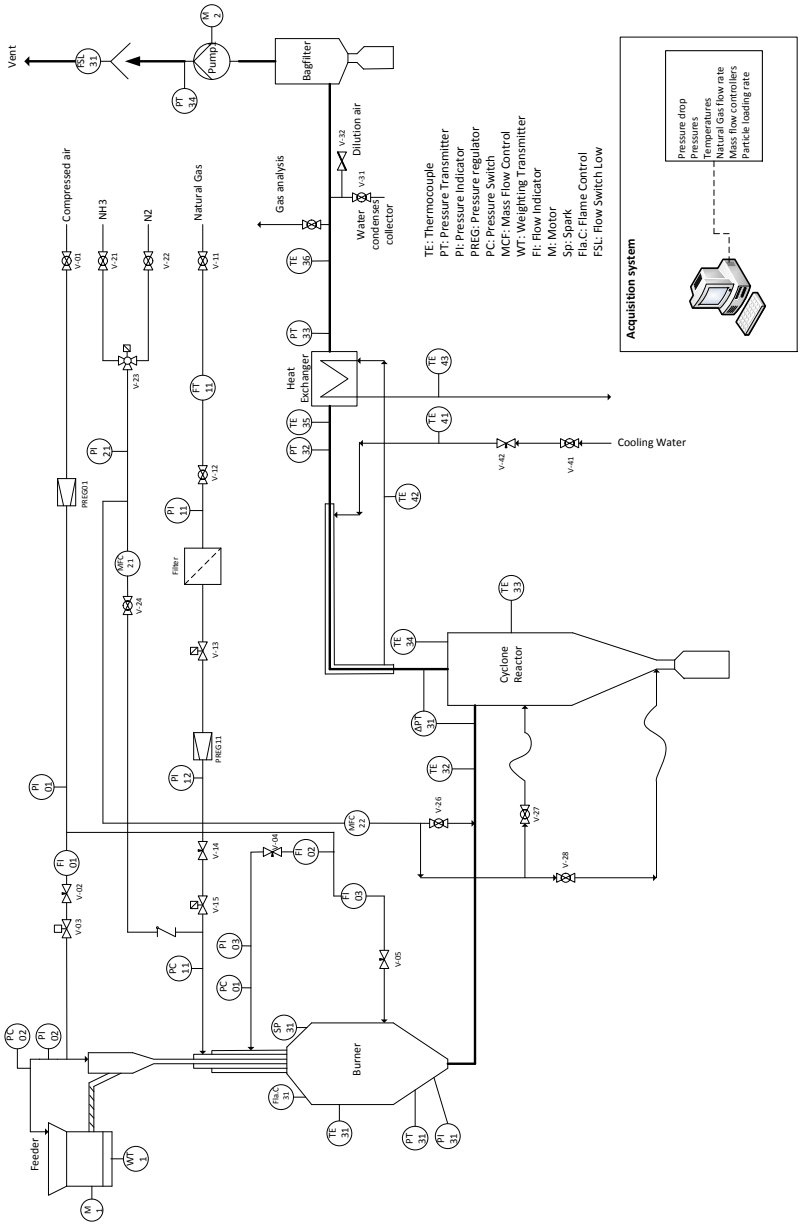

Figure 3.1: Schematic diagram of the experimental setup used for experiments

Table 3.2: The natural gas composition (July 2016) [155]

CH_4	mol. %	88.64
C_2H_6	mol. %	6.11
C_3H_8	mol. %	2.55
$i-C_4H_{10}$	mol. %	0.39
$n-C_4H_{10}$	mol. %	0.61
$i-C_5H_{12}$	mol. %	0.13
$n-C_5H_{12}$	mol. %	0.09
C_6^+	mol. %	0.04
N_2	mol. %	0.33
CO_2	mol. %	1.11
Lower caloric value	MJ/Nm^3	39.673
Density	kg/Nm^3	0.8298

The combustion air is supplied from the centralized compressed air system. The feed rate of the air is controlled by ball valves manually and a pressure regulator and monitored on rotameters. There are three air flows available with their rotameters and ball valves to control, tangential air flow to the outer annular (FI-02, V-04 in Figure(3.1)), feeder air to the solids feeding (FI-01, V-02 in Figure(3.1)) and secondary air (FI-03, V-05 in Figure(3.1)) that can be fed at any gas port on the combustor.

3.2 Swirl burner

The swirl burner is mounted on the top of the combustion chamber and is down-fired to avoid particle accumulation due to the limited length of injection during particle loading. Also, another aim of using swirl burner is heating the particles before inserting into the cyclone. During the combustion inside the combuster, the swirl flow inside the combustor can provide enough residence time for particles to reach the gas temperature. The burner is made up of concentric tubes, with a central tube for injection of the particles, an outer annulus for swirl air (tangential air flow) and the middle annulus for the natural gas. For transporting particles, another air stream (Feeder air) is fed into the inner tube. The ratio between air flows from tangential air and feeder air determines the swirl intensity (the swirl number).

The proper combustion in a swirl burner depends on an appropriate shape of the burner quarl. The burner and the quarl are assembled on a flange as shown in Figure(3.2). The quarl is made up of high-density refractory cement. At the edge of the quarl, there is a flame detector and an ignition spark.

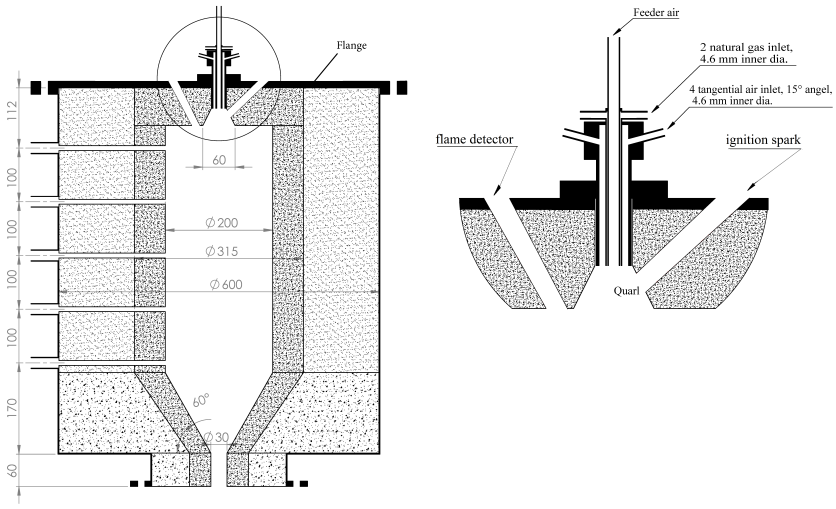

Figure 3.2: Detailed sketch of combustion chamber and swirl burner

3.3 Combustion chamber

The combustion chamber has an inner diameter of $200mm$ and a height of $700mm$ with a reduced diameter ($200mm$ to $30mm$ with $60°$ angel) at the bottom to obtain high velocity to avoid particle accumulation. A cross-section of the combustion chamber is shown in Figure(3.2). The combustion chamber is made up of three rings of different materials. The first ring with $57.5mm$ thickness is a high-density refractory cement withdrawing to high temperature. The second ring with $140.5mm$ thickness is low-density isolation for good insulation and the third ring is steel shell with $2mm$ thickness.

There are 6 ports (5 ports on body and one port at top), which can be used for temperature measuring, gas sampling, pressure measuring and gas injecting. In this work, one port is used to control the temperature of the combustion chamber for the safety of the system, one to control the pressure and one to add air as secondary air. The latter can be used to control the temperature in some cases. All of the ports can be used alternatively for all the purposes mentioned.

3.4 Cyclone reactor

The standard Starinmand cyclone shown in Figure(3.3) has been designed. Table(3.3) shows the design data for the full dimension of the cyclone. The cyclone reactor, same as the combustion chamber, has three rings (two refractory and one steel) insulated with a two-layer refractory lining. The cyclone is connected to the bottom of the combustion chamber also with a two-layer refractory tube to avoid the heat loss.

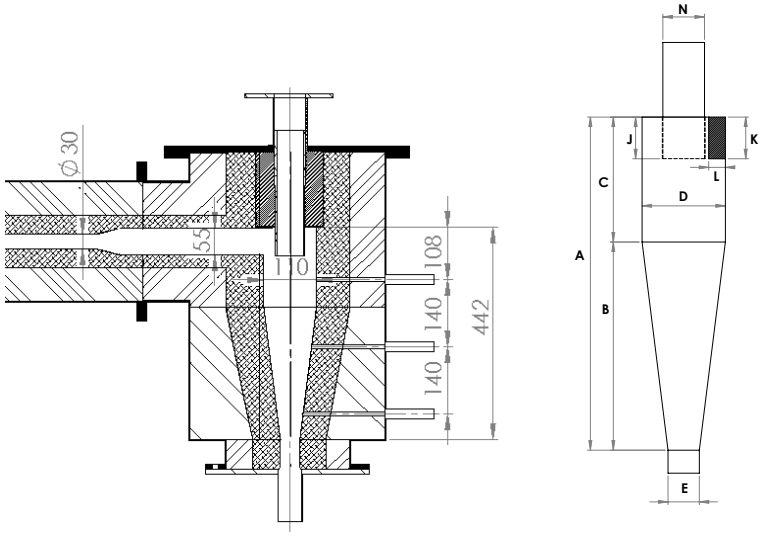

Figure 3.3: Detailed sketch of the cyclone reactor

Table 3.3: Full dimension of the cyclone reactor

	D	**A**	**B**	**C**	**E**	**J**	**K**	**L**	**N**
Dimension (mm)	110	440	275	165	41.25	55	55	22	55

Four ports are available to access the main body of the cyclone, namely Port0, Port1, Port2 and Port3 in Figure(3.4). Port0 is located on the top of the cyclone, oriented vertically, more detail on top-view in Figure(3.4). Port1 is located $108mm$ below the roof of the cyclone (inside), oriented horizontally. Port2 and Port3 are located $140mm$ and $280mm$ downward of Port1, respectively. In addition, three ports in the connector tube are considered. One of them is used to measure the temperature, one for pressure drop and one for ammonia injection, namely P_{in} in Figure(3.4).

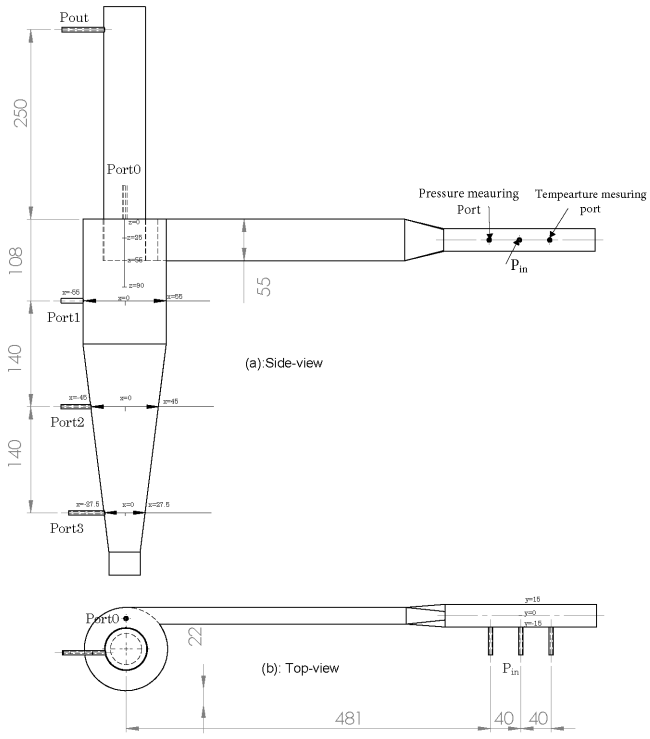

Figure 3.4: Position of the ports in the cyclone reactor

3.5 Particle loading system

A screw feeder is installed at the top of the burner to load the particles into the central tube of the burner. The reason is heating particles up to flue gas temperatures before entering the cyclone. A screw feeder is connected to a vertical tube with an inner diameter of $22mm$. The solids drop down into the entrance of the inner tube of the burner. The feeder air is introduced above the exit of the screw to avoid particle blocking and push the particles inside the swirl burner. An installed pressure switch (PC-02 in Figure(3.1)) on feeder air line is to shut down the particle loading if any blocking in particle loading system happens.

The feeder is put on a scale. The scale is connected to the setup PC for logging

the data of the particle feed rate. The capacity of the feeder is $0.13kg/h \sim 105kg/h$. The normal accuracy achieved with this feeder is between ± 1.5 and 2.5% of set point.

3.6 Ammonia injection system

The ammonia injection system is composed of an ammonia cylinder, nitrogen line from the utility, 3-way magnetic valve, two mass flow controllers and six ball valves Figure(3.5). Ammonia gas flows from cylinder to set-up with approx. $2bar$ pressure for production NOx by injecting to natural gas and reduction of NOx by injecting to cyclone reactor for SNCR.

This 3-way magnetic valve is designed to make sure of the system safety. It is switched to ammonia when activated from the labview-system and automatically switched back to N_2 in any risky situation, e.g., when the burner is not operating or temperature is below a certain defined level.

All the piping of ammonia to the setup is stainless steel. Close to the ammonia injection ports (for a reduction in cyclone reactor) stainless steel piping is connected to the adjustable ceramic tube by using a Teflon tube. This ceramic tube will be inserted into the cyclone with high temperature. Ammonia gas decomposes at high temperatures with metal tubes into nitrogen and hydrogen. Using the ceramic tube significantly decreases this fact. The ceramic tube can be horizontally adjusted to different distances from the cyclone wall to inject ammonia in different horizontal positions.

The ammonia flows are controlled by two mass flow controllers, one (MFC-21 in Figure(3.5)) for natural gas to obtain the specific NOx concentration in flue gas and the other one (MFC-22 in Figure(3.5)) to inject ammonia as a reduction agent in different positions in reactor with using provided valves (V-26,V-27 and V-28 in Figure(3.5)). The range of MFC's are 0–$1305Nl/min$. If the set-point of MFC is in the range of 0–$260Nl/min$, the accuracy will be $\pm 0.18\%$ of set-point whereas if the set-point is in the range of 260–$1305Nl/min$, the accuracy will be $\pm$ 0.9% of set-point.

3.7 Post-reactor system

This system consists of flue gas cooling, water removing and particle removing sub-systems. The flue gas after cyclone reactor is first cooled with two water jackets and then with a heat exchanger.

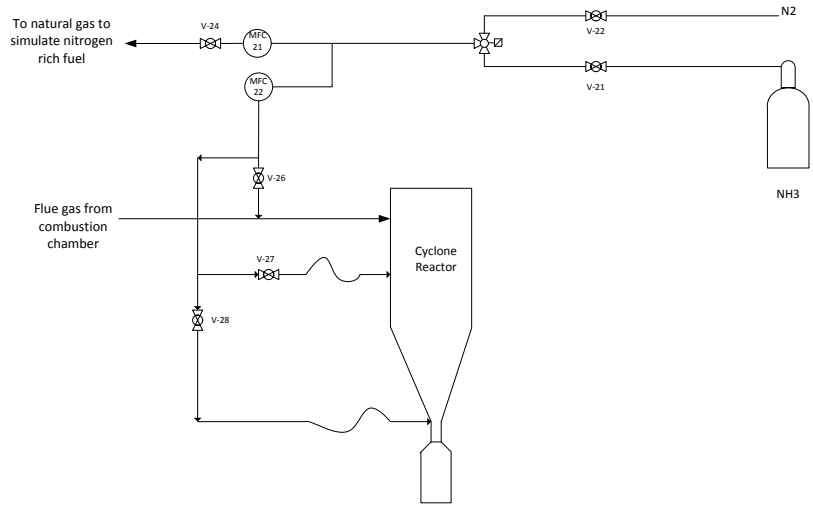

Figure 3.5: Ammonia injection system

The cooling water passes counter-current through the water jacket and follows up the cooling in an exhaust gas heat exchanger. The heat exchanger is shell and tube type. Heat exchanger is a single-pass flue gas/cooling water exchanger with 20 tubes of $34mm$ inner diameter in which exhaust gas passes through tubes and cooling water in shell counter-currently. The cooling water ends up in the DTU cooling water closed-loop system.

The water produced through combustion, which is condensed in the cooling system, is trapped before the bag filter and drained after all.

A ball valve (v-32 in Figure(3.1)) is also embedded before the bag filter to open a dilution air to flue gas if the temperature becomes higher than 90°C before the bag filter to avoid damage of the bag filter.

The flue gas passes a bag filter to remove fine particles before connecting to building the main ventilation.

3.8 Control system

The system is operated at a presser lower than atmospheric pressure to avoid the leakage the flue gas and ammonia gas to the surroundings. The exhaust fan is operated automatically and controlled by the pressure in the combustor

(PT-31 in Figure(3.1)).

To ensure the safe and smooth start-up and operation of the burner, a control system is designed.

The burner control system is composed of a control box, monitoring devices (flame detector, pressure trans-meters and thermocouple) and action device (magnetic valves, gas pressure switches, ignition spark). The startup sequence is controlled by a microcomputer inside the control box, which is described as follows.

By starting the control box (Pressing start the burner), air flow check is performed by a pressure switch on tangential air by PC-11 (Figure(3.1)). The magnetic valves (V-13 and V-15 in Figure(3.1)) on natural gas are automatically opened $30 seconds$ after combustion air is detected. During 30 seconds, the combustion air needs to flow into the combustor to remove any gases remaining from the previous experiments before starting the ignition. The ignition spark starts immediately when the magnetic valves (V-13, V-15) open for natural gas. If the ignition is not successful, the signal from flame detector orders the magnetic valve to close and the above procedure will be repeated by pressing *start-up burner* manually until the ignition is successful.

Another controller is also provided which controls the temperatures, pressures, ammonia injection, particle loading, water cooling flow and ventilation. This safety-controller is connected to the burner controller and installed to handle several safety situations in the whole system by closing the magnetic valves' communication by burner controller. As some practical examples, if the flame is extinguished accidentally / combustion air feeding stops / blocking in system happened / temperature is high in some points / cooling water flow is low or cut / ventilation cut-off happened, the natural gas feeding will stop. Also, the 3-way magnetic valve switch to nitrogen and particle loading stops if it is operating.

3.9 Gas sampling system

The gas sampling system includes filtering, quenching, water removal, and pumping to gas analyzer which pass through a scrubber to get rid of ammonia.

The gas samples are taken out with $1 Nl/min$ flow rate from designed sampling point or as an alternative with a sampling probe from any places of the cyclone using designed ports (see Figure(3.4) for detail studies). The designed sampling point itself is placed after heat exchanger shown in Figure(3.1). The taken

sample is passing a pretreatment station near the set-up including filtration to remove fine particles, quenching and water condensing. Then the dry gas sample is pumped into the scrubber to remove ammonia with oxalic acid before reaching the central gas analyzer. There will be a second treatment which is provided for the central gas analyzer to ensure the gas sample is dry and free of ammonia. The sampled flue gas flows to a series of three gas analyzers.

- Fischer-Rosemount NGA 2000 analyzer to measure CO, CO_2 and O_2 concentrations
- Fischer-Rosemount NGA 2000 to measure NO
- CLD 700 EL to measure the NO and NO_2 (NO_x is the sum of these two)

The concentration of the gases are transferred via the internal network and logged to a computer.

The continuous gas analyzers must be calibrated using N_2 for zero-point adjustment and calibration gases with a 2% accuracy for span gases.

3.10 Data acquisition

The data acquisition system is designed for further analysis of the results. All process parameters (temperatures, pressures, pressure drop, flue gas composition, natural gas flow rate, ammonia flow rates, particle loading rate), except air flow (which is monitored by rotameters), are acquired on-line by a PC using the Labview software via a convector. Converted from voltage or milliampere, the output of the data was expressed in proper engineering units such as $^{\circ}C$ for temperature, Pa for pressure or pressure drop, ppm or % for gas concentrations and kg/s for feed rate of particles, Nl/min for natural gas flow rate and Nml/min for ammonia flow rate.

3.11 Experiments procedure

The procedure for experiments is presented here for a case with flue gas properties as listed in Table(3.4) and reduction by the molar ratio (NH_3/NOx) 1.25.

The velocity of flue gas is an important operating parameter which needs to be constant as a defined value in all experiments. Assuming flue gas is an ideal gas, the velocity is a function of moles of the flue gas and temperature.

Table 3.4: Considering wet flue gas composition for simulation

Component	N_2	H_2O	O_2	CO_2	CO
mole fraction wet (%)	75.63	10.58	8.11	5.68	0
mole fraction dry (%)	84.52	0	8.9	6.8	0

The starting point is a first estimate based on a calculation (more details of calculations are in Appendix(A)) in ideal conditions. Then it needs some practical adjustment to achieve defined values as expected for experiments.

In this project the system was working with the first estimated values of natural gas flow $16.7 Nl/min$, air flow on $270 Nl/min$ (50% FI-01 and 50% FI-02 in Figure(3.1)).

In the next step, gas analyzers have to be turned on. Since the most flexible parameter is oxygen concentration, the air flow could be adjusted to reach a defined gas composition (CO_2 6.8%, O_2 8.9%, CO $1.5 ppm$, NOx $96 ppm$ (produced from NG combustion)) once the system becomes steady state with regard to temperature. Then oxygen concentration (over 8.5%) and the operating temperature ($1010°C$) were applied in most experiments which provide the defined inlet gas velocity($21 m/s$)) and 96 m^3/hr flue gas.

To follow the SNCR reduction, the initial NOx value is also important. This initial NOx is provided partly from the natural gas combustion (almost $90 ppm$) and the rest from adding ammonia to the natural gas. This is also practically started from a first estimate based on a calculation of conversion of the ammonia to NOx in ideal and stoichiometric conditions. Then the total produced NOx in the system is measured which is different from the calculation. This experiment has been done for low ($200 ppm$), moderate ($500 ppm$) and high ($700 ppm$) concentrations of NOx and an average conversion (conversion of NH_3 to NOx) based on the operating condition is obtained 54% which applied in the rest of the experiments. Therefore, to get $500 ppm$ NOx in the mentioned flue gas $254 Nml/min$ ammonia was injected to natural gas.

Based on calculation, the ammonia needed for reduction of $500 ppm$ initial NOx with a molar ratio 1.25 is 245 Nml/min which this amount of ammonia was injected into the cyclone to reduce NOx.

Temperature profiles were obtained by inserting the thermocouple in different ports, vertical temperature profile by inserting the thermocouple at Port0 and horizontal temperature profile by inserting at Port1, Port2 and Port3.

To study the detailed reaction zone, NOx concentration was measured by tacking sample at Port0, Port1, Port2, and Port3 by inserting a ceramic tube in the

specified point of the cyclone.

For experiments with particles, the particles were added from the middle of the swirl burner with mass loading $2.2kg/hr$, density $2550kg/m^3$ and particle distribution 3–$150\mu m$ to combustor to heat up particles before entering the cyclone.

Chapter 4

Experiments, SNCR in cyclone reactor

4.1 Introduction

In recent years, NOx emission control has become stricter worldwide. Selective Non-Catalytic Reduction (SNCR) with reduction capabilities from 25% to 75% over a range of industrial applications is an effective and economical method for the reduction of NOx emission based on injecting nitrogen agents such as ammonia (NH_3) and urea ($CO(NH_2)_2$) in flue gas containing NOx at high temperatures. In practice, NOx reduction efficiency is primarily dependent on three factors: temperature, mixing, and residence time.

The SNCR process is very sensitive to temperature and only happens in a narrow temperature window. At high temperatures, the selectivity of chemical reactions desires oxidation of reductive N-containing species to form NOx, and at optimum temperatures of temperature window, selectivity desires the reduction of NOx. At low temperatures the reaction rate is slow, so NOx reduction will be slower and leads to more reductant slip.

Rapid mixing of injected reductant into the flue gas is also necessary in high temperatures. If mixing is too slow, selectivity desires the oxidation of reductants to NO because of the locally very high NH_3 concentration [89]. Therefore,

it is highly important to gain knowledge about mixing behavior and temperature profile inside the cyclone to provide effective inputs for practical studies/applications.

Most of the studies on SNCR have been conducted in furnaces/kilns/boilers, and there is a large body of literature on different operating parameters and chemical reaction/reduced kinetics to provide preferred reaction conditions. In this study, the focus is on cyclones instead of the furnaces/kilns/boilers as a preferred reactor for SNCR, on which there have not been many studies performed.

Studies have shown that cyclones seem to ensure excellent heat transfer efficiencies between carrier gas, solid particles and walls [21]. Moreover, the residence time in cyclones is within the range of a few seconds. Consequently, it can be anticipated that cyclones would be well suited for carrying out fast reactions. In this case, SNCR is also categorized as a fast reaction. In addition, turbulent flow inside a cyclone provides better mixing conditions. All the benefits mentioned could contribute to getting a higher reduction efficiency for SNCR.

There is need to provide more knowledge in different aspects of SNCR reaction, e.g., mixing, residence time, and particle effect to achieve a better understanding of the reactions inside the cyclone.

In this section, the first SNCR inside the cyclone is studied without particles. Also, the experiment set is designed to explain the effect of temperature, NOx distribution, ammonia injection position, reaction zone, initial NOx, molar ratio and ammonia injection velocity in detail. The effect of temperature and molar ratio is also studied with a consideration of particle loading.

These studies are planned to provide experiment-based knowledge about the system and how it works in real cases, to better explain and improve the mixing and residence time inside the cyclone.

4.2 Experimental approach and methodology

The objective for this section is to find the most effective reaction zone in the cyclone, to investigate mixing behavior and to study the effect of ammonia injection from different positions to compare the reaction condition in different temperatures (higher and lower temperatures of the temperature window). Eventually, we will be able to find out where to inject ammonia into the cyclone to get the best reduction rate for NOx.

All experiments are designed to provide a detailed study of temperature profile

and concentration distributions inside the cyclone to monitor the reactions with different operation conditions, such as initial NOx concentration or Ammonia molar ratio.

The experiments are primarily divided into two main groups. First, a detailed study is performed on the cyclone reactor without particle loading. Then, one set of targeted experiments are done with particle loading based on the results from a former set of experiments (without particles).

To provide flexibility for injection, measurement and sampling in different positions of the cyclone, four adjustable ports (Port0, Port1, Port2, and Port3 in Figure(3.4)) are placed on the body of the cyclone. Additionally, P_{in} in the inlet channel is fixed for both measurement and injection. In addition to the adjustable ports and P_{in}, two more ports are used, namely Main port and P_{out} in Figure(3.4). Main port is used only for gas sampling at the end of the stream and P_{out} is mostly used to measure pressure/temperature at the cyclone outlet. P_{out} can also provide gas sampling at the cyclone outlet if needed.

A series of operating parameters, which are kept constant in all experiments, are listed in Table(4.1), and the rest of the parameters will be presented separately in each experiment.

It is worth mentioning that in the second set of experiments, where particle loading is performed, to compensate for the heat used to warm up the particles, the natural gas flow is increased to some extent, while keeping oxygen concentration in dry flue gas still above 8%. More details will come in Section(4.4).

Table 4.1: Constant parameters for all experiments

Natural gas	16.71[1] Nl/min
Air flow rate	266 Nl/min
Oxygen concentration in dry flue gas	>8 %
CO concentration	1-5 ppm
Temperature in inlet of cyclone (TE-32)	1010 °C
Velocity in inlet of cyclone	18.8 m/s

1 For experiments with particle loading, this would be increased to 17.21

The experimental set is explained in detail (Considering objectives, measurements, sampling and injection ports) in Table(4.2), including investigation of temperature profile (Case1-Case4), NOx distribution (Case5), ammonia injection position (Case6-Case9), reaction zone (Case10-Case12), initial NOx (Case13), molar ratio (Case14) and ammonia injection velocity (Case15) without parti-

cle loading and investigation of temperature profile (Case16-Case17) and molar ratio (Case18) with particle loading.

The results of these experiments are explained in detail following this section.

4.3 Experiments and results without particles

4.3.1 Temperature Profile and NOx distribution

Temperature plays a key role in NOx reduction in the SNCR process. Therefore, it is important to monitor the effect of flow (velocity) on the temperature profile and also NOx distribution inside the cyclone before adding the reduction agent.

Details of the conditions for experiments in this section are shown in Table(4.1) and Table(4.2). All the experiments have been performed with three replicates.

In general, the temperature profile is obtained by inserting the thermocouple in different ports. The thermocouple typeS-class2 (Pt10%RH-Pt) is used to measure the temperature with an accuracy of 1.5°C for the range (0-1100°C), excluding the measuring error caused by radiation. The radiation effect is ignored in the experiments of this project.

The vertical temperature profile of the cyclone is obtained by inserting the thermocouple at Port0. Radial temperature profile is also studied at Port1, Port2 and Port3. With these experiments, the radial temperature profile is observed at the top, middle and bottom of the cyclone.

In the next step, NOx concentration is measured at Port0, Port1, Port2, and Port3. This helps to know if concentration distribution for NOx is homogeneous inside the cyclone due to the flow. For this part of experiments, 500 *ppm* NOx has been produced by adding ammonia in natural gas since the amount of NOx within the natural gas is not enough for our experiments (It is normally below 100ppm). Following this experiment, a case is investigated without adding ammonia (which would later be added for the purpose of NOx reduction) to monitor the NOx distribution inside the cyclone.

4.3.1.1 Vertical Temperature Profile

The vertical temperature profile is shown in Figure(4.1).

As can be seen, the temperature is not uniform inside the cyclone reactor which

Table 4.2: General overview of experiments

	Cases	Objective	Measurement[a]	Ammonia Injection Port	Sampling Port	Notes
Without particles	Case1	Vertical Temperature Profile	Temperature	-	Port0	
	Case2	Radial Temperature Profile	Temperature	-	Port1, Port2, Port3	
	Case3					
	Case4					
	Case5	NOx distribution	NOx Concentration	-	Main, Port0, Port1, Port2, Port3	
	Case6	Investigation of ammonia injection position	NOx Concentration	Pin in 2 point	Main port	
	Case7			Port1-Vertically in different points	Main port	
	Case8			Port2-Verticaly in different points	Main port	
	Case9			Port3-Verticaly in different points	Main port	
	Case10	Investigation of reaction zone	NOx Concentration	Port1, Port2, Port3	Main, Port0, Port2, Port3	
	Case11			Port3	Port1 and Port2-Radialy	
	Case12			Port1, Port2, Port3	Port0-Verticaly	
	Case13	Investigation of initial NOx	NOx Concentration	Port1	Main port	NO_{x_i}= 200, 350, 500, 700ppm
	Case14	Investigation of molar ratio	NOx Concentration	Port1	Main port	Molar ratio=0.5, 0.75, 1, 1.25, 1.5, 1.75, 2
	Case15	Investigation of ammonia injection velocity	NOx Concentration	Pin, Port0 and Port1	Main port	
With particles	Case16	Vertical Temperature Profile	Temperature	-	Port0	
	Case17	Radial Temperature Profile	Temperature	-	Port1, Port2, Port3	
	Case18	Investigation of molar ratio	NOx Concentration	Port1	Main port	Molar ratio=1, 1.25, 1.5, 1.75, 2

[a]This means specific measurement for a case while all measurements are done and recorded

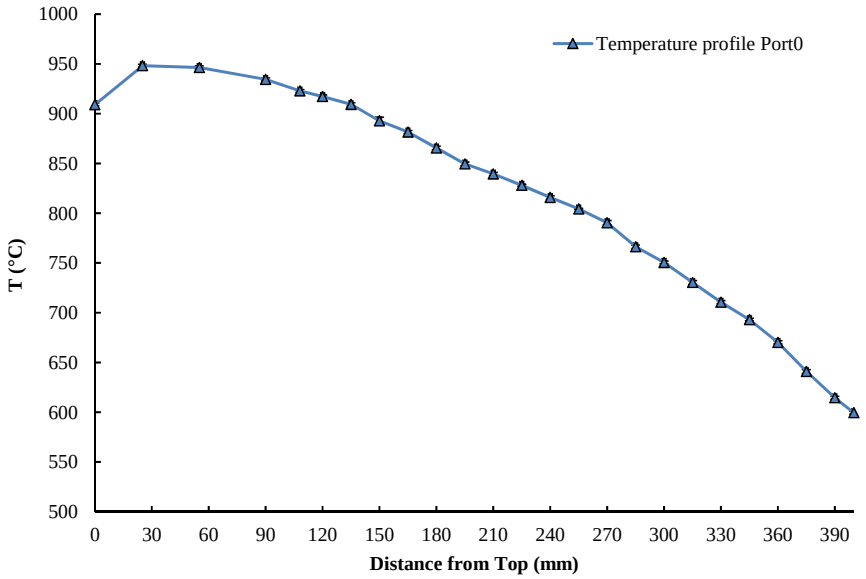

Figure 4.1: Vertical temperature profile based on dimension on Figure(3.4)

means that the reactor is non-isothermal. A set of support experiments with changing the operational conditions (such as air flow and natural gas flow to increase the inlet velocity), shows no effective improvements to provide uniform temperature and consider the reactor as isothermal.

A non-isothermal condition in the cyclone shows that the gas flow (with high temperature) does not reach the bottom of the cyclone and makes the bottom of the cyclone cold compared to the top. Knowing that the convection has the main role in heat transfer, increasing temperature will change flue gas properties (increasing viscosity and decreasing density). This could be improved by higher injection velocity or a smaller cyclone inlet area, which is practically impossible considering erosion problems.

Another possible solution to get a uniform temperature could be changing the height of the vortex finder inside the cyclone. Sun et al. [156] and Gao et al. [139] used the cyclone as a gasifier with a long vortex finder.

In addition to all the above, in practice cyclone always works with particles according to its main application, and it is expected that the system turns to be more uniform in temperature when operating with particles.

The measured temperature in the inlet channel of the cyclone (P_{in} in Figure(3.4)) is 1010°C whereas the maximum temperature inside the cyclone is 950°C at the top of the cyclone as a case study.

Considering the temperature window for reduction, it is possible to have both reduction of NOx and oxidation of ammonia during ammonia injection at P_{in} and Port0. By injecting ammonia at Port1 and Port2, the possibility of reduction is higher than oxidation, whereas close to Port3, the temperature is lower than the temperature window and thus a reduction cannot take place, considering only the temperature effect.

In general, the results of temperature profile studies show that NOx reduction can take place in the inlet channel and from the top of the cyclone down to 340mm depth from the top.

4.3.1.2 Radial Temperature Profile

Port1: The radial temperature profile for Port1 is shown in Figure(4.2). The temperature range in this port is 880–910°C. The temperature measured close to the port is low because of heat loss rate from the wall of the cyclone, and it is lowest close to the center as expected (fluid from bottom flows in the inner vortex).

By considering the temperature window for reduction, Port1 could be the best choice for reductant injection. The radial profile is not symmetric as can be seen in Figure(4.2) which shows that the inner vortex is slightly asymmetric. The proof of this theory is provided by studying the flow patterns using CFD modeling later.

Port2: The experiments are repeated in the same conditions for Port2 and Port3 to find the radial temperature profiles. The results for Port2 are shown in Figure(4.3).

The temperature profile in Port2 shows approximately constant temperature for different radial positions while in Port1 there are significant differences in different positions. The average temperature for this port is 780°C which is in the minimum range of the temperature window for reduction. It means, by injecting ammonia from this port, the reduction efficiency is expected to be low.

Port3: The same results as Port2 (approximately constant temperature) are obtained for Port3 as shown in Figure(4.4). The temperature in this port is

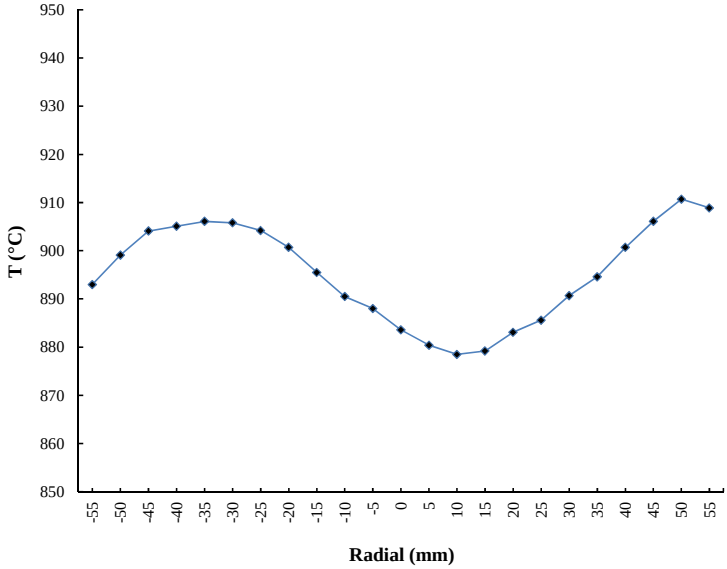

Figure 4.2: Radial temperature profile for Port1

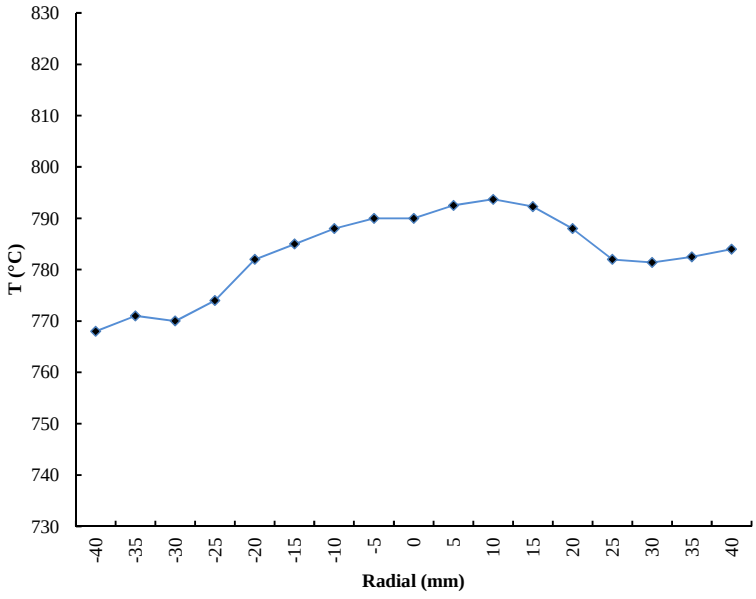

Figure 4.3: Radial temperature profile for Port2

lower than the temperature window range. This means, with an injection of ammonia at this port, the reduction of NOx could not take place in this area.

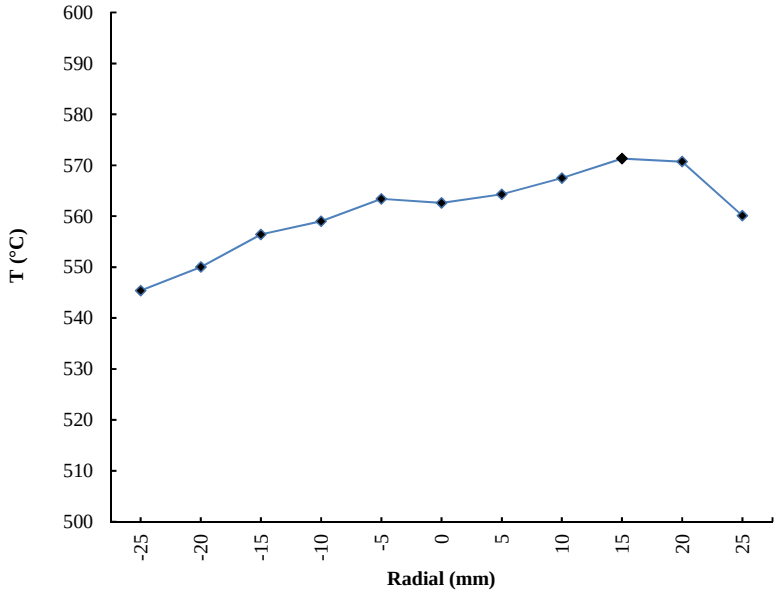

Figure 4.4: Radial temperature profile for Port3

The difference in temperature profiles in Port1, compared to Port2 and Port3, raises the idea of the presence of an unexpected, non-cyclonic flow in this area of the cyclone. This idea will be considered and elaborated on in the flow pattern studies in the following chapter on CFD modeling.

4.3.1.3 Initial NOx distribution

In this part of the experiments, 500*ppm* NOx has been produced by adding ammonia to natural gas. Besides, no ammonia is added into the cyclone for reduction. The main objective of this experiment is to investigate the NOx distribution and to observe NOx flow inside the cyclone following Table(4.2). Sampling was done by inserting a probe in different ports of the cyclone and in different insertion depths within each port. To avoid decomposition of ammonia at a high temperature with metal tube, a ceramic tube has been used. The results of this experiment are illustrated in Figure(4.5).

As it can be seen, there is a negligible difference among Main port, Port0, Port1, Port2 and Port3 which confirms that the distribution of initial NOx

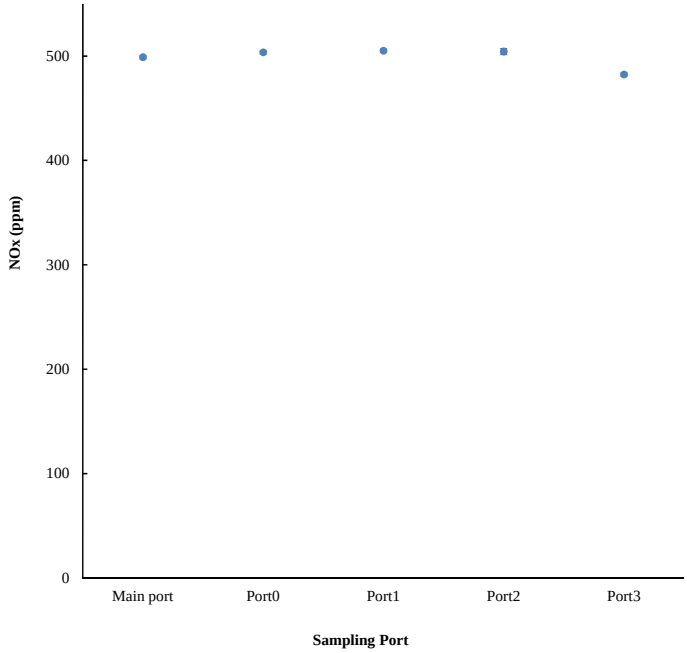

Figure 4.5: NOx concentration by sampling from different ports without reduction

inside the cyclone is uniform. This experiment shows that the initial NOx can be distributed uniformly in the cyclone and thus any differences in the presence of ammonia are evidence of reaction.

4.3.2 Investigation of ammonia injection position

The main objective of this part of the study is to find the best position for ammonia injection and its effect on reduction efficiency considering temperature profile, mixing and residence time.

The temperature window is the range of temperatures in which considerable reduction of NOx takes place. This interval is relatively narrow (750°C- 1100°C). Below 750°C the reaction is too slow to give any reduction and most of the injected NH_3 remains unreacted. At higher temperatures (higher than 1200°C) NH_3 tends to oxidize to form NO. The optimum temperature is approx. 900°C for the SNCR process with ammonia. The reduction efficiency is increased with

increasing the temperature until optimum temperature. By going higher than optimum temperature, reduction decreases partly due to ammonia oxidization. It is then of high importance to inject ammonia to the most effective zone of the cyclone with regard to possible temperature differences.

The mixing and residence time effect is also bound to the Temperature effect. The reaction shows different behaviors from higher to lower temperatures.

At high temperatures of the temperature window, the reaction is limited mostly by mixing while at low temperatures the reaction rate is slow and residence time limits the NOx reduction. Therefore, residence time becomes one of the most important parameters in SNCR in low temperature because of slow reduction, and mixing is more important at high temperatures.

In this section, with a survey on the ammonia injection zone, it is demonstrated that in different cyclone zones the reaction behavior is different.

4.3.2.1 Injecting ammonia from different ports

In this set of experiments, by injecting ammonia in different ports, the reduction of NOx in different zones of the cyclone is studied. (see Table(4.1) and Table(4.2))

P_{in}: Temperature range from the injection port until the cyclone inlet is 960–1010°C which is characterized by high temperatures in the temperature window. The results of adding ammonia at P_{in} in two vertical positions show reasonable reduction efficiency as expected in this high temperature. The NOx level decreases from 505*ppm* to 197*ppm* (61%).

P_{in} provides the longest route for the flue gas passing through the cyclone, which means a higher residence time compared to the other ports. On the other hand, high reduction efficiency in high temperature confirms that the mixing effect as the limiting parameter is good enough, leading to a reduction in such temperature.

As a result, injecting ammonia in this injection port has satisfied all three important criteria for reduction: temperature condition, mixing and residence time.

Port0: Adding ammonia at Port0 in two vertical positions to reduce NOx, as illustrated in Figure(4.6), results show around less than 50*ppm* decrease in NOx concentration. Low reduction efficiency despite having a high temperature in

this area is proof of slow mixing. This slow mixing in high temperature also provides the possibility for ammonia oxidation. Thus, having approximately the same rate for NOx reduction and NH_3 oxidation results in low reduction efficiency. It is also probable in this case that NH_3 leaves the cyclone without participating in the reaction. This could be further discussed if we would be able to measure NH_3 concentration in the outlet of the cyclone.

To follow up the mixing effect in this port, another support experiment will be discussed in Section(4.3.5) with a higher ammonia injection velocity that provides better mixing at the injection position. The results will be discussed briefly in Section 4.3.5.

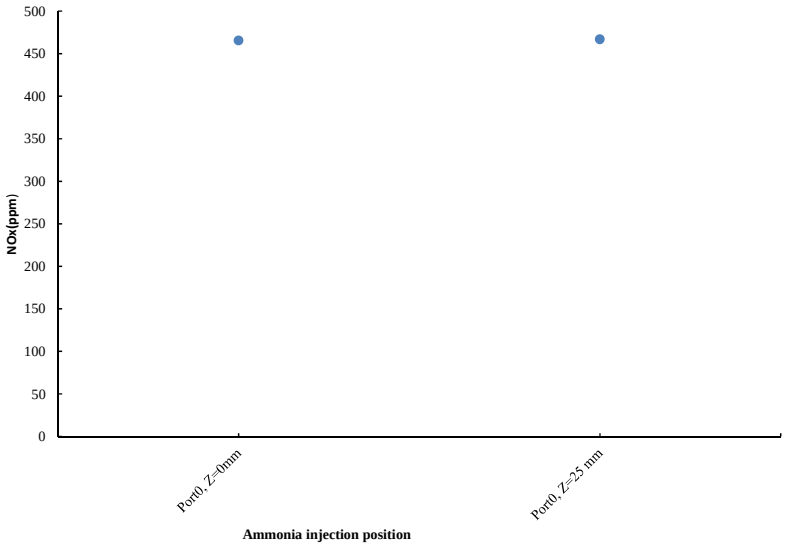

Figure 4.6: NOx concentration in outlet by adding ammonia from Port0 in two vertical positions: ($NOx_{initial}$=500ppm, O_2=8.85%, Molar ratio=1.25)

Port1: After adding ammonia at different radial locations (different probe insertion depths) in Port1, NOx level is obtained and illustrated in Figure(4.7) (exactly the same locations used for temperature measurements).

The temperature range in this area is 880–910°C which is characterized by the optimum temperature range for SNCR because the ammonia oxidation probability is low. The reduction efficiency is high, which confirms the good mixing in this area. Higher reduction efficiency takes place at 5–15mm distance from

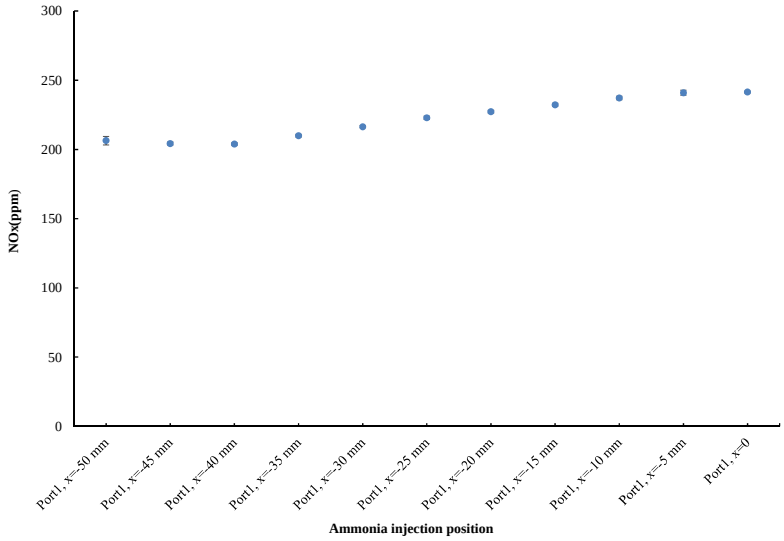

Figure 4.7: NOx concentration in outlet by adding ammonia from Port1 in different radial positions:($NOx_{initial}$=500ppm, O_2=8.85%, Molar Ratio=1.25)

the wall (between x=-50mm and x=-40mm) because in this distance ammonia meets downward swirl flow which provides a higher residence time. Temperature conditions, fast mixing and enough residence time lead to a satisfactory reduction level by being injected in this area.

By injecting ammonia to the x=-30mm and further to the center (x=0), the reduction efficiency is decreased exactly following the temperature profile in Figure(4.2). The residence time is also decreased by adding ammonia in this area. However, the average reduction efficiency of adding ammonia in Port1 is still high (57%), confirming the effect of mixing in this area. The results show that when temperature is high enough for SNCR, by adding ammonia in all radial positions regarding cyclonic flow, the mixing is good enough to provide a high reduction efficiency.

Port 2: The experiments are repeated in the same condition for Port 2. The results for Port2 are shown in Figure(4.8).

Considering temperature condition (minimum range of temperature window for reduction), lower reduction efficiency is obtained by injecting ammonia at this port. However, the results show 52% reduction efficiency, which is higher than

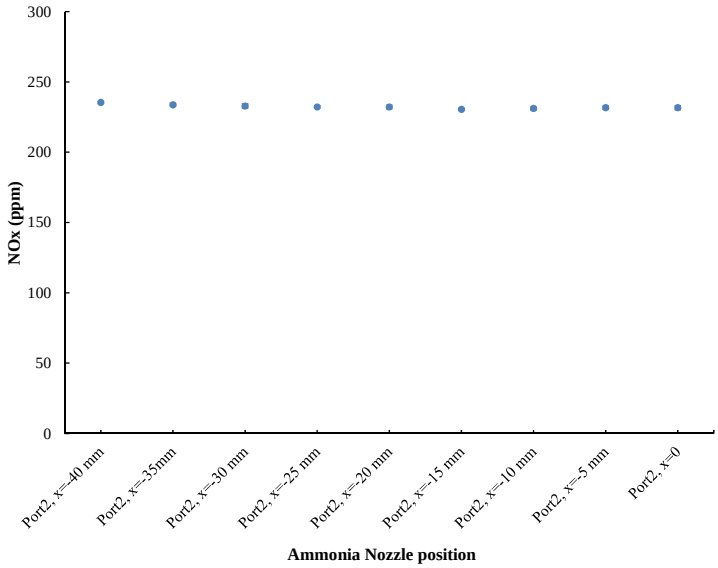

Figure 4.8: NOx concentration in outlet by adding ammonia from Port2 in different radial positions: ($NOx_{initial}$=500ppm, O_2=8.85%, Molar Ratio=1.25)

expected.

It was also expected to have a lower reduction efficiency by injecting ammonia in positions close to the center because the residence time of reactant is larger when ammonia is injected into the main vortex spiral downward compared to when it is injected into the inner vortex spiral upward. However, results show a constant reduction. This needs more study to explain the phenomenon that happens in this zone, which is further discussed in Section(4.3.2.2).

Port3: The experiment is repeated for Port3, similar to the former experiments for Port1 and Port2. The results are shown in Figure(4.9).

The temperature profiles in Port3, Figure(4.4), show that the temperature in this port is lower than the temperature window. However, by adding ammonia in different radial positions at Port 3, reduction efficiency is more than expected (51%) (See Figure(4.9)).

This result shows that the ammonia injected from this port still has enough residence time to meet the high-temperature areas inside the cyclone. As it is

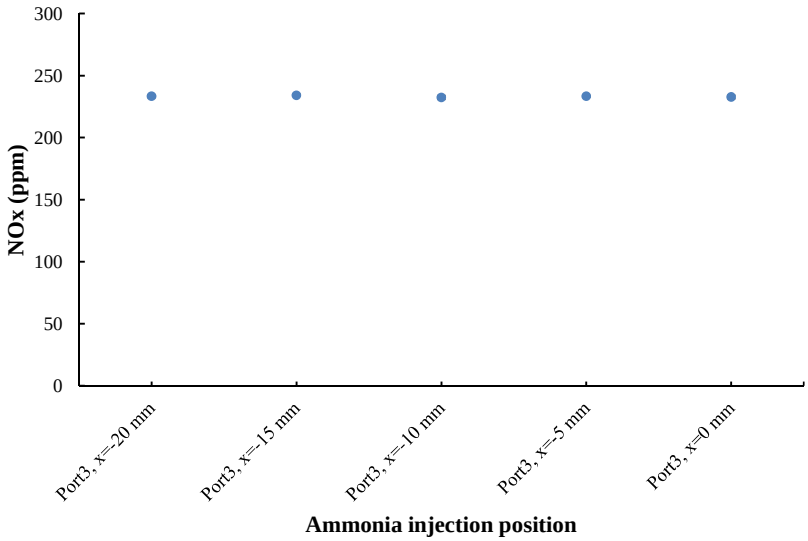

Figure 4.9: NOx concentration in outlet by adding ammonia from Port3 in different radial positions: ($NOx_{initial}$=500ppm, O_2=8.85%, Molar Ratio=1.25)

explained before, in low temperatures the residence time limits the reduction. Having the high reduction efficiency at this port confirms the effect of the high residence time of ammonia, which together with upward flow leads ammonia to reach the high-temperature area of the cyclone.

To explain the reaction inside the cyclone, some experiments are developed to support the former results which will be discussed later in the next Section(4.3.2.2).

4.3.2.2 Investigation of reaction zone

As the results show in the previous section, by injecting ammonia in places with low temperature, remarkable reduction efficiency was obtained which needs more study to explain the details inside the cyclone.

It is also important to be sure about the sealing of the cyclone, especially at Port2 and Port3 area. So some experiments are done by having an initial 500ppm NOx and no reduction. By measuring the NOx and other gases concentration, it is proved that no leakage exists in the system.

Also, as setup provides us with the possibility of taking a sample from different ports, some experiments are done by injecting ammonia at a port and taking samples from the rest of the ports, both vertically and radially, which will help to find the reduction zones.

Injecting ammonia at a port and sampling from the rest of the ports

In these sets of experiments, ammonia is added from one of the ports (Port1, Port2 and Port3) and sampling is done from other ports, including Port0 and Main port (in the former section, samples were taken only from Main port). Results are illustrated in Figures(4.10, 4.11 and 4.12) when ammonia is injected from Port1, Port2 and Port3, respectively. Afterwards, NOx reduction is studied in different zones of the cyclone.

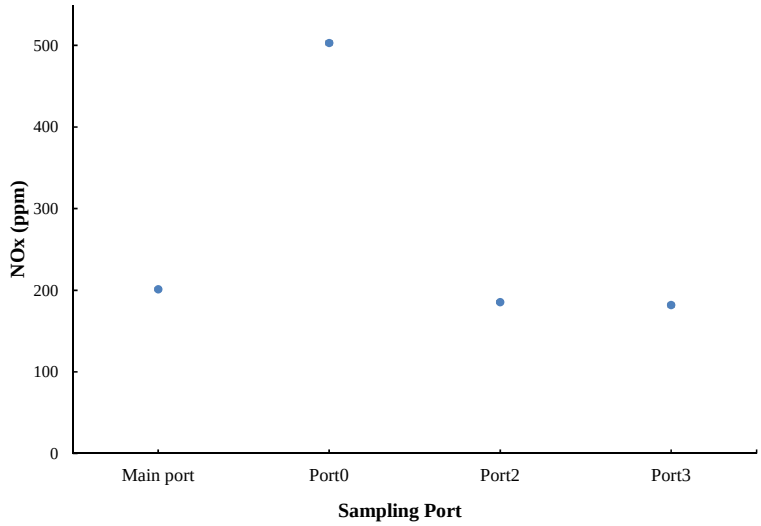

Figure 4.10: NOx concentration by sampling from different ports, ammonia injected from Port1: ($NOx_{initial}$=500ppm, O_2=8.8%, Molar Ratio=1.25)

The results of NOx concentration measurement from Main port follows the results obtained from the former section showing the same reduction efficiency (confirms reproducibility).

Results as depicted in Figures(4.10, 4.11 and 4.12), which show that with adding ammonia from any of the ports (Port1, Port2 and Port3), NOx concentration in the zone close to Port0 is almost the same as initial NOx, confirming that

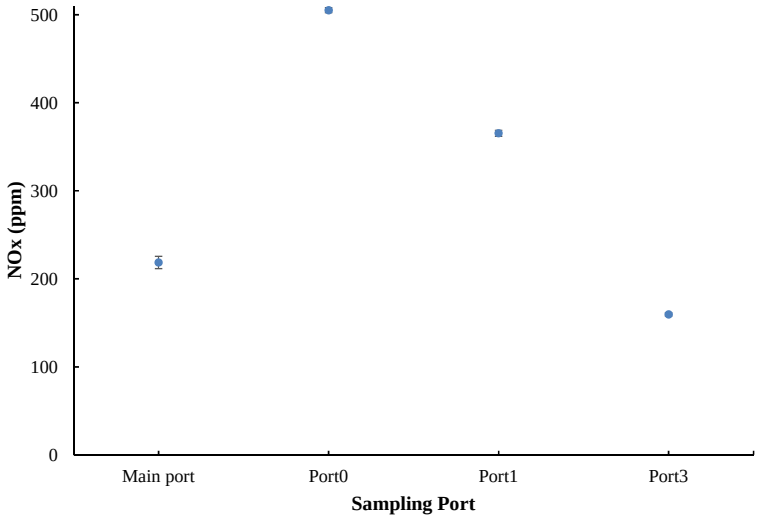

Figure 4.11: NOx concentration by sampling from different ports, ammonia injected from Port2: ($NOx_{initial}$=500ppm, O_2=8.8%, Molar Ratio=1.25)

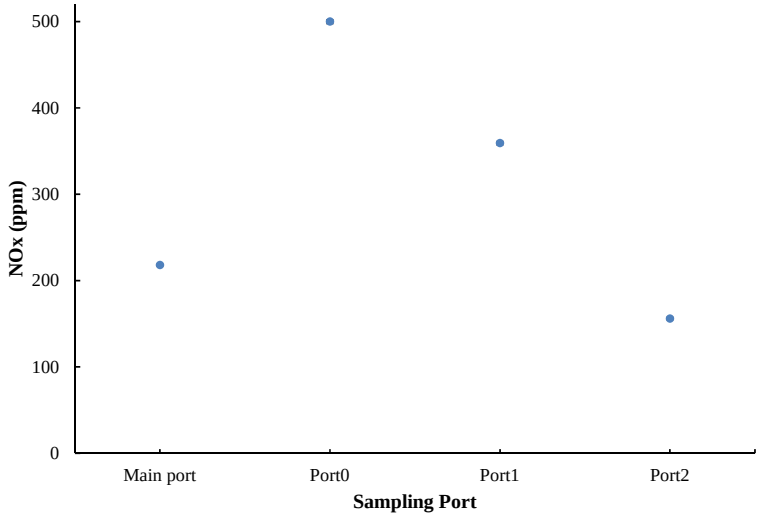

Figure 4.12: NOx concentration by sampling from different ports, ammonia injected from Port3: ($NOx_{initial}$=500ppm, O_2=8.8%, Molar Ratio=1.25)

ammonia will not reach the top of the cyclone. In this area, the sample is more affected by inlet flow.

Also, these results show that the NOx concentration in the zone close to Port2 and Port3 is low even though the temperature is low for a reduction in this area of the cyclone. Temperature condition in this area limits NOx reduction. Therefore, the low amount of NOx is the result of NOx reduction in the area with proper temperature when flue gas passes through the cyclone. This fact, on the other hand, supports the effect of cyclonic flow to provide proper mixing for fast reactions.

To sum up, by adding ammonia in one of ports (Port1, Port2 and Port3), reduction mainly takes place in the area of the cyclone which has the right temperature. Considering former results, the proper temperature is mostly in the area between Port1 and Port2. This latter conclusion needs more experimental support which will be presented in the following experiments.

Injecting ammonia at Port3 and sampling from Port2 and Port1

Two more experiments have been performed to identify the reduction zone by observing radial NOx concentration distribution in the zone close to Port1 and Port2 when ammonia is added to Port3. Results are illustrated in Figure(4.13) and Figure(4.14).

Radial concentration profile in Port1, Figure(4.13), shows low NOx concentration when getting close to the center and increasing near to the wall, as expected from the flow pattern.

However, NOx radial profile in Port2, Figure(4.14), is clearly different. A minimum NOx concentration happened before the center, while in the center, it is maximum and then again decreases.

This difference shows that the flow pattern in the area of Port2 is different from the cyclonic flow. This phenomenon has been recognized in the temperature profile study in the former section. In general, details about flow pattern are needed to make a clear explanation for this phenomenon. This is targeted in CFD modeling chapter.

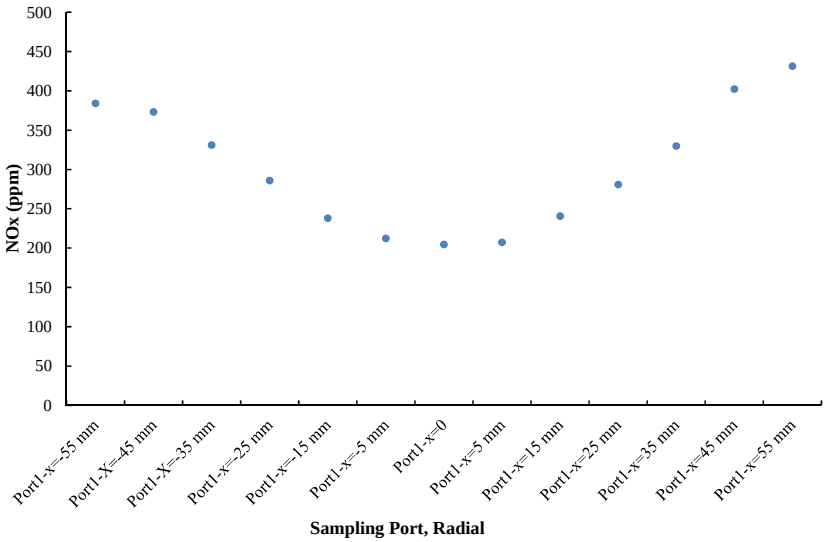

Figure 4.13: NOx concentration in sampling from Port1 radially, ammonia injected from Port3 ($NOx_{initial}$=500ppm, R=1.25)

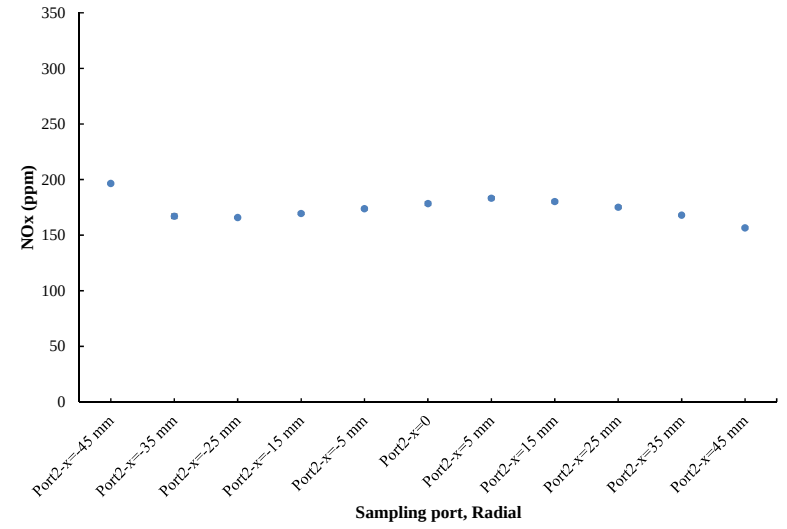

Figure 4.14: NOx concentration in sampling from Port2 radially, ammonia injected from Port3 ($NOx_{initial}$=500ppm, R=1.25)

Injecting ammonia at Port1, Port2, Port3 and sampling from Port0 vertically

The average temperature at Port1, Port2 and Port3 are 900°C, 780°C and 560°C, respectively. Considering the temperature window for a reduction, the probability of a reduction by adding ammonia at Port2 is very low and at Port3 is not possible at all. However, the results from previous experiments (Figure(4.8) and Figure(4.9)) show a remarkable reduction by adding ammonia at these two ports. By vertically sampling at Port0 during adding ammonia at these three ports, we may be able to explain what happens inside a cyclone and where the reaction zone happens to be.

Figure(4.15) shows the results of the NOx concentration by sampling from different zones vertically while adding ammonia from Port1, Port2 and Port3.

As can be seen, a sharp decrease of NOx concentration happens in the zone between Port1 and Port2. Such a fast decrease shows that the maximum reduction takes place in this area. The proper temperature in this area and good mixing ensures a high probability of reaction.

In general, even with adding ammonia to Port2 and Port3, the gas flow carries ammonia onto the zone between Port1 and Port2, which provides a good reduction condition.

As it can be seen for Port2 and Port3, the drop in NOx concentration (reduction) is happed before Port2 (150mm), which means in any condition ammonia gets the chance of being in the reaction zone while mixing and being carried on by upwards flow.

According to the results, the most part of the reduction takes place in the area between Port1 and Port2 when ammonia is injected at Port1, Port2 and Port3. This area has the optimum temperature and is supported by a cyclonic flow (swirling flow) when ammonia is added from Port1 (recommended) and is also supported by mixing with upwards flow when ammonia is being added from Port2 and Port3. General conclusion confirms the ability of the cyclone reactor in reducing NOx for approx. 60% which is similar to the efficiency reported for conventional reactors [69, 72, 76, 79–81]. The fact of having a good reduction, even with adding ammonia from areas of lower temperature, makes the cyclone reactor flexible with regard to ammonia injection and makes this process easy to apply for design and optimization approaches. However, it is strongly recommended to add ammonia from the proper temperature zones when it is practically possible to get the highest possible efficiency.

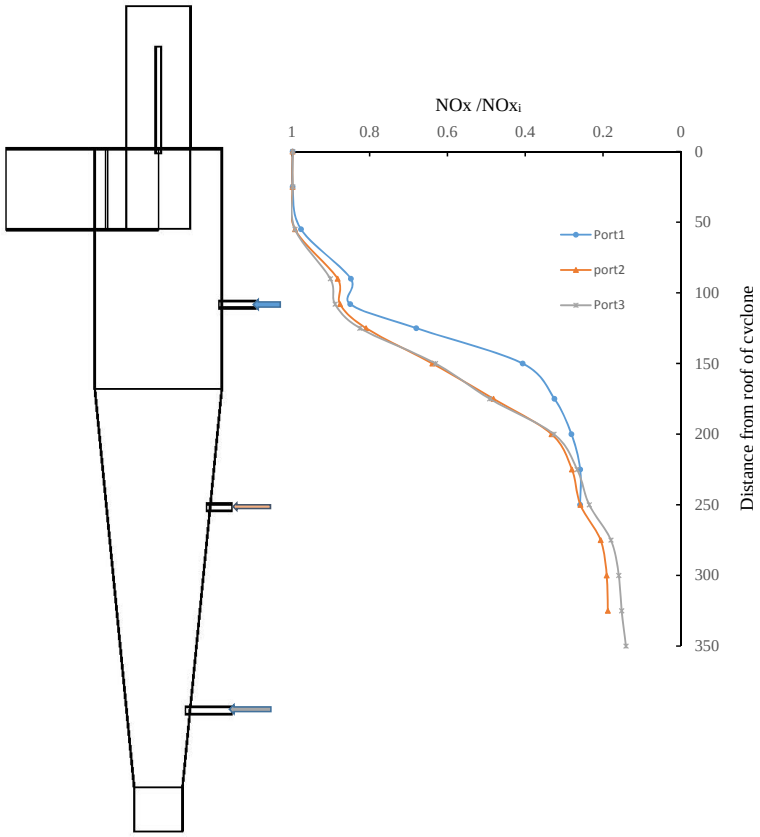

Figure 4.15: NOx concentration with sampling from Port0 vertically on cyclone, ammonia injected from Port1, Port2, Port3 ($NOx_{initial}$=500ppm, R=1.25)

4.3.3 Investigation of initial NOx

The effect of initial NOx concentration is studied by ammonia injection at Port1 by initial NOx; 200, 350, 500 and 700ppm in molar ratio constant 1.25. Ammonia flow rates are 96, 169, 240 and 336Nml/min, respectively. The results for this case are presented as reduction efficiency in Figure(4.16).

The results indicate that increasing the initial NOx from 200ppm to 350ppm has less effect on total reduction efficiency, while in higher NOx concentrations, the final reduction efficiency increases with increasing initial NOx at the same molar ratio. Higher initial NOx with a constant molar ratio increases the probability

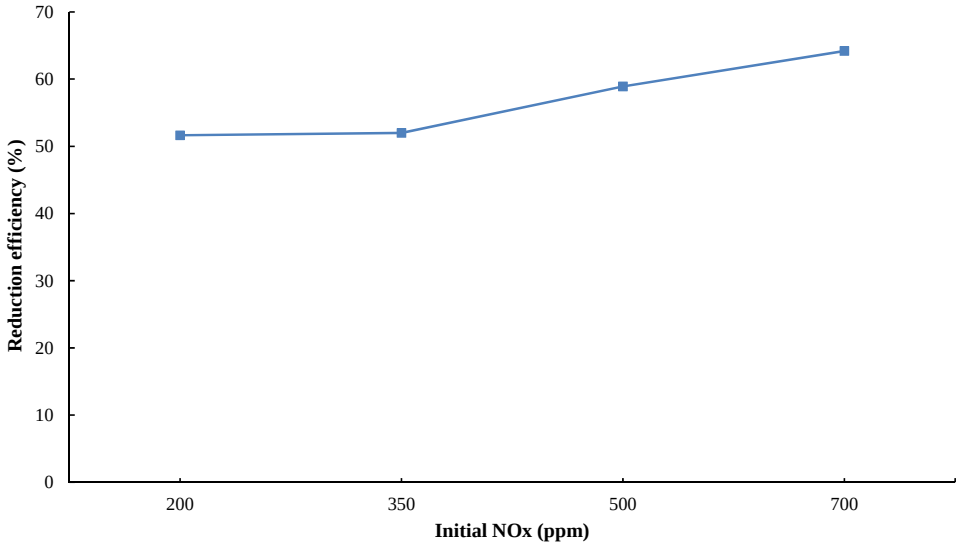

Figure 4.16: NOx reduction efficiency w.r.t various initial NOx, ammonia injected at Port1 (R=1.25)

of effective molecular contact and hence increases reduction efficiency to 64%. Results show that the system can achieve high reduction efficiency in the presence of a higher amount of initial NOx and also confirms system reliability in a broad range of initial NOx concentration, which is good for real case emission control studies.

4.3.4 Investigation of molar ratio

The effect of molar ratio is studied by injecting ammonia at Port1 with 500ppm initial NOx and molar ratios; 0.5, 0.75, 1, 1.25, 1.5, 1.75 and 2. Results illustrated in Figure(4.17) indicate that the effect of increasing molar ratio is only significant up to R=1.5, beyond which a low increase in NOx reduction is observed, which leads to increasing ammonia slip.

4.3.5 Investigation of ammonia injection velocity

The effect of ammonia injection velocity in reduction is studied by injecting ammonia at Port1, Port0 and P_{in}. Nitrogen gas is added to ammonia line to increase the injection velocity as a carrier gas. Ammonia with flow rate

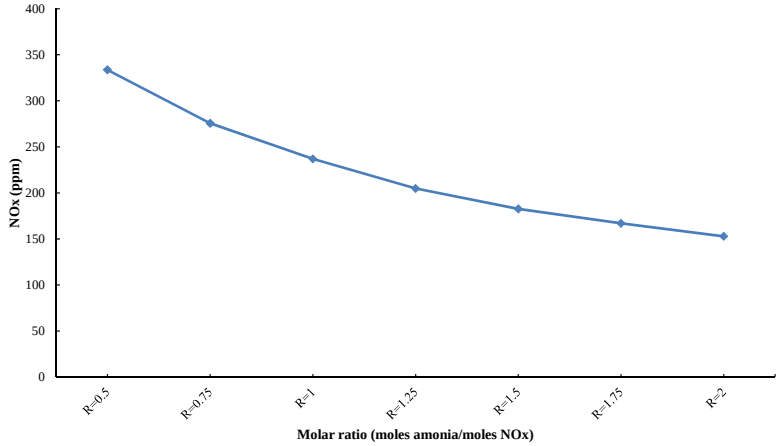

Figure 4.17: NOx concentration in various molar ratio by adding ammonia at Port1 ($NOx_{initial}$=500ppm)

$245Nml/min$ is diluted with nitrogen gas to get 1.1, 4,6.7,14.7,22.6 m/s with nitrogen flows of 0, 0.5, 1, 2.5, $4Nl/min$, respectively.

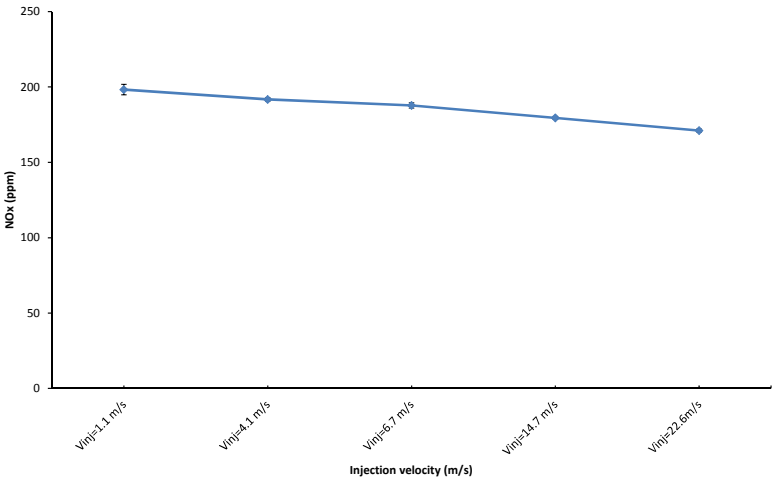

Figure 4.18: NOx concentration in various injection velocity at P_{in} with $NOx_{initial}$=500ppm, R=1.25 diluted by N_2 gas

The effect of injection velocity at P_{in} is illustrated in Figure(4.18). As observed, increasing the injection velocity leads to some increase in the reduction efficiency, yet not significantly. In this case, ammonia with any injection velocity will also

mix very fast with flue gas and gets the chance of reacting with NOx.

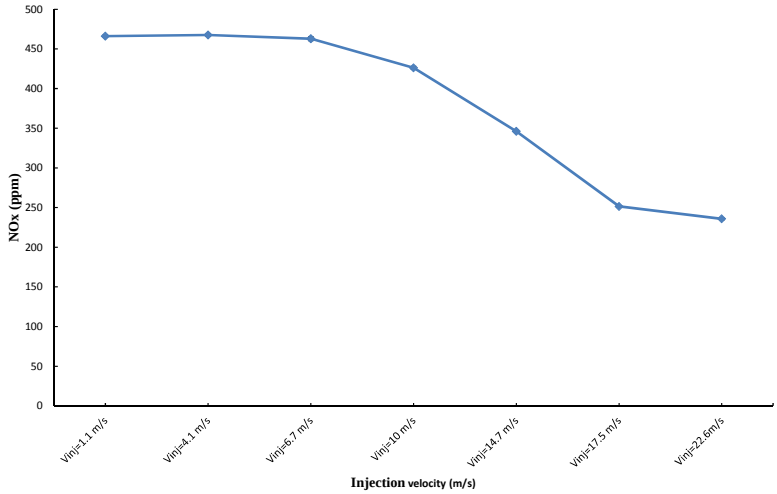

Figure 4.19: NOx concentration in various injection velocity at Port0 (near the wall, Z=0) with $NOx_{initial}$=500ppm, R=1.25 diluted by N_2 gas

Figure (4.19) and Figure(4.20) show the effect of injection velocity while adding ammonia at Port0 at Z=0 (near the roof of the cyclone) and Z=25mm (25mm far from the roof of the cyclone). A significant change is observed when the injection velocity is higher than 6.7 m/s. With increasing velocity up to 17.6m/s, reduction efficiency increases. This confirms the presence of fast mixing of ammonia with NOx in the inlet of the cyclone. Besides, by increasing the velocity, ammonia is distributed in full cross-section of the inlet of the cyclone. This effect gets decreased when velocity goes higher than 17.6m/s. Increasing the injection velocity to more than 17.6m/s has no effect on reduction efficiency.

Figure(4.21) shows the NOx level in different injection velocities for Port1. As it can be seen, increasing injection velocity has no effect on reduction in the investigated velocity range. Ammonia with any injection velocity will mix very fast with flue gas and get the chance of reacting with NOx.

4.4 Experiments and results with particles

To understand the effect of particles on temperature profiles and consequently the NOx reduction efficiency inside the cyclone, some experiments are done with

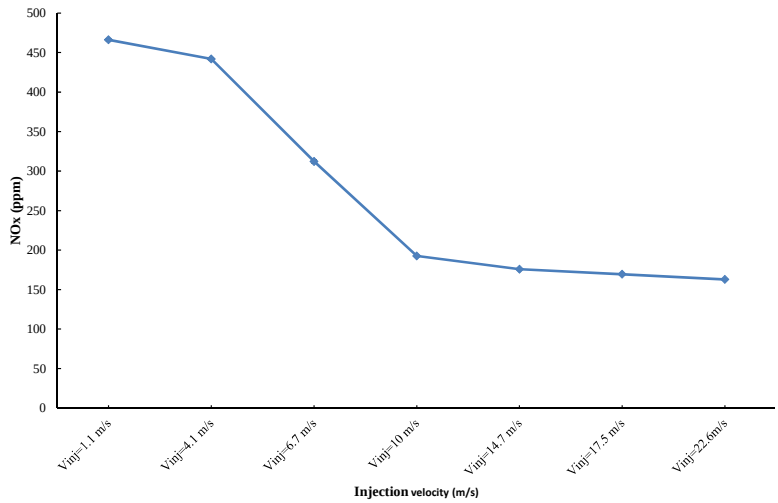

Figure 4.20: NOx concentration in various injection velocity at Port0 (Z=25 mm) with $NOx_{initial}$=500ppm, R=1.25 diluted by N_2 gas

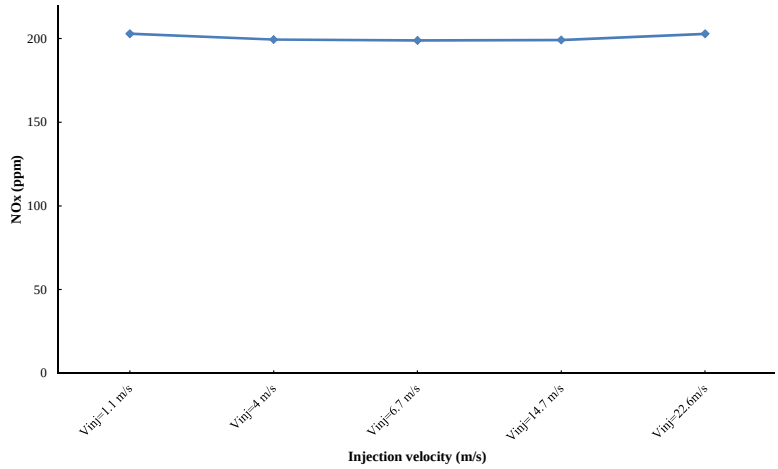

Figure 4.21: NOx concentration in various injection velocity at Port1 with $NOx_{initial}$=500ppm, R=1.25 diluted by N_2 gas

sand particles (inert particles regarding SNCR reaction, however it should be check in high temperature).

The applied sand particles have the particle distribution of 3–200μm, particle density of 2700 kg/m^3 and bulk density of 1300kg/m^3 (illustrated in Fig-

ure(4.22)).

To compare with former results, it is important to keep the conditions as close as possible to those of former experiments. If the air flow rate and natural gas flow are kept constant, the temperature of flue gas will be decreased due to energy consumption for heating up the particles before entering the cyclone. In considering the importance of effective parameters on SNCR, i.e., temperatures, oxygen and CO concentrations, to compensate temperature decrease, one possible way is to increase the natural gas flow. However, it also leads to a decrease in the oxygen concentration level, yet higher than the considered oxygen concentration (% O_2> 8%). Calculation shows that to heat-up $2.2kg/hr$ sand particles to flue gas temperature, approx. $0.3kW$ energy is needed. By increasing the natural gas flow from $16.71Nl/min$ to $17.21Nl/min$, this energy is provided. By increasing the amount of natural gas flow and keeping the air flow constant, new flue gas properties are obtained for comparison with experiments without particle (% O_2=8.28, CO=1.2ppm, CO_2=6.73 in dry flue gas).

In practice, for experiments with particles, when the system becomes steady in proper natural gas and air flow, the particles are heated with loading in the middle of the swirl burner before entering the cyclone.

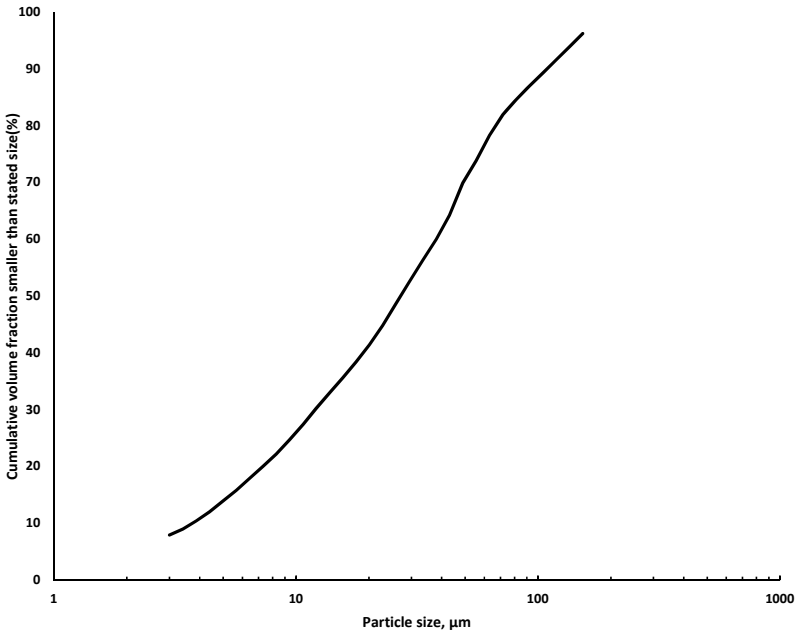

Figure 4.22: Particle size distribution-sand 74/200

4.4.1 Temperature Profile in the presence of particles

The vertical temperature profile of cyclone with particles is illustrated in Figure(4.23) to compare with the same experiment without particle. As it can be seen, particle loading increases the temperature and follows almost the same upside-down regime compared to the experiments without particles. However, at the bottom of the cyclone, the temperature is increased around 100°C in the presence of particles. Meaning that, even though the reactor is still non-isothermal, the temperature difference up-down the cyclone is lower and the temperature is distributed better with loading particles.

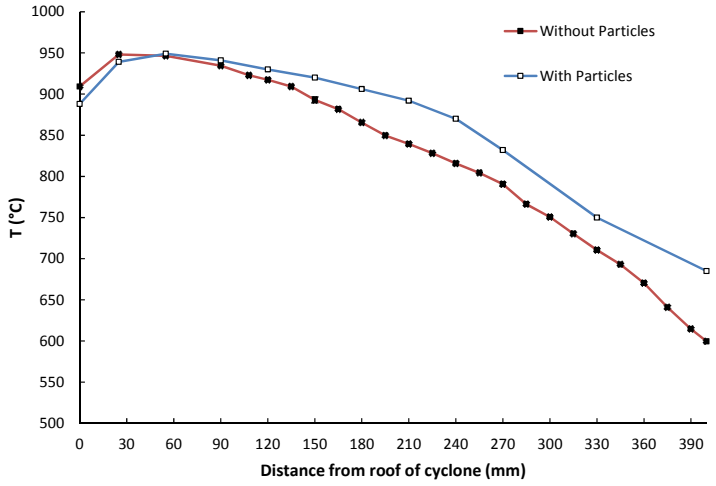

Figure 4.23: Vertical temperature profile of cyclone with and without particles

4.4.2 Investigation of NOx reduction in varying molar ratio in the presence of particles

To study the effect of particles on SNCR, some experiments are carried out by injecting ammonia from Port1 and sampling from Main port with $500ppm$ initial NOx and molar ratios: 1, 1.25, 1.5, 1.75 and 2. An investigation of NOx distribution is also done and results are compared (with and without particles). This is illustrated in Figure(4.24).

Reduction efficiency is lower than the case without particles, as illustrated in Figure(4.24). Ammonia is injected at optimum temperature (considering the

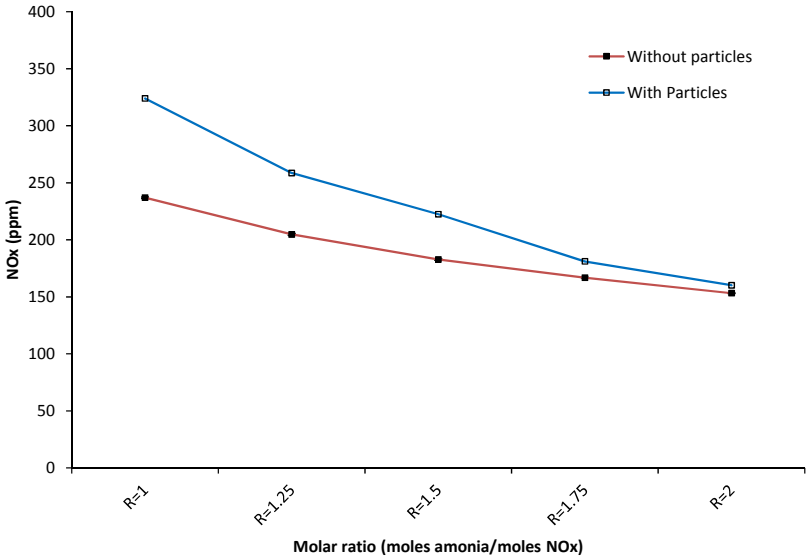

Figure 4.24: NOx level at different Molar ratios in the cyclone with and without particles

optimum temperature of app. 950°C) to the Port1 of the cyclone. In this area, the temperature is high, and by adding pre-heated particles, it is probable for the temperature to be higher compared to the case without particles. However, the measured temperature is almost the same. The temperature measurement system has some errors due to radiation; therefore, in high temperature, the system's temperature could be higher than the measured value. Temperature tolerance is enough to provide a chance for ammonia oxidation. According to Figure(4.24), by adding particles, temperature shifts to higher amounts through the cyclone, which provides a chance of oxidation on high-temperature zones of the cyclone. Any ammonia oxidation in this case leads to a decrease in reduction efficiency. It is also probable that sand particles play a catalytic effect in this temperature (need to analyse the sand compositions).

Considering the results of the study on the molar ratio, by increasing ammonia molar ratio, the NOx reduction efficiency gets increased (Figure(4.24)). Therefore, higher amounts of ammonia mostly increase the reduction in competition with the oxidation, meaning that the chance of oxidation or catalytic effect is still limited due to the mixing effect. If ammonia does not distribute well by mixing, the oxidation rate must be increased by adding more ammonia, which is not the case here. Results show that while temperature provides a chance

for oxidation, the mixing effect still provides a better chance of reduction for ammonia in competition with oxidation.

4.5 Conclusion

Due to the importance of temperature and mixing effect on SNCR, there is a strong need to study the temperature profile and mixing behavior under different conditions.

In this project, some experiments are performed to obtain the temperature profile and to know more about the effective zones with the proper temperature for NOx reduction. Another set of experiments are also performed to investigate the mixing behavior based on NOx reduction efficiency.

With these experiments, the cyclone has been targeted as a reactor to find efficient reduction zone by providing vertical and radial NOx concentration distribution.

The first series provide the temperature profile vertically and radially (in different ports). There is a temperature difference up-down of approx. 350°C. Considering the temperature window for reduction, the possibility of having both reduction of NOx and oxidation of ammonia in P_{in} and Port0 is higher when injecting ammonia at Port1 and Port2. In general, temperature profile study shows that reduction can take place in an inlet channel and from the top of the cyclone down to $340mm$ depth from the top. Results show more efficiency when injecting ammonia from Port1 because the average temperature in this area is 900°C, which is the optimum temperature for SNCR NOx reduction.

In addition, the results of radial experiments show that the optimum position for adding ammonia from Port1 is 5–15mm distance from the wall (vortex-flow downward). The NOx reduction efficiency was maximum in this condition (60%), and it is expected because of temperature profile and cyclonic flow pattern. Larfeldt et al. [153] concluded that by adding ammonia in the inner vortex in the cyclone in CFB boilers (close to Port1 in this project), NOx reduction efficiency is improved by at least 30%.

A further detailed study shows that reduction efficiency is still high (54%) by injecting ammonia at Port2 and Port3, even though the temperature is at the lowest level of the temperature window in Port2 and below the temperature window for Port3. Further studies have been performed to monitor the reduction pattern by injecting ammonia from one port and point measurement of NOx concentration vertically and radially (minimum of 10 points for each). The results

of these experiments show that reduction mostly takes place in the zone between Port1 and Port2 when ammonia is injected from any of the side ports (Port1, Port2 and Port3), which is the main reason behind achieving high reduction efficiency, even with injecting ammonia in low-temperature zones. Comparing the radial concentration distribution in sampling from Port1 and Port2 (ammonia is injected at Port3), the parabolic concentration profile is obtained for Port1 but not for Port2, as expected from the swirl flow inside the cyclone. Results of temperature profile at the same condition also show the parabolic temperature profile for Port1 and non-parabolic for Port2 and Port3. This is the result of an unexpected flow (recycling) in this area which provides mixing towards a proper temperature area and leads to high reduction efficiency (54%).

Following the experimental plan, investigation of initial NOx concentration shows that by an increase in initial NOx concentration in constant molar ratio, reduction efficiency gets increased.

It is also concluded from our study on a molar ratio with constant initial NOx ($500ppm$) that with increasing molar ratio, reduction efficiency gets increased. However, the rate of increase is low after molar ratio R = 1.5.

Further investigation on injection velocity shows that, by increasing injection velocity for Port0, reduction efficiency gets increased because mixing is performed better and faster which avoids ammonia oxidation. However, no increasing pattern is recognized for P_{in} and Port1 in this range of injection velocities. The mixing effect under the cyclonic flow condition is more effective in Port1.

A complementary experiment with adding particles to the cyclone shows that the system works as a non-isothermal reactor but the temperature difference up-down the cyclone is 100°C, lower in the presence of particles. A comparative study of molar ratio with and without particles shows a lower reduction efficiency in the presence of particles.

In general, results show that, in cyclone reactor, wherever the swirl flow plays the main role, the mixing effect is extensively good. With regard to the temperature profile and NOx distribution, the swirl flow is well-generated in the area between Port1 and Port2. This mixing function of swirl flow together with temperature conditions provides a potential reaction zone in this area (between Port1 and Port2). Adding to flow effect and temperature, with the high residence time of reactants inside the cyclone, it is highly probable for the reactants to meet this reaction zone even when the ammonia is injected from the lower temperature zones, which altogether provides high reduction efficiency and flexible design availability for real case studies.

In the following chapter, all of the above will be discussed with CFD modeling of the same cyclone. Results of CFD will clarify the flow pattern inside the

cyclone and be further applied to discuss the experimental results.

Chapter 5

CFD of SNCR in the cyclone reactor

Introduction

CFD is a method of calculating fluid flows, heat and mass transfer, chemical reactions and similar phenomena by numerical solving mathematical expression [157]. CFD has emerged to be one of the most important fields of study that plays a key role in the modern engineering environment. As global industries tend to demonstrate a growing demand for innovative designing, engineering, and manufacturing processes, it is becoming imperative to understand thermal and fluid dynamics of innovation and seamless solutions for core problem areas. Despite the fact that fluid dynamics have always been widely used in design and manufacturing, it is the significance of computer technology and rapid advancements that have made CFD an element of precise and accurate computation in the engineering industry.

The accuracy of the solutions is dependent on the following properties:

- Consistency: The discretization error should approach zero for infinite small grid sizes or time steps. For this case, the algebraic finite difference equations become equal to the original partial differential equations.
- Stability: Numerical errors should be bounded for each iteration step and

not diverge the solution.

- Convergence: A numerical method is convergent if its solution approaches that of the partial differential equation for decreasing grid sizes and time steps and if numerical errors are bounded. This means that both consistency and stability are required to achieve convergence.

In this Ph.D. project, the CFD simulations are performed with the commercial software program ANSYS-FLUEN 16.

In this part of study the focus is CFD modeling of cyclones as a preferred reactor for SNCR to provide more knowledge in different aspects, e.g., flow pattern, mixing and residence time to achieve a better understanding of the reaction inside the cyclone.

Therefore, to explain the effect of mixing and map the role of fluid dynamics in the cyclone reactor, CFD modeling is preferred. With CFD, the reactor is modeled by considering both fluid dynamics and reaction.

The lack of knowledge of fluid dynamics and NOx reduction inside the cyclone is because the fluid dynamics within a cyclone is complex. Moreover, the inclusion of parameters, such as residence time, reactant concentration distribution, as well as other relevant physical properties (e.g., viscosity, density, temperature effects, rotational effects), add further complexities. CFD simulations of the fluid in the cyclones provide an effective tool for understanding the details of the flow and reaction within the cyclones. However, the system to be used for the simulations with a detailed reaction scheme is very complicated and the computational time consumption is high even with powerful computers. To reach a reasonable computational time, the system needs to be simplified. The main aim of this project is to map the relative importance of fluid dynamics and SNCR with the involvement of flow pattern and transport phenomena with reduced chemical kinetics and to propose a methodology for process simplification for modeling. The results could be applied for optimization and scale-up, e.g., in the cement industry and power plants.

5.1 CFD approach and methodology

In this chapter, the governing equations applied in this study are explained. The next step is CFD modeling to simulate the cyclone reactor. The CFD modeling is divided into three steps:

- Develop a reliable fluid dynamic model, which will be validated by exper-

iments (cold mode study).

- Develop a model with heat transfer
- Implement SNCR reactions with mass and heat transfer taken into consideration.

In a cold mode simulation, the basic setting is designed and optimized which is applied for the rest of the study. In the heat transfer section, the temperature profile is obtained to compare with the experimental results and to define a reliable boundary condition for the last section (SNCR). In the last section, SNCR process is simulated with Finite-Eddy/dissipation model. The developed model would then be used to predict the performance parameters of the cyclone reactors, such as pressure drop, temperature profile, NOx reduction efficiency, Reaction zones and ammonia slip.

5.2 The governing equations for the gas phase

The behavior of flows is described by the equation of conservation of mass (continuity equation), the equation of motion (Navier-Stokes for Newtonian fluids) and the equation of energy.

Conservation of mass: The continuity equation describes the change of mass in a control volume by means of the transport of mass through the faces of the volume. Its general equation for conservation of mass or continuity equation can be written [158]:

$$\frac{\partial \rho}{\partial t} + \nabla . (\rho \vec{v}) = S_m \tag{5.1}$$

Conservation of momentum: The momentum balance for each direction over the control volume is calculated by [159]:

$$\frac{\partial}{\partial t} (\rho \vec{v}) + \nabla . (\rho \vec{v} \vec{v}) = -\nabla p + \nabla . \bar{\bar{\tau}} + \rho \vec{g} + \vec{F} \tag{5.2}$$

Where P is the statics pressure, $\bar{\bar{\tau}}$ is the stress tensor, and $\rho \vec{g}$ and $\vec{F}$ are the gravitational body force and external body forces, respectively. The stress tensor is given by:

$$\bar{\bar{\tau}} = \mu \left[\left(\nabla \vec{v} + \nabla \vec{v}^T \right) - \frac{2}{3} \nabla . \vec{v} I \right] \tag{5.3}$$

where μ is the molecular viscosity, $\vec{v}^T$ is the transpose of the velocity vector, I is the unit tensor, and the second term on the right-hand side is the effect of volume dilation.

Conservation of energy: ANSYS-FLUENT solves the energy equation in the following form:

$$\frac{\partial}{\partial t} (\rho E) + \nabla . \left(\vec{v} \left(\rho E + p \right) \right) = \nabla . \left(k \nabla T - \sum_i h_i \vec{J}_i + \left(\bar{\bar{\tau}} . \vec{v} \right) \right) + S_h \tag{5.4}$$

where k is the thermal conductivity, and $\vec{J}_i$ is the diffusion flux of species i. The first three terms on the right-hand side of Eq.(5.4) represent energy transfer due to conduction, species diffusion, and viscous dissipation, respectively. S_h is the energy source and includes the heat of chemical reaction as well as any other volumetric heat sources.

In Eq.(5.4),

$$E = h - \frac{p}{\rho} + \frac{1}{2} v^2 \tag{5.5}$$

where sensible enthalpy, h, is defined for ideal gases as

$$h = \sum_i Y_i h_i \tag{5.6}$$

Conservation of species: In ANSYS-FLUENT, a local mass fraction of each species, Y, is predicted through the solution of a convection-diffusion equation for the species. Tis conservation equation takes the following general form:

$$\frac{\partial}{\partial t} (\rho Y_i) + \nabla . \left(\rho \vec{v} Y_i \right) = -\nabla . \vec{J}_i + R_i + S_i \tag{5.7}$$

where R_i is the net rate of production of species by chemical reaction and S_i the rate of creation by addition from the other sources.

An equation of this form will be solved for $N - 1$ species where N is the total number of fluid phase chemical species present in the system. $\vec{J}_i$ is the diffusion

flux of species, which arises due to gradients of concentration and temperature. We consider Fick's law to model mass diffusion due to concentration gradients for laminar flows, under which the diffusion flux can be written as:

$$\vec{J_i} = -\rho D_{i,m} \nabla Y_i - D_{T,i} \frac{\nabla T}{T} \tag{5.8}$$

$D_{i,m}$ is the molecular mass diffusion coefficient of species i in the mixture, and $D_{T,i}$ is the thermal diffusion coefficient.

Turbulence equation: The fluid flow studied in this research is highly turbulent. In this project, static techniques are used to capture the character of chaotic and random motions in turbulence, as velocity, pressure and other parameters vary continuously with time. The solution variables are decomposed into the mean (ensemble-averaged or time-averaged) and fluctuating components. For the velocity components:

$$u_i = \bar{u_i} + u_i' \tag{5.9}$$

where $\bar{u_i}$ and u_i' are the mean fluctuating velocity components ($i = x, y, z$).

Likewise, for pressure and other scalar quantities:

$$\phi = \overline{\phi} + \phi' \tag{5.10}$$

where ϕ denotes a scalar such as pressure, energy, or species concentration.

The averaging method is usually based on time averaging of flow properties. After the application of averaging rules on the flow equations, the Reynolds averaged form of Navier–Stokes equations are derived with the additions of several unclosed terms like Reynolds stresses for the Navier–Stokes equations and other extra terms of turbulent transport. Continuity, momentum and energy equations are rewritten as Eq.(5.11) to Eq.(5.13).

$$\frac{\partial \rho}{\partial t} + \frac{\partial}{\partial x_i} \left(\rho \overline{u}_i \right) = S_m \tag{5.11}$$

$$\frac{\partial}{\partial t}\left(\rho\overline{u}_i\right)+\frac{\partial}{\partial x_i}\left(\rho\overline{u}_i\overline{u}_j\right)=-\frac{\partial\overline{p}}{\partial x_i}+\frac{\partial}{\partial x_j}\left[\mu_{eff}\left(\frac{\partial\overline{u}_i}{\partial x_j}+\frac{\partial\overline{u}_j}{\partial x_i}-\frac{2}{3}\delta_{ij}\frac{\partial\overline{u}_l}{\partial x_l}\right)\right]+\frac{\partial}{\partial x_j}\left(-\rho\overline{u_i'u_j'}\right) \tag{5.12}$$

$$\frac{\partial}{\partial t}\left(\rho E\right)+\frac{\partial}{\partial x_i}\left[\overline{u}_i\left(\rho E+\overline{p}\right)\right]=\frac{\partial}{\partial x_i}\left(k_{eff}\frac{\partial\overline{T}}{\partial x_i}-\sum_i h_i\vec{J}_i+\overline{u}_i\left(\tau_{ij}\right)_{eff}\right)+S_h \tag{5.13}$$

In Eq.(5.13), $k_{eff}=k+k_t$ is the effective conductivity, where k_t is the turbulent thermal conductivity, defined according to the turbulent model being used. And $\left(\tau_{ij}\right)_{eff}$ is the deviatoric stress tensor, defined as:

$$\left(\tau_{ij}\right)_{eff}=\mu_{eff}\left(\frac{\partial\overline{u}_j}{\partial x_i}+\frac{\partial\overline{u}_i}{\partial x_j}\right)-\frac{2}{3}\mu_{eff}\frac{\partial\overline{u}_k}{\partial x_k}\delta_{ij} \tag{5.14}$$

Where μ_{eff} is the effective viscosity same as the effective conductivity; $\mu_{eff}=\mu+\mu_t$.

Also, in turbulent flows, the mass diffusion is captured in the following form:

$$\vec{J}_i=-\left(\rho D_{i,m}+\frac{\mu_t}{Sc_t}\right)\nabla Y_i-D_{T,i}\frac{\nabla T}{T} \tag{5.15}$$

where Sc_t is the turbulent Schmidt number equal to ($\frac{\mu_t}{\rho D_t}$). μ_t is the turbulent viscosity and D_t is the turbulent diffusivity.

In Eq.(5.12), $\overline{u_i'u_j'}$ represents the correlation between fluctuating velocities and is called the Reynolds stress tensor. All the effects of turbulent fluid motion on the mean flow are lumped into this single term by the process of averaging.

It is the main task of turbulence to derive expressions and develop computational schemes of sufficient accuracy to calculate the Reynolds stresses and the turbulence transport term.

Reynold Stress Model: The Reynolds stress model is the most elaborate type of RANS turbulence model. Abandoning the isotropic eddy-viscosity hy-

pothesis, the RSM closes the Reynolds-averaged Navier–Stokes equations by solving transport equations for the Reynolds stresses, together with an equation for the dissipation rate. This means that seven additional transport equations are required in 3D flows.

Since the RSM accounts for the effects of streamline curvature, swirl, rotation, and rapid changes in strain rate in a more rigorous manner than one-equation and two-equation models, it has greater potential to give accurate predictions for complex flows.

The exact transport equations for the transport of the Reynolds stresses, $\rho\overline{u_i' u_j'}$, may be written as follows:

$$\underbrace{\frac{\partial}{\partial t}\left(\rho\overline{u_i' u_j'}\right)}_{\text{Local Time Derivative}} + \underbrace{\frac{\partial}{\partial x_k}\left(\rho u_k \overline{u_i' u_j'}\right)}_{C_{ij} \equiv \text{Convection}} = \underbrace{-\frac{\partial}{\partial x_k}\left[\rho\overline{u_i' u_j' u_k'} + \overline{p'\left(\delta_{kj} u_i' + \delta_{ik} u_j'\right)}\right]}_{D_{T,ij} \equiv \text{Turbulent Diffusion}}$$
$$+ \underbrace{\frac{\partial}{\partial x_k}\left[\mu\frac{\partial}{\partial x_k}\left(\overline{u_i' u_j'}\right)\right]}_{D_{L,ij} \equiv \text{Molecular Diffusion}}$$
$$\underbrace{-\rho\left(\overline{u_i' u_k'}\frac{\partial u_j}{\partial x_k} + \overline{u_j' u_k'}\frac{\partial u_i}{\partial x_k}\right)}_{P_{ij} \equiv \text{Stress Production}}$$
$$\underbrace{-\rho\beta\left(g_i\overline{u_j'\theta} + g_j\overline{u_i'\theta}\right)}_{G_{ij} \equiv \text{Buoyancy Production}}$$
$$+ \underbrace{\overline{p'\left(\frac{\partial u_i'}{\partial x_j} + \frac{\partial u_j'}{\partial x_i}\right)}}_{\phi_{ij} \equiv \text{Pressure Strain}}$$
$$\underbrace{- 2\mu\overline{\frac{\partial u_i'}{\partial x_k}\frac{\partial u_j'}{\partial x_k}}}_{\varepsilon_{ij} \equiv \text{Dissipation}}$$
$$\underbrace{-2\rho\Omega_k\left(\overline{u_j' u_m'}\varepsilon_{ikm} + \overline{u_i' u_m'}\varepsilon_{jkm}\right)}_{F_{ij} \equiv \text{Production by System Rotation}}$$
$$+ \underbrace{S_{user}}_{\text{User-Defined Source Term}}$$

5.3 CFD modeling of cyclone in cold mode

The aim of this part is to develop fluid dynamics model for the cyclone. The designed cyclone reactor is considered for high temperatures. For the cold model, the only parameters for validation are pressure drop and collection efficiency which are not enough to validate fluid dynamics. Considering the geometric similarity and important dimensionless numbers in the cyclone (Reynolds, Euler and Stk_{50}), Hoekstra's experimental result [121] for a cyclone with 290mm diameter is selected to validate CFD modeling. After validation of the devel-

oped model, it is scaled down to 110mm (designed cyclone for this project) and used for the next steps of the project with the same grid and model settings.

Among many known discretization schemes, the finite volume method is one of the most popular methods since it is relatively simple to understand and implement in computer code. The method can accommodate any type of grid which makes it suitable for complex geometries used in the industry.

In this section, the computational domain and boundary conditions are presented followed by turbulence model selection. Then, mesh generation and grid independency study are presented. In the next step, solver settings are defined to present phenomena in a cyclone. All the items mentioned are applied to the heat transfer and reaction studies as well. Results of the cold model are discussed at the end of this section.

5.3.1 Computational Domain and boundary Condition

Figure(5.1) illustrates the geometry of Stairmand high efficiency cyclone [160] and corresponding dimensions with the definition of the coordinate system that will be used throughout the thesis. According to [121], the reference diameter is selected as $D = 290$mm.

A computational domain can also be seen in this figure. Flow enters to the cyclone from a tangential inlet duct (violet face) to generate the swirl flow and leaves through the exit pipe at the top (red face) which is famous for vortex finder. The particles leave the cyclone from the bottom of the cyclone.

Velocity inlet boundary condition is applied at the inlet of the cyclone, outflow at gas outlet and wall (no-slip) boundary condition at all other boundaries. The air linear inlet velocity is equal of $v_{in} = 16.1$ m/s, corresponding to the experimental study of Hoekstra [121]. The air density of 1.225 kg/m^3 and viscosity of 1.7894×10^{-5}kg/m.s were defined in this part of the study.

The turbulence quantities (kinetic energy and dissipation rate) are uniformly found at the inlet by using the following correlations [161]:

$$k_{in} = \frac{3}{2}\left(I v_{in}\right)^2 \tag{5.16}$$

$$\varepsilon_{in} = C_{\mu}^{\frac{3}{4}} k_{in}^{\frac{3}{2}} / L \tag{5.17}$$

The turbulence intensity, I, equals 10%, and C_{μ} is an empirical constant equal

to 0.09 and the turbulence characteristic length (L in Eq(5.17)) equals 0.07 times the inlet width of the cyclone [121] are considered. At the cyclone's inlet, the Reynolds stress specific method in ANSYS-FLUENT solver is the Reynolds stress components. The diagonal components of the Reynolds stress tensor (normal stresses) are assigned to $2/3k_{in}$. The shear stresses (non-diagonal components) at the inlet are set to zero. The solutions are hardly sensitive to the exact inlet values for k_{in} and ε_{in}. These values are entered from the [121] to this study.

The boundary condition at the gas outlet is the outflow boundary condition provided by Fluent [162], where all transport variables have a zero normal gradient ($\partial/\partial n$). This boundary condition is valid for fully developed flow.

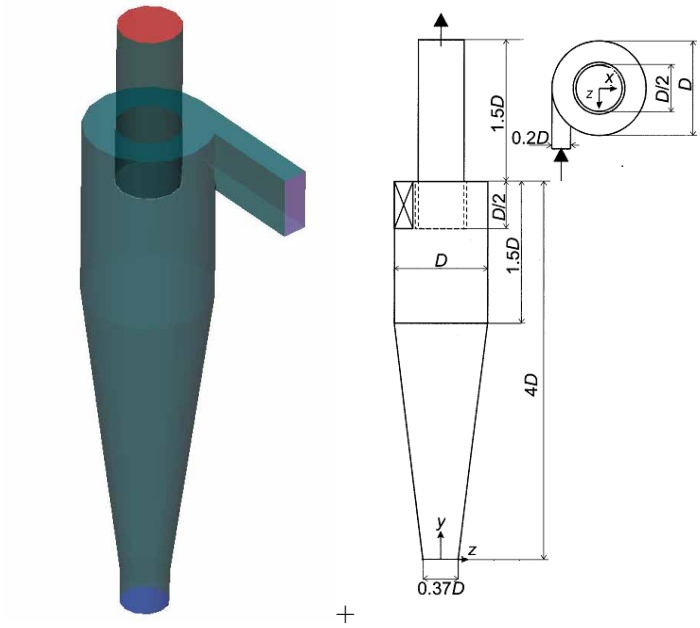

Figure 5.1: Geometry of Stairmand high efficiency cyclone

5.3.2 Turbulence model selection

For the turbulent flow in a cyclone, the key to the success of the CFD lies with the accurate description of the turbulent behavior of the flow. To model the swirling turbulent flow in a cyclone separator, a series (families) of turbulence models are available in ANSYS-FLUENT. Some of the Fluent turbulence models are listed below:

- $k-\varepsilon$ model family: 1-Standard, 2-Realizable and 3- RNG[1]
- $k-\omega$ model family: 1-Standard, 2-SST[2] and 3- BSL[3]
- RSM[4] family: 1-Linear Pressure Strain (RSM-LPS), 2-Quadratic Pressure Strain (RSM-QPS) and 3- Stress-Omega (RSM-SW)

The k-ε model involves the solution of transport equations for the kinetic energy of turbulence and its dissipation rate and the calculation of a turbulent contribution to the viscosity at each computational cell. The models of this family are not optimized for strongly swirling flows typically found in cyclones. Turbulence may be stabilized or destabilized in parts of the flow domain where a strong streamline curvature is present. The Reynolds stress model requires the solution of transport equations for each of the Reynolds stress components as well as for dissipation transport without the necessity to calculate an isotropic turbulent viscosity field. This means that seven additional transport equations are required in 3D flows. The Reynolds Stress turbulence model yields an accurate prediction of swirl flow pattern, axial velocity, tangential velocity and pressure drop on cyclone simulations.

In the present study, some turbulence models are tested. Axial and radial velocity profiles illustrate that the RSM models resulted in a better solution than the others. Figure(5.5) compares the different turbulence models' performance for flow in our cyclone.

5.3.3 Mesh Generation and Grid Independence Study

Industrial leading software ICEM-CFD has been used to discrete the fluid domain to generate the control volumes over which the governing equations are solved. A total number of 34 blocks are used to fill the entire cyclone domain to generate a body-fitted mesh. Blocking technique facilitates easy mesh generation with full control over the mesh density at appropriate locations. Figure(5.2) illustrates the hexahedral mesh of the cyclone. After grid generation, the mesh is imported and simulated using Fluent commercial finite volume solver.

The grid in the dependency study has been performed by comparing axial velocity profile for different grids. Three levels of grid fineness for the cyclone have been tested, to be sure that the obtained results are grid-independent. Table(5.1) depicts the generated grid information. Axial velocity profiles are

[1] Re-Normalisation Group
[2] Shear Stress Transport
[3] Baseline
[4] Reynolds Stress Model

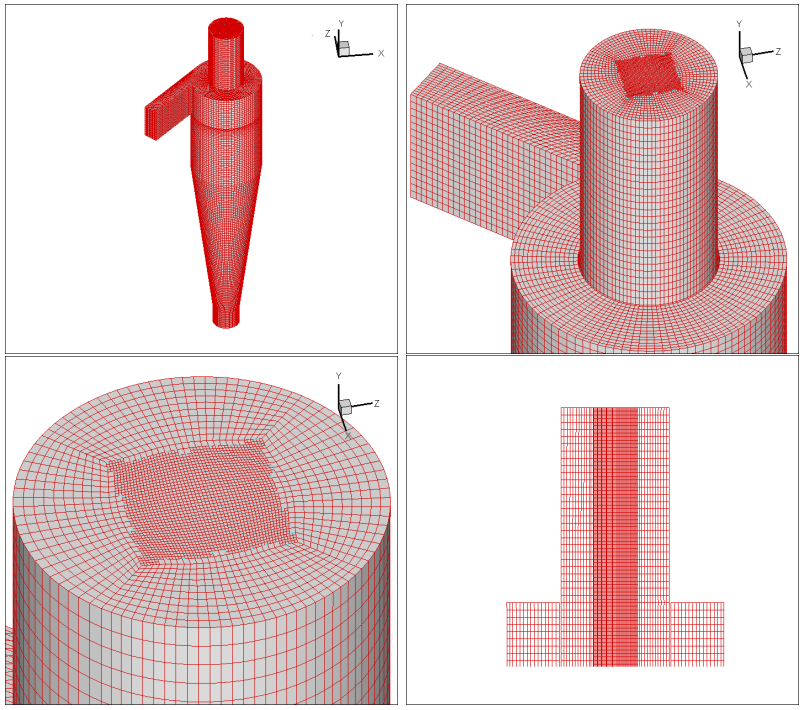

Figure 5.2: Structured grid generated for cyclone

compared for the three grids in Figure(5.3). It can be seen that the Fine and Medium grids matched each other but the course grid result has a small discrepancy; thus the medium grid is selected for simulations.

Table 5.1: Mesh information for simulated cyclone

Grid	No. of elements	No. of nodes
Course	325962	337192
Medium	444782	458030
Fine	692132	709424

5.3.4 Simulation strategy

Two aspects should be considered regarding the convergence criteria. Firstly, the scaled residuals should be below 10^{-5} [112]. Secondly, some representative quantities such as velocity and pressure should be monitored until they are constant.

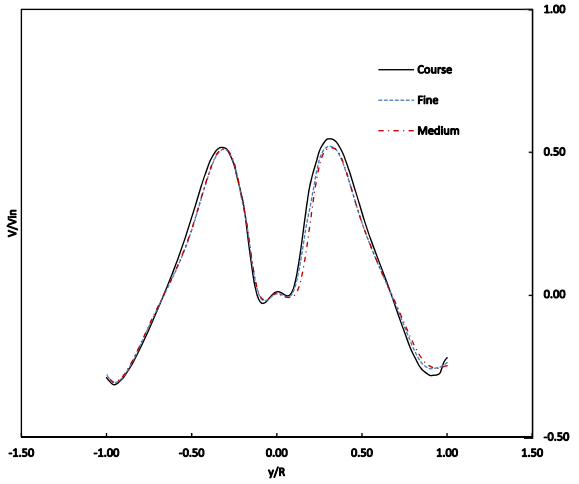

Figure 5.3: Grid independence study: Comparison of axial velocity profile along the y-axis (at $z = 3.25D$).

The solution of the cyclone simulation is started by running the steady solver for 5000 iterations where residuals start to exhibit periodical oscillations. From there, the unsteady solver, first order, then second order, and finally QUICk and third order implicit formulation options are enabled, and a fixed time step size of 10^{-4}s is employed in the simulation of the cyclone. The solution converged at each time step with preset scaled residuals of 10^{-5} as convergence criterion for all solution variables and the data sampling for time statistics is carried out over each time step. The simulation is carried out until the flow becomes statistically steady.

The present simulations were conversed at about $t = 1.9 - 2$s, they are terminated at $t = 2.5$s to get more accurate time-averaged values. The total CPU running time was about (140hr for each case) on 16 nodes CPU Opteron 64 Linux cluster using ANSYS-FLUENT 16 commercial solver. All simulations have been converged with the selected time step (10^{-4}s).

The residual and x-velocity convergence plots can be seen in Figure(5.4).

5.3.5 Solver Settings

The presence of some phenomena in cyclones such as strong swirl, sharp pressure gradients and high anisotropy demands a robust and efficient algorithm. For

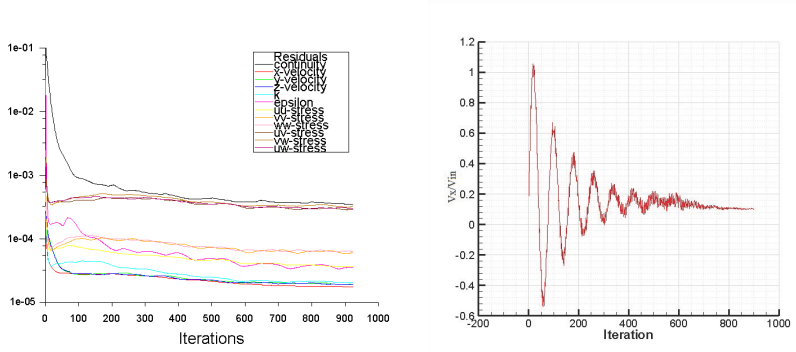

Figure 5.4: Residual and x-velocity v.s. iteration.

pressure-velocity coupling, SIMPLEC[5] algorithm of van Doormaal and Raithby [163] is used.

PRESTO[6] interpolation scheme as suggested by Shukla et al. [164] is used for pressure, QUICK[7] (2nd order) and MUSCL[8] (3rd order) for momentum-$k-\varepsilon$ equations, and Reynolds stresses equations scheme gives better predictions when compared with the experimental data. Solver residual set-point for all the conservation equations is set to 10^{-5}. In the near-wall region, the fluid flow is modeled using the standard wall function.

5.3.6 Results

In the present study, some turbulence models are tested. Figure(5.5) compares the different turbulence models performance compared to experimental data of Hoekstra's experiments [121].

The axial and radial velocity profiles show that the RSM–2nd order QUICK models resulted in better solutions than the other selected turbulence models.

For the next step of the simulation, the validated results (by Hokestra's Experimental results) of the developed model for cold mode will be used. Considering dimension difference, geometry in CFD modeling is scaled down from 29cm to 11cm. In the present geometry, a similar number of grids are generated, and turbulence model and solver settings are used as it is obtained from cold mode

[5]Semi-Implicit Method Pressure-Linked Equations Consistent
[6]PREssure STaggered Option
[7]Quadratic Upstream Interpolation for Convective Kinetics
[8]Monotone Upstream-Centered Schemes for Conservation Laws

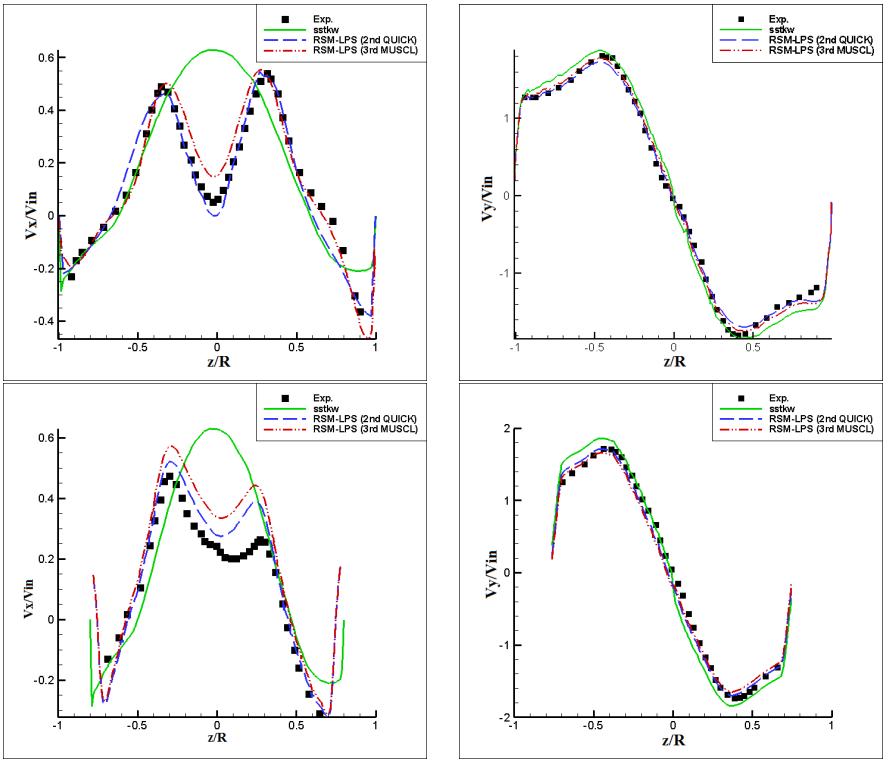

Figure 5.5: Non-dimensional velocity profiles along the z-axis v.s. non-dimensional y position (at $y = 3.25Dandy = 1.5D$).

study.

5.4 CFD modeling of heat transfer in a cyclone reactor

The fluid dynamics for cold mode modeling are obtained and validated from the previous section in which the results and setting are used to study accurate results for heat transfer. In this part of the simulation, the solver setting, including proper grid number, turbulent model, solution methods and time step are chosen same as the cold mode.

Considering a high-temperature situation, heat transfer is specifically important. In this project, regarding the gas phase reaction the radiation has been excluded

from the heat transfer methods. It means that in our CFD model, heat transfer is considered with conduction and convection. The radiation is more important in the presence of solid particles with remarkable higher radiation surface.

In this step, boundary conditions and fluid species are different with the cold mode which are presented below.

5.4.1 Considering fluid species in heat transfer modeling

The fluid used in this step is flue gas with compositions listed in Table(5.2) instead of air in cold mode.

Table 5.2: Considering wet flue gas composition for simulation

Component	N_2	H_2O	O_2	CO_2	CO
Mol fraction (%)	75.63	10.58	8.11	5.68	0

Because the temperature of flue gas inside the cyclone is not constant, the polynomial method with four coefficients as a function of temperature is used for heat capacity, thermal conductivity and viscosity for flue gas properties in ANSYS-FLUENT. The ideal gas is considered as an available option for density in ANSYS-FLUENT. Table(5.3) shows the flue gas properties in different temperatures.

Table 5.3: Flue gas properties as a function of temperatures [165]

T[°C]	ρ **[kg/m^3]**	**C$_p$ [j/kg.k]**	**k [w/m.K]**	μ **[Pa.s]**
200	0.722433	1109.931	0.037368	2.47E-05
300	0.597489	1134.233	0.043423	2.83E-05
400	0.507785	1159.373	0.049132	3.16E-05
500	0.44211	1185.351	0.054495	3.46E-05
600	0.392452	1210.91	0.059685	3.75E-05
700	0.352406	1236.469	0.064702	4.01E-05
800	0.318767	1260.771	0.069719	4.26E-05
900	0.291536	1283.816	0.07439	0.000045
1000	0.26911	1305.185	0.078888	4.73E-05
1100	0.249888	1324.459	0.083386	4.95E-05
1200	0.232268	1341.219	0.087711	5.17E-05
1300	0.217851	1354.627	0.091863	5.37E-05

5.4.2 Boundary Conditions

In this part of the simulation, the constant mass-flow-inlet is selected as an inlet boundary condition. Species according to Table(5.2) are implemented with inlet temperature $1240K$. For outlet, "outflow" B.C. type is selected which means all normal gradients are zero $\partial/\partial n$ and no-slip B.C. are implemented at the other boundaries.

For the simulation of heat transfer, first the heat loss is roughly estimated by measuring the temperatures of the outer body of the cyclone of the pilot in different parts during experiments in steady-state conditions. It is estimated at approx. $1150watt$. Then, assuming this amount is equal to the heat loss from the body of the cyclone, it is considered in the boundary condition of the wall in the cyclone as a heat flux. To overcome the non-uniformity of temperature in the outer surface of the cyclone reactor, UDF [9] is helpful. Heat loss flux from the cyclone is divided into 11 levels. The average calculated amount of heat-loss flux is considered for each part. UDF used in this part is in Appendix(B).

5.4.3 Simulation strategy

In this part, for convergence criteria, two aspects are considered. First, the scaled residuals should be below 10^{-5}. Second, temperature and velocity as representative quantities are monitored until they reach steady values. For turbulence flow, there is fluctuation for parameters like temperatures and velocity.

The stepwise solution of the heat transfer simulation is including first, solving by steady solver for 8000 iterations, then the unsteady solver, first order, second order and finally QUICk implicit formulation options are used (These stepwise is used to decrease computational time) and a fixed time step size of 10^{-4}s is employed in the simulation of the cyclone.

The solution is converged at each time step with preset scaled residuals of 10^{-5} as convergence criterion for all solution variables.

5.4.4 Results and validation

The model validation is done by comparing the measured temperature profiles in 2 ports (Port1 and Port3 in Figure(3.4)).

[9] User Defined Function

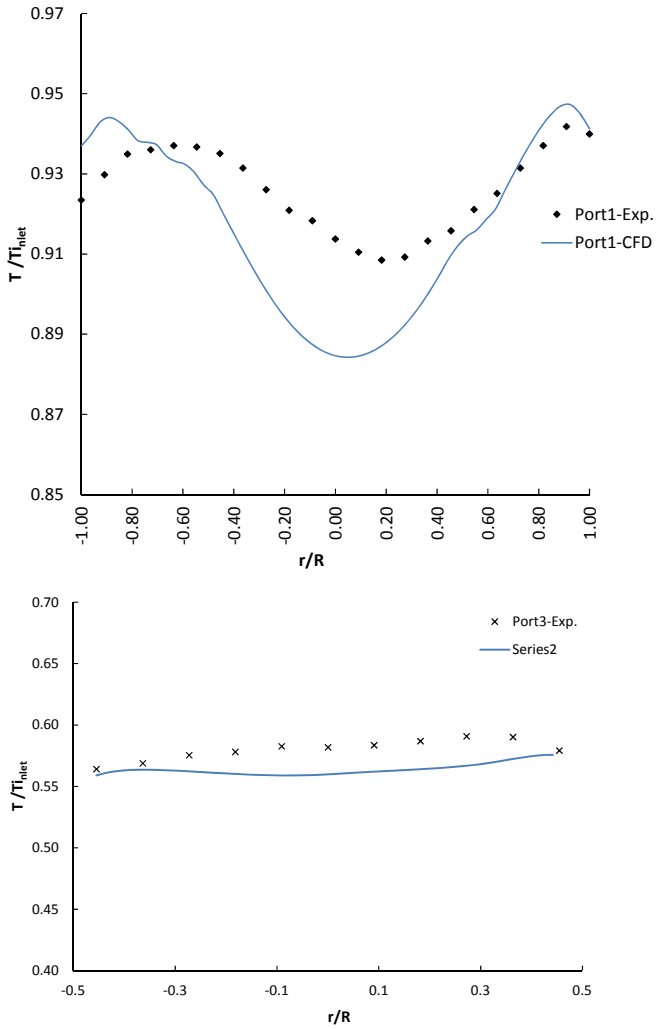

Figure 5.6: Non-dimensional temperature along radial Port 1, Port 2 and Port3

As it can be seen in Figure(5.6) the CFD modeling can low the experiments especially close to the wall.

In Figure(5.7), the contours of the temperature are shown. The temperature in different zones of the cyclone and hence the temperature difference is also clear, which supports the former conclusion from experiments.

Considering the temperature window for the SNCR process, a minimum temperature of $1100K$ (727°C) is needed for SNCR. This area is clearly illustrated in Figure(5.7). Also, the red colors in Figure(5.7) are area in which NH_3 oxidation is more probable to the temperature. In this figure, the green-yellow area shows the proper temperature for SNCR, which is in good agreement with experimental results and the conclusion about the reaction zones.

In the next step of CFD modeling these results and boundary conditions are used.

5.5 CFD modeling of NOx reduction in the cyclone reactor

In this part, the CFD modeling of the SNCR process with injection of ammonia from Port1 in flue gas inside the cyclone is presented and the results are compared with the experimental data.

5.5.1 Modeling approach

In order to understand the SNCR process inside a cyclone reactor CFD program, ANSYS-FLUENT is used in considering the results obtained from the cold mode and heat transfer steps (number of mesh, turbulence model, heat flux as a heat loss and solutions schemes). The finite-rate/eddy dissipation model (see Section(5.5.1)) is used to consider the effects of turbulence-chemistry in the flow.

Boundary conditions The flue gas with flow rate $96m^3/hr$ (equal 0.00733kg/s) at $1240k$ (967°C) is injected into the cyclone (composition of flue gas with NO is listed in Table(5.4)). The flue gas contains $500ppm$ initial NOx in dry flue gas. The ammonia with a molar ratio of 1.25 and a mass-flow rate of $3.043\times10^{-6}kg/s$ is injected from Port1 by a $2mm$ inner diameter nozzle.

Table 5.4: Wet flue gas composition in the inlet of cyclone for the simulation of SNCR

Component	N_2	H_2O	O_2	CO_2	NO
Mole fraction (%)	Balance	10.58	8.11	5.68	0.0497

For predicting the binary mass diffusion coefficient, the method presented by Reid et al. [166] is used. The methodology is based on the Chapman–Enskog

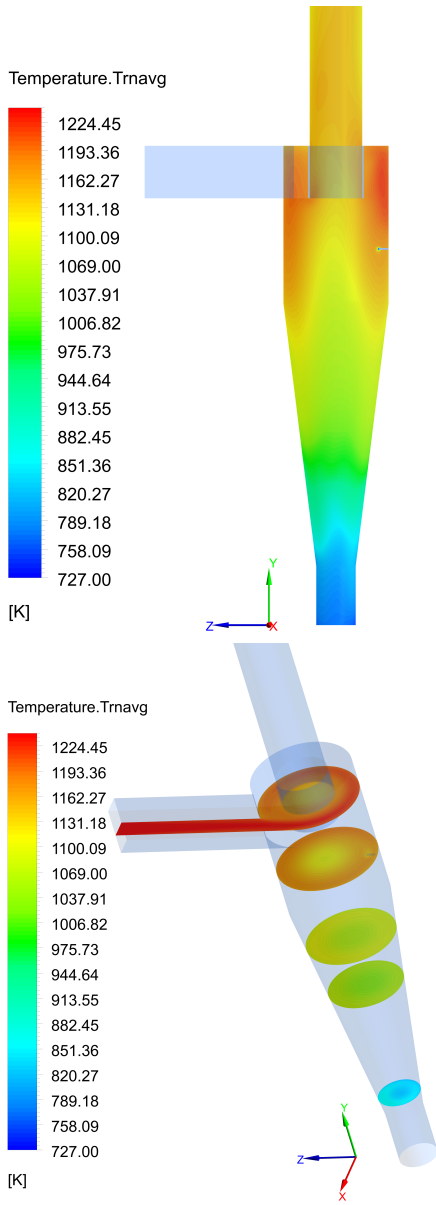

Figure 5.7: Contour of temperature (K)

theoretical description of binary mixtures of gases at low to moderate pressures. The detail is presented in Appendix(C). Because of dependency of the diffusion

coefficient on temperature, the mass diffusion coefficient is defined as a function of temperature by the polynomial function of the temperature by three coefficients in ANSYS-FLUENT.

Kinetics: Mathematical modeling of reaction, especially fast reactions, in turbulent flow is the problem of modeling turbulent flow and chemical kinetics as well as the interaction between the flow and the chemical reactions. In systems where reactions take place in bulk with turbulence flow, the flow description becomes more complicated due to the coupling between the fluid dynamics and the chemical kinetics. In this kind of systems, chemical kinetics is not enough to study the reactions. Turbulent fluctuations may change the apparent chemical production rate. On the other hand, the change in the local mole fraction is thus due to both the mixing and conversion of the reactant. So the mixing of the reactant plays a major role in the reaction rate of the reactant. In mathematical modeling, to simulate the systems, including the reactions, the number of reacting species and thus the number of partial differential equations that describe the change of the mole fraction becomes large, and furthermore the wide spread in length and time scales makes the PDEs stiff, which requires an increased solution time. Therefore, in this kind of system, using a reduced mechanism is recommended to simplify the total model. Also, a link between flow and chemical kinetics needs to be established. Among different approaches, Eddy Dissipation model developed by Magnussen and Hjertager [167] is widely used.

Among several proposed models for the SNCR process, to obtain an acceptable computational time, a simple, practical application of an empirical model proposed by Duo et al. [168] and reduced chemical kinetics mechanism proposed by Brouwer et al. [94] are used. The reaction rates are calculated from Arrhenius rate expressions.

The two-reaction mechanism proposed by Duo et al. [168] includes the following overall reactions: one leading to a reduction (R29) and the other to a formation (R30).

$$NO + NH_3 + \frac{1}{4}O_2 \rightarrow N_2 + \frac{3}{2}H_2O \tag{R29}$$

$$NH_3 + \frac{5}{4}O_2 \rightarrow NO + \frac{3}{2}H_2O \tag{R30}$$

Duo et al. [168] developed a simple kinetic model in a constant O_2 concentration (4% O_2). The rate of reactions are:

$$r_{red.} = k_r \, [NO] \, [NH_3] \tag{5.18}$$

$$r_{ox.} = k_{ox} \, [NH_3] \tag{5.19}$$

This model did not include the influence of the O_2 concentration. Kasuya et al. [169] observed that Duo et al.'s [168] model is valid for the range of 1–20% oxygen concentration. The rate of reaction for NO and NH_3 are:

$$r_{NO} = k_{ox.} \, [NH_3] - k_{red.} \, [NH_3] \, [NO] \tag{5.20}$$

$$r_{NH_3} = -k_{ox.} \, [NH_3] - k_{red.} \, [NH_3] \, [NO] \tag{5.21}$$

The other kinetics model that is considered was developed by Brouwer et al.[94]. The kinetic model is solved for ammonia by considering the two following reactions:

$$NO + NH_3 \rightarrow N_2 + H_2O + H \tag{R31}$$

$$NH_3 + O_2 \rightarrow NO + H_2O + H \tag{R32}$$

The rate of reactions for NO reduction and NH_3 oxidation are:

$$r_{NO} = k_{ox.} \, [NH_3] \, [O_2] - k_{red.} \, [NH_3] \, [NO] \tag{5.22}$$

$$r_{NH_3} = -k_{ox.} \, [NH_3] \, [O_2] - k_{red.} \, [NH_3] \, [NO] \tag{5.23}$$

The rate constant is modeled by the Arrhenius equation in Fluent:

$$K = A_r T^{b_r} exp\left(\frac{-E_r}{RT}\right) \tag{5.24}$$

where A_r is the pre-exponent, b_r the temperature exponent, E_r the activation energy, and R the universal gas constant. The used Arrhenius equation parameters in simulation for mechanisms are listed in Table(5.5).

Table 5.5: Arrhenius parameters used in CFD

	Reaction	A_r	b_r	E_r (J/kmol)
Duo et al. [168]	red	$2.45 \times 10^{17} (m^3/kmole.s)$	0	2.44×10^8
	ox	$2.21 \times 10^{14} (1/s)$	0	3.17×10^8
Brouwer et al. [94]	red	$4.24 \times 10^5 (m^3/kmole.K^{5.3}.s)$	5.3	3.50×10^8
	ox	$350 (m^3/kmole.K^{7.56}.s)$	7.56	5.24×10^8

Some approaches have been suggested to find the interaction between flow and chemical kinetics. One of them, which is widely used, is the Eddy Dissipation model. Eddy dissipation model was originally introduced by Spalding [170] and later generalized by Magnussen and Hjertager [167].

The net rate of production of species i due to the reaction r, $R_{i,r}$ is given by the smaller (i.e., limiting value) of the two expressions below:

Based on the mass fraction of reactants:

$$R_{i,r} = \nu_{i,r} M_{w,i} A \rho \frac{\varepsilon}{k} min_R \left(\frac{Y_R}{\nu_{R,r} M_{w,R}}\right) \tag{5.25}$$

Based on the mass fraction of products:

$$R_{i,r} = \nu_{i,r} M_{w,i} A B \rho \frac{\varepsilon}{k} \frac{\sum_P Y_P}{\sum_j^N \nu_{j,r} M_{w,j}} \tag{5.26}$$

Where k is turbulence kinetic energy, ε is turbulence dissipation rate, Y_p and Y_R are mass fraction of products and reactants, $M_{w,i}$ is molecular weight, subscripts R, P are reactant and products, $\nu_{i,r}$ is stoichiometric coefficient in reaction. A and B are empirical Magnussen constants for reactants. The model constants A and B need to be empirically adjusted for each reaction in each system. The default values of 4 and 0.5 respectively were determined for one and two-step combustion processes by Magnussen [167].

In ANSYS-FLUENT [161], by choosing the Finite-rate/eddy dissipation model, the rate of reaction for species i in reaction r with reactant j is given by the smallest value of Equation(5.22)/Equation(5.20), Equation(5.25) and Equation(5.26). On the other hand, the slowest reaction rate is used to make a more reliable model in any turbulent situation:

- If turbulence is low, mixing is slow and this will limit the reaction rate.
- If turbulence is high, but the kinetic rate is low, this will limit the reaction rate

The system acts as a flexible model to cover different flow patterns and will provide more realistic results.

5.5.2 Results

CFD modeling of the SNCR process inside the cyclone for a case with injecting ammonia in Port1 is done. RSM turbulence model, mesh, and modeling schemes are applied from previous steps together with the finite rate/eddy dissipation model for reactions by using two mechanisms. The results of CFD modeling of NOx concentration in the outlet of the cyclone together with experimental data for a case by adding ammonia in Port1 are listed in Table(5.6) for both mechanisms. The better prediction of the NOx level is obtained with Duo et al.'s [168] mechanism:

$$ppm_{NO} = \frac{molefraction_{NO} \times 10^6}{1 - molefraction_{H_2O}} \tag{5.27}$$

	NOx (ppm)	Error (%)
Exp.	205	
CFD- Duo et al.	216	3.6
CFD- Brouwer et al.	325	38.9881

Table 5.6: Comparing NOx concentration results of CFD modeling's and experimental results for a case by injecting ammonia in Port1 in an outlet of the cyclone in the SNCR process (500ppm initial NOx and 1.25 molar ratio)

To validate the model in this step, detailed NOx concentrations got from CFD results are compared with experimental measurements by taking a sample from

Port0 in different points of the cyclone by inserting a sampling probe in the cyclone, Figure(5.8).

The result shows that the trend of CFD results and experimental data are in good agreement. As can be seen in the upper part of the cyclone, the result is not as good as predicted in the bottom of the cyclone. This difference explains the higher complexity of the system in the upper parts where reaction takes place.

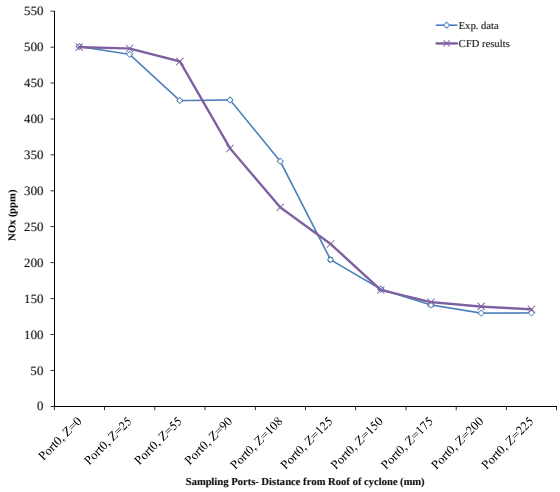

Figure 5.8: Comparing NOx concentration results from CFD with experimental data

To provide knowledge for better understanding, the reaction zone inside the cyclone, important parameters such as residence time, mixing and temperature profile are further analyzed. In the next step, the residence time of ammonia is studied by considering ammonia injection from different ports by DPM [10] method.

Residence time of ammonia and ammonia trajectories by interjection from different ports without considering reactions: In order to obtain of RTD [11], particle tracking by DPM (two phases model) has been used [171,172]. RTD is deduced from the simulation of a pulse injection of a sufficient number of particles (more than 500 particles). The trajectory of a particle (ammonia) is predicted by integrating the force balance on the particle in a Lagrangian

[10] Discrete Phase Model
[11] Residence Time Distribution

reference frame [162]. The characteristics of these particles have been chosen such as they can be considered as perfect tracers of the fluid flow. The diameter of particles are considered $10^{-9}m$ and they have the same density as ammonia. The turbulent dispersion of particles is also taken into account (particles in a turbulent flow are influenced by a randomly varying flow field).

The residence time of ammonia for each port is shown in Figure(5.9). The histograms show the amount of ammonia(%) which has a specific residence time. As an example, for ammonia injecting from Port1, Figure(5.9c), 22.5% ammonia has the residence time of $0.1Second$ and 3.5% of the ammonia shows $1.15Second$.

The mean residence time is listed in Table(5.7). As the results show, ammonia injected in Port3 has the maximum mean residence time among all ports. Considering the ordinary path based on Port3's position and the flows, residence time of the particles when adding to (Port3) upward flow must be less than when it added to the downward flow (Port1). This higher residence time is caused by a different flow at the bottom of the cyclone. The latter conclusion can be observed in the flow pattern study results.

Residence time (s)	**Pin**	**Port0**	**Port1**	**Port2**	**Port3**
average	0.279408	0.141856	0.312476	0.420342	0.725398
min.	0.042886	0.039883	0.036936	0.054456	0.12123
max.	1.6607	0.55767	1.4463	2.0679	3.1121

Table 5.7: Residence time of ammonia by injecting from different ports

In Figure(5.10) and Figure(5.11), the ammonia path-line by injection from different ports are illustrated. For P_{in} it was expected to have the maximum residence time among the other ports; however, the results show that injecting from P_{in} only provides a longer residence time than Port0. As it can be seen in Figure(5.10a), ammonia mostly shortcuts through the vortex finder (in Port0) instead of entering the outer vortex. This shortcut is what makes ammonia residence time less than it was expected to be from the route (distance in a cyclone) for both Port0 and P_{in}.

In a complementary study, Figure(5.11) also shows among the body ports; Port3 has the maximum mean residence time because the velocity at the bottom part of the cyclone is low and, therefore, more time is required to enter the inner vortex to leave the cyclone.

To clarify the flow pattern in the cyclone, the velocity in different heights of the cyclone will be discussed in the next step.

These results show the ammonia trajectories in the cyclone when injecting from

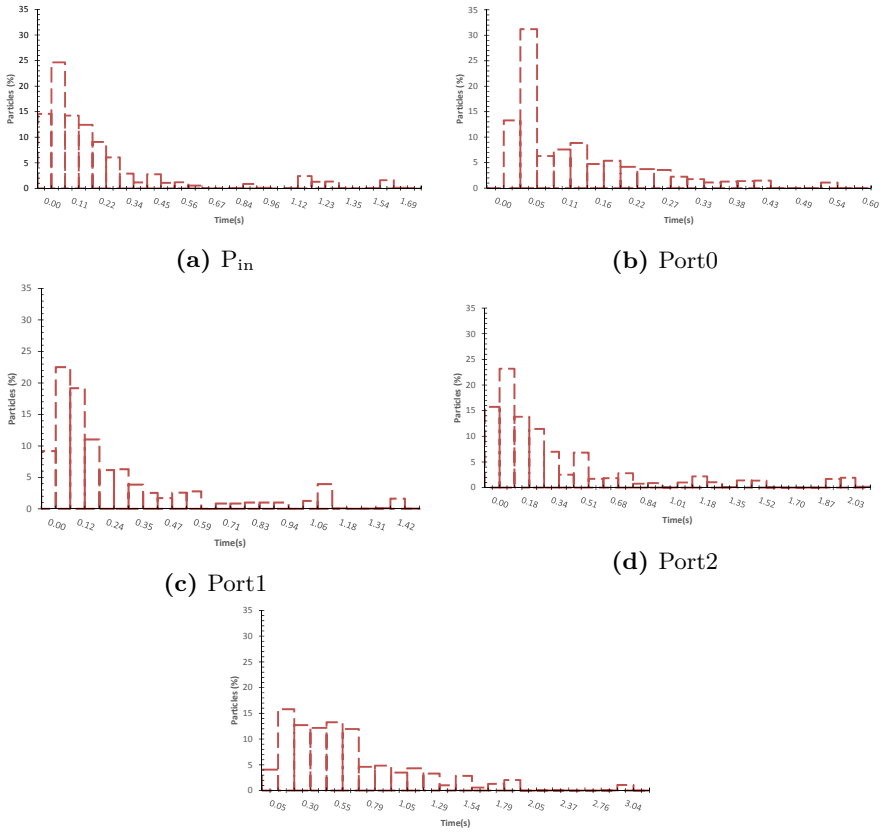

(a) P_{in} **(b)** Port0

(c) Port1 **(d)** Port2

(e) Port3

Figure 5.9: CFD results of residence time of ammonia by injecting from different ports found by DFM (Lagrangian-Lagrangian method)

different ports also show that the residence time is mostly dependent on the fact that ammonia meet the upward flow or downward flow. This knowledge helps to manage both injection position and injection velocity.

As a general conclusion, by adding ammonia from different Ports in the body of the cyclone, ammonia will enter to the exit flow with different residence times. This will provide enough time for ammonia to participate in the reaction when meeting the proper conditions.

Reaction zone: Figure(5.12) shows the streamlines of the flue gas inside the cyclone based on time. As it can be seen, the main part of the flue gas exits the

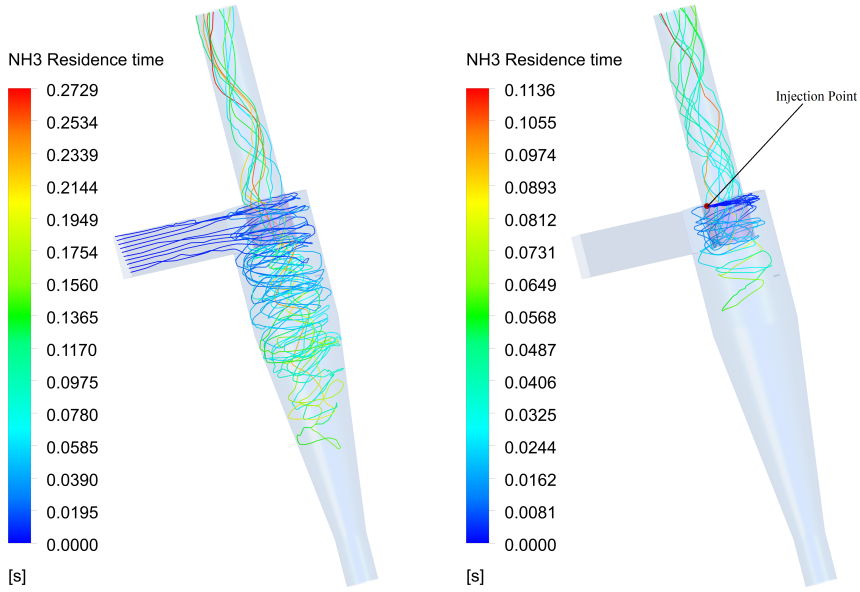

(a) P_{in} **(b)** Port0

Figure 5.10: Ammonia residence time inside the cyclone by adding ammonia from P_{in} an Port0

cyclone without passing the bottom of the cyclone. Most parts of the flue gas enter the inner vortex in the middle of the cyclone and only a very small part of the flue gas reaches deeper to the bottom of the cyclone, the number of stream lines in this figure shows the flue gas behavior in the cyclone.

Considering this result, and back to the Figure(5.11c) for Port3, with injecting ammonia into Port3, the ammonia injected below the main part of the flow (flue gas enters the inner vortex at the middle of the cyclone) and thus cannot meet the upward flow very fast. The high residence time also confirms that ammonia is somehow trapped below the main flow and needs more time to join the main flow-upward.

This phenomenon is supported by a study on flow pattern of the flue gas shown in Figure(5.13) where the streamlines of the flue gas and velocity vector in YZ plane are illustrated. As can be seen in Figure(5.13a), the flue gas with approx. $25m/s$ is fed into the cyclone to create a turbulent swirling flow. The flue gas flows downward in the outer part of the swirl and upward in the center. The change of the flow direction (downward to upward) happened in the middle of the cyclone (of a distance of $260mm$ from the roof of the cyclone in Figure(5.13b)). The slow

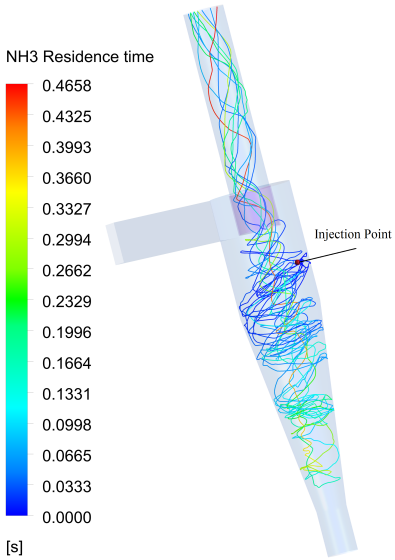

(a) Port1

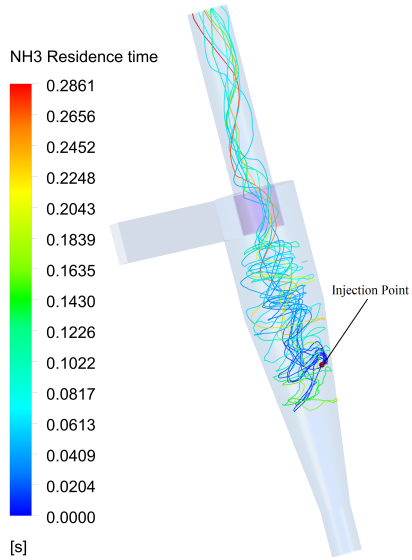

(b) Port2

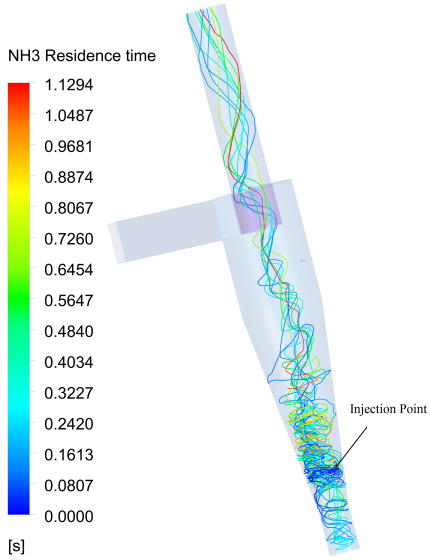

(c) Port3

Figure 5.11: Ammonia residence time inside the cyclone by adding ammonia from Port1, Port2 and Port3

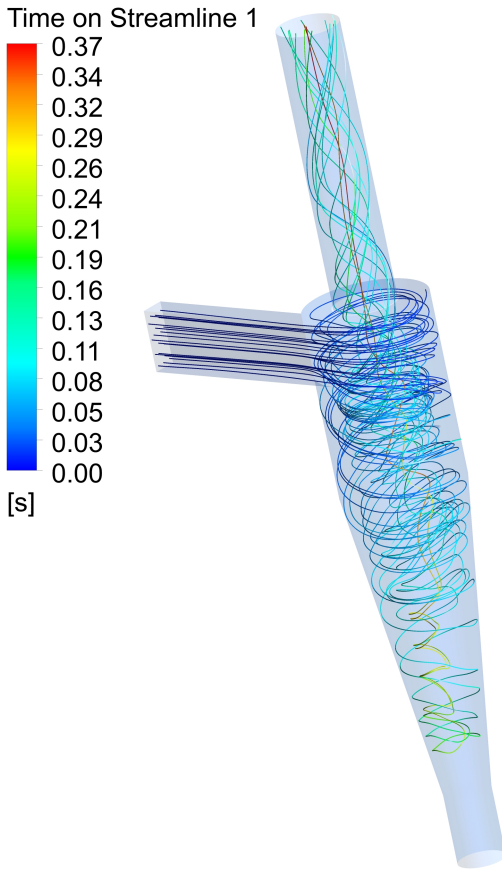

Figure 5.12: streamline inside cyclone based on time on streamline

secondary flow is also presented at the bottom of the cyclone (Figure(5.13a)).

The flow pattern is clearer when velocity vectors are compared for different distances from the roof of the cyclone in horizontal sections (Figure5.14). In Figure(5.14a), the conventional vortex flow can be seen, while in Figure(5.14b) gas flow starts to move toward the wall of the cyclone. In Figure(5.14c), gas in distance $260mm$ from the roof of the cyclone meets the wall, and most parts of the gas enter the inner vortex, the rest angled from the wall directed downward and meet the opposite wall of the cyclone (Figure(5.14d)), explaining the secondary flow behavior. In addition to the fluid direction and pattern planes,

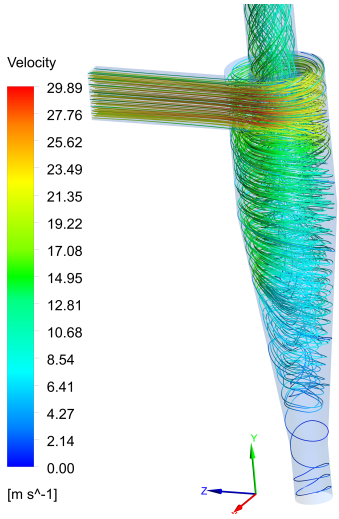

(a) Stream line based on velocity of flue gas

(b) Velocity vector at YZ palne

Figure 5.13: Flow pattern of flue gas inside cyclone

Figure(5.14) also provides knowledge about low-high gas velocity pattern. The higher the velocity, the bolder the vectors. It means in the bottom of the cyclone the velocity of gas is low.

The contours of turbulence intensity are illustrated in Figure(5.15) in the YZ

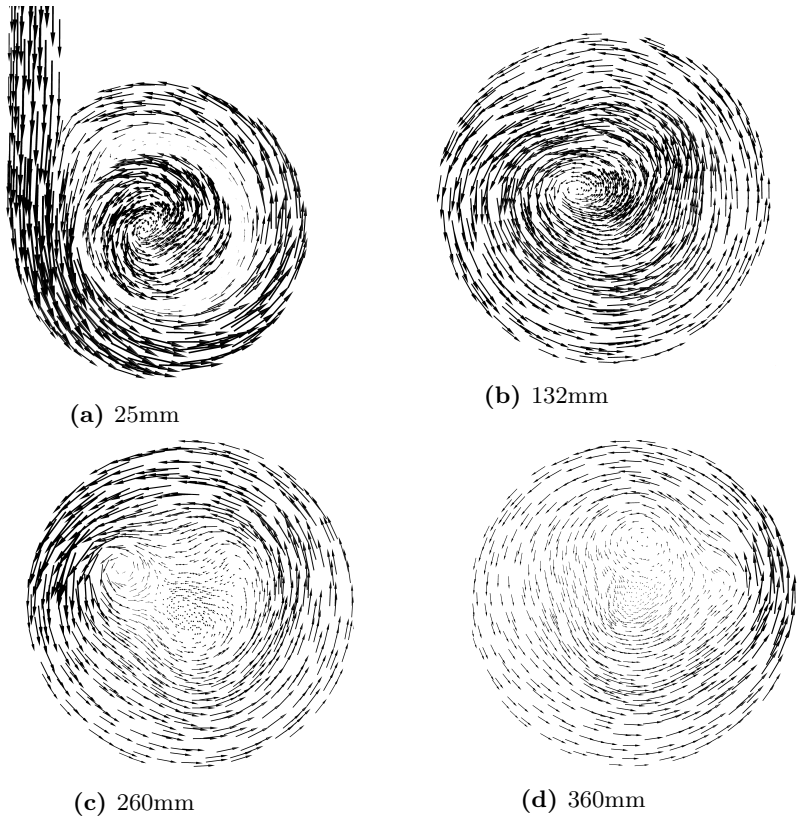

(a) 25mm **(b)** 132mm **(c)** 260mm **(d)** 360mm

Figure 5.14: Velocity vectors at different distance from roof of cyclone

plane. As it can be seen, the turbulence effect is stronger in the inlet of the cyclone and the beginning of vortex finder than in other parts. The turbulence intensity, I, is defined as the ratio of the root-mean-square of the velocity fluctuations to the mean flow velocity.

A turbulence intensity of 1% or less is generally considered low and intensities greater than 10% are considered high. In general, the higher the intensity, the higher the turbulence, which leads to better mixing. In this case, Figure(5.15) shows average intensities approx. 3, showing that injecting ammonia in this area provides good mixing and leads to a higher reaction possibility. This will be clearly mapped in the discussion about reaction zone in the following section.

To study more details on reaction zone, NO concentration distribution provides supportive knowledge about the reaction based on the reaction results in different areas of the cyclone. The results of NO concentration will be presented in

the next step.

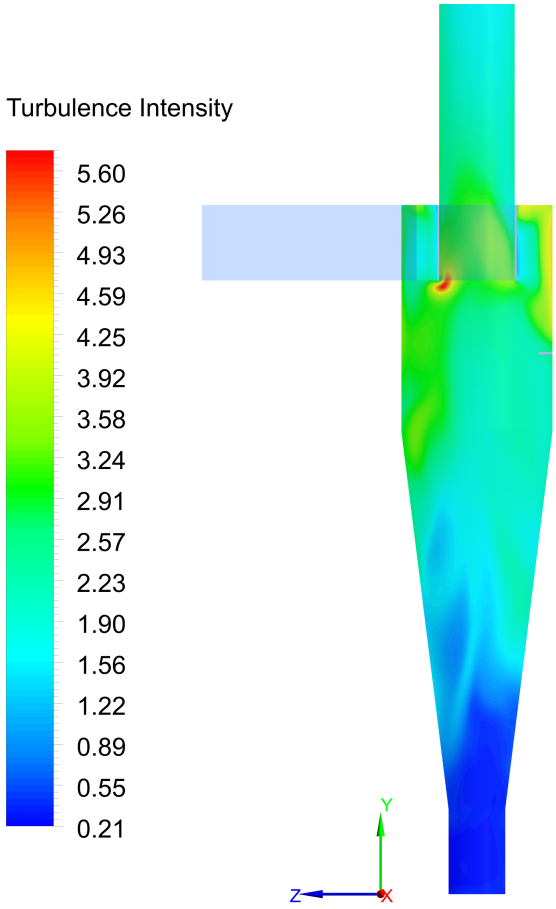

Figure 5.15: Contour of Turbulent intensity in the center of the cyclone in the YZ plane

In this part, contour of NO concentration in *ppm* is illustrated in Figure(5.16), to study the reaction. The ammonia is injected from Port1.

As it can be seen, NO concentration decreases very fast down to the bottom of the cyclone. This shows again that reaction is fast enough to reduce the high amount of NO when ammonia is added from Port1.

The gas flow in the downward direction has a low concentration of NO which is high at the bottom of the cyclone. Considering the initial situation (before injecting ammonia) and the slow flow at the bottom of the cyclone, there is still

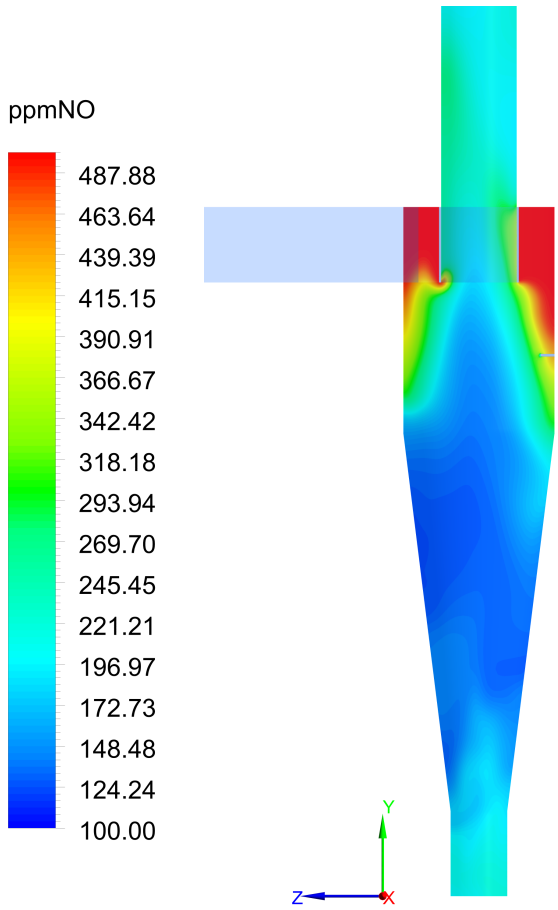

Figure 5.16: Contour of NO concentration in YZ plane(ppm)

a higher amount of NO in this area, which will be decreased with continuing the solution of the CFD model a couple of seconds more. Contour of NO in Figure(5.16) is the result after $8s$. If the solution would continue for a longer period, then the system had enough time to become homogenized at the bottom of the cyclone.

Putting all together, Figure(5.17) illustrates the contour of NO reduction rate. This figure shows that in the upper part of the cyclone, the reaction rate is higher than other parts and the residence time is enough to provide good mixing under the effect of flow pattern and the consequent reaction. Reduction takes place mostly immediately after injecting ammonia. There is also a high chance for reduction of the unreacted parts when passing through the cyclone

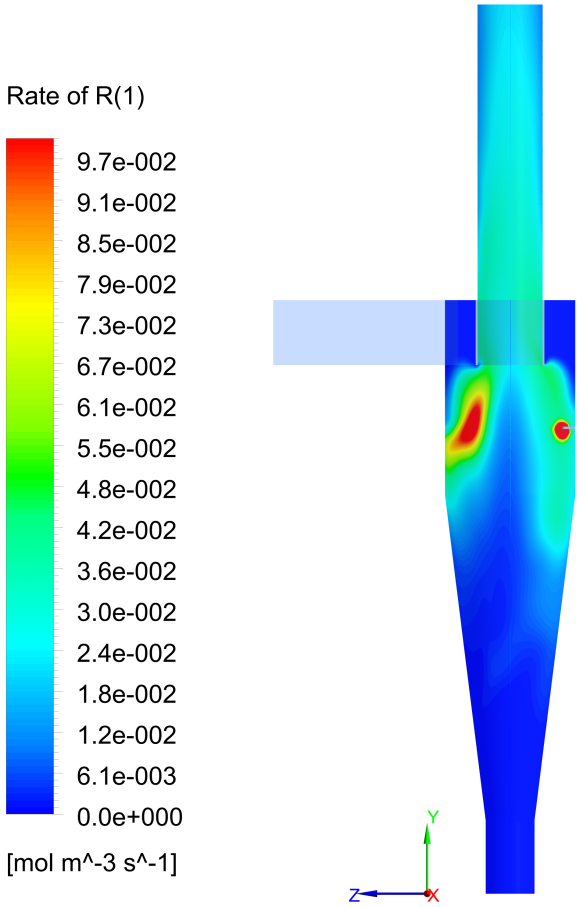

Figure 5.17: Contour of rate of Reaction(R29) in the YZ plane

following the flow pattern and being back to the high-temperature zone. The cyclone swirl flow provides a high residence time for both NO and ammonia. In addition, it provides good mixing conditions so that most of the NO in the cyclone would be reacted. The flow pattern, reaction coutures and concentration distributions explain the high efficiency of the SNCR in the cyclone reactor even when ammonia is injected into regions with low temperature.

To sum up the CFD predictions, results of NO concentration Figure(5.16), temperature profile Figure(5.7), and turbulent intensity Figure(5.15) show that the reaction is most likely to take place in the area between Port1 and Port2 which is named the reaction zone. In the reaction zone, the temperature is in the optimum range, the turbulence is stronger in this zone, which provides better

mixing, and the residence time in this zone with adding ammonia from Port1 is longer (reactants meet the reaction zone both downward and upward). Furthermore, even with adding ammonia from other ports in the body of the cyclone, the reactants still have the chance of meeting the reaction zone following the flow pattern.

Comparing the results of the CFD model with experiments, the model accurately predicted the experimental results. The experiment results also provide the same conclusion about the reaction zone. The CFD model explains the swirl flow effect on both mixing and residence time in detail and maps the flow pattern of the reactants and the reaction detail.

According to the CFD results, the reduction mainly takes place in the zone between Port1 and Port2, where the temperature is in the optimum range of the temperature window for reduction and reactants have the high probability to react due to the mixing effect and residence time.

5.6 Conclusion

The CFD model presented is a part of the study carried out to develop a practical method to provide knowledge about flow patterns and reaction inside a cyclone reactor. CFD simulations have been carried out for simplified reactions and two mechanisms of Duo et al. [168] and Brouwer et al. [94] have been considered. Duo et al.'s mechanism predicts the SNCR reaction in this system better.

The CFD model was first developed for the cold mode. The first step has been validated with the former experiments from the literature.

This first step simulation has been further developed for high temperatures to explain the heat transfer phenomenon inside the cyclone and find the temperature profile as the cyclone reactor is non-isothermal.

CFD results of this step are validated by the experimental results and show good agreement with the experiments.

Afterwards, the SNCR reactions are added to the calculation and all the reaction parameters are discussed and explained.

For the considered reactions, the results of calculations have been verified with the results of experimental measurements presented in the section on experiments performed in a pilot-scale cyclone reactor.

The results have been further employed in the parametric analysis of the reaction

inside the cyclone to study the effect of flow on the reaction in cyclone reactor and recognize the reaction zone, location in which reaction has the most chance of happening.

The results could be applied to optimization, scale-up and design projects considering the importance of fluid dynamics in cyclone reactor.

The developed CFD model provides reasonable results for flow pattern of flue gas, heat transfer, residence time, NO concentration distribution and reaction. With this comprehensive study, the CFD provides a detailed explanation of how swirl flow produces a higher residence time/better mixing in the cyclone.

Results show that the reaction mostly takes place in the upper part of the cyclone which also has proper temperature.

It is also concluded that even when ammonia is injected from the low-temperature zone, reactants still find a chance to be in the high-temperature zone under the effect of swirl flow. So it is expected to have a high SNCR efficiency in the cyclone reactor.

All the stepwise results provide a detailed understanding of the SNCR reactions and flow patterns inside the cyclone reactor which can be used in many different applications. According to the results, the cyclone reactor provides a good mixing and high residence time for reactants mixing together with mapping a reaction zone with the proper temperature.

The CFD model has the potential of being developed further for more focused targets such as design, scale-up and optimization purposes.

Chapter 6

General conclusions and suggestion for future work

6.1 Conclusions

The main objective of this thesis was to provide science-based knowledge regarding the transport phenomenon inside the cyclone reactor for SNCR. In order to achieve this objective, studies were carried out in different steps to understand the process systemically. The three steps are: 1. Design and construction of pilot set-up, 2. Experiments in pilot scale, 3. CFD modeling.

The pilot set-up is designed considering all the practical and theoretical demands of this study. The system can support measurements from many different parts of the cyclone. This flexible measurement potential provides the ability of a detailed experimental study on SNCR in the cyclone reactor.

A large series of experiments are performed to provide a detailed study on both temperature profile and reaction inside the cyclone. Results from these experiments provide practical knowledge about SNCR in a cyclone reactor and could also be used in the validation of our developed CFD model.

A CFD model is then developed to map the flow pattern inside the cyclone reactor and provide a reliable base for a more detailed discussion on mixing and

residence time which has a key role in SNCR. The model is initiated for the cold mode and developed stepwise for supporting all details of the SNCR process in the cyclone reactor considering fluid dynamics. CFD is then validated with pilot scale experiments.

Based on systematic investigations, the main conclusions are summarized as follows:

This cyclone reactor works as a non-isothermal reactor. From both experiments and CFD results, it can be concluded that, in the upper part of the cyclone, the temperature is high enough for NOx reduction. The SNCR process is very sensitive to temperature. At high temperatures, the selectivity of chemical reactions desires oxidation of ammonia to form NOx, and at low temperatures selectivity desires a reduction of NOx. The area which is called reaction zone in this thesis has an optimum temperature range for NOx reduction and avoids ammonia oxidation.

Results show that the reaction mostly takes place in the upper part of the cyclone. In general, in cyclone reactor, wherever the swirl flow plays the main role, the mixing effect is extensively good. With regard to the temperature profile and NOx distribution, the swirl flow is well-generated in the area between Port1 and Port2. This mixing function of swirl flow together with temperature conditions provides a potential reaction zone in this area (between Port1 and Port2).

Adding to the flow effect and temperature, with the high residence time of reactants inside the cyclone, it is highly probable for the reactants to meet this reaction zone even when ammonia is injected from the lower temperature zones, which altogether provides high reduction efficiency and flexible design availability for real case studies.

In the reaction zone, there is a high chance of reaction even for the unreacted reactants which are on the way out of the cyclone (upward flow). Reduction efficiency in different conditions is obtained 54-60%. The higher reduction efficiency (60%) is obtained when ammonia gets injected from the upper part of the cyclone (reaction zone).

Following the parametric experimental investigation, with increasing initial NOx (constant molar ratio) or increase in the molar ratio (constant initial NOx), reduction efficiency will increase.

An investigation in injection velocity is also provided. The effect of injection velocity on reduction efficiency has been chosen as an indicator of mixing. The mixing effect is highly important in SNCR reaction in high temperature to avoid ammonia accumulation and decrease the chance of ammonia oxidation.

Ammonia, therefore, must have dispersed fast into the cross flow (cyclonic flow) and pass through the cyclone downward.

In this part of the study, different ammonia injection velocities have been studied in 3 different injection ports. It is necessary to mention that in all of these three ports ammonia is injected into the high-temperature zone of the cyclone. Adding ammonia into the port inlet, ammonia first meets the inlet cross flow experiments and show no significant effect with increasing injection velocity. There is a chance of ammonia accumulation and hence ammonia oxidation in inlet port which concurred with the reduction and, therefore, no significant increase in reduction efficiency can be seen.

Adding ammonia to Port0 is the most important example to show the relative importance of mixing and interaction of the jet flow and cross flow in the general cyclone efficiency. In this port, ammonia is injected into the upper part of the hot zone of the cyclone. Considering temperature, there is a chance of ammonia oxidation in this area; therefore, it is important that ammonia mixed with cyclonic flow fast and moves to the lower zones where the temperature is lower and oxidation has no chance to take place. Results show that by an increase in ammonia jet velocity, the efficiency is increased significantly until a certain level of velocity, confirming that by increasing the injection velocity the ammonia is mixed fast enough to avoid oxidation and the effect of cyclonic flow to carry ammonia down through the cyclone. Results of the same study with injecting ammonia to Port1 shows no significant effect with the studied jet flows. The efficiency is still slightly increased with increasing ammonia jet flow. Results show that by adding ammonia to Port1, jet flow is distributed into crossflow even with low ammonia injection velocity because the reduction efficiency is at a high level compared to the other experiments. The effect of injection velocity can practically explain the importance of cyclonic flow in providing fast mixing in the cyclone reactor; however, the former Droplet diffusion model [93] and the Damkohler number cannot explain this phenomenon (finding characteristic time scales for mixing) in the presence of the swirl flow. This, of course, needs a comprehensive theoretical study on the importance of mixing in the cyclone reactor which is suggested in future work section.

A complementary experiment on adding particles to the cyclone shows that the system works as a non-isothermal reactor but the temperature difference up-down the cyclone is 100°C lower in the presence of particles. A comparative study on a molar ratio with and without particles shows a lower reduction efficiency in the presence of particles. Results also show that by adding higher amounts of ammonia, the efficiency will increase. This part is also added as a step toward a more realistic approach for an industrial application, which almost always involves particles inside the cyclone. Although it is, in general, concluded that the cyclone reactor is an effective reactor for the SNCR reaction

in the presence of inert particles, there is still need for a detailed study on the cyclone reactor in the presence of different particle types which is recommended for future studies in the next section.

The developed CFD model is predictive for flow pattern (residence time, streamlines, velocity vectors, velocity streamline), turbulent intensity, NO concentration distribution and reaction. Results of CFD model is in good agreement with experimental study. The reaction zone is more clearly investigated with CFD results.

With this comprehensive study, CFD provides a detailed explanation of how swirl flow provides a higher residence time/better mixing in the cyclone. CFD model also has the potential of being further developed for more focused targets such as design, scale-up and optimization purposes.

As a general conclusion, results of experiments and CFD study show that all the stepwise results provide detailed knowledge about the SNCR reactions and flow pattern inside the cyclone reactor which can be a support to any further development study on cyclone reactors. The developed model together with experimental results can be applied to different industrial and research applications.

6.2 Future work

In the current study, the focus was mainly put on the experimental challenges of using cyclone as a reactor and providing flexible measurements to follow the reaction condition in different reaction conditions and injection conditions. The study is also supported by a CFD modeling part which applied to describe the role of the fluid dynamics in providing good reaction conditions and to map more details in the cyclone reactor. The study concluded that cyclone as a reactor has a comparable efficiency for the selected reaction. Different reaction conditions and injection positions have been discussed in detail, which could be used for more practical industrial applications. However, further theoretical, experimental and modeling studies could be targeted specifically to develop more practical theories for the cyclone reactor. Based on the challenges in this study and following the current results, a list of suggestions is provided here. These suggestions are valuable and have a direct focus upon:

- A theoretical study of the cyclonic flow and the importance of the mixing through the cyclone under different conditions of injected gas and cyclonic crossflow is highly recommended because the current theories cannot explain the cyclone reactor situation due to its specific flow. This should be

included as a part explaining both when the gas is injected vertically into the cyclonic flow and radial to the cyclonic flow. There are also possibilities of creating a side flow, distortion or tunneling, which is an interesting subject for discussion. This theoretical study can be sufficiently supported by doing experiments in the presented pilot in its current situation.

- It is also recommended to provide a targeted CFD study to extract mixing time in different conditions. The CFD results could also be validated with some experiments in this pilot. Having a more realistic mixing time estimations is highly beneficial for design purposes.

- As a complementary study with an experimental scope, a study on changing the length of the vortex finder which is expected to affect the flow pattern and temperature profile is suggested. This suggested study is beneficial to carry the injected gas to a more determined temperature zone and practice the changes precisely. This suggested study is more helpful to cover complicated reaction conditions, e.g., in the presence of more reactant spices.

- CFD modeling of SNCR with particle-loaded cyclone and investigation of fluid dynamics under different particle loading situations.

- Study on a gas-solid reaction inside cyclone considering particle flow pattern and the effect of fluid dynamics in cyclone reactor for a gas-solid reaction.

- Application of CFD modeling for scale-up purposes to provide supportive knowledge for SNCR of NOx reduction in large-scale cyclone reactors which can potentially be applied in design and developments in emission control industries.

- CFD study on cyclone geometry for further design studies, this can provide knowledge to be used in designing the new plant (pilot, real scale) and considering the parameters in a preliminary study.

- Industrial application of SNCR in cyclone reactor and investigation of the reaction efficiency, this could be definitely done together with CFD modeling for optimization of the effective parameters and experimental plan.

Appendix A

Flue gas compositions

The fuel used in this system is natural gas which connect to national grid. Daily and monthly composition of natural gas is available in website([155]). In this study the monthly composition (as an example for July 2016) is reported in Table(A.1).

Table A.1: The natural gas composition (July 2016) [155]

CH_4	mol. %	88.64
C_2H_6	mol. %	6.11
C_3H_8	mol. %	2.55
$i-C_4H_{10}$	mol. %	0.39
$n-C_4H_{10}$	mol. %	0.61
$i-C_5H_{12}$	mol. %	0.13
$n-C_5H_{12}$	mol. %	0.09
C_6^+	mol. %	0.04
N_2	mol. %	0.33
CO_2	mol. %	1.11
Lower caloric value	MJ/Nm^3	39.673
Density	kg/Nm^3	0.8298

The target for experiments for example is preparation flue gas with 9% oxygen in dry flue gas and outlet temperature (TE-32 in Figure(3.4)) 1010°C.

As mentioned in Table(A.1), natural gas including; methane, ethane, propane, butane and propane. which mainly is methane. Here the calculation related to methane which is the main of natural gas and air only with considering the nitrogen and oxygen is explained, detailed including the other component of natural gas and air has the same method which is reported in a table to find the final flue gas composition (Calculation basis is combustion of $1 gmol$ methane with oxygen to get 9% oxygen in dry flue gas).

The methane combustion involving the following reaction:

$$CH_4 + 2O_2 \rightarrow CO_2 + 2H_2O \tag{R33}$$

Since the percentage of excess air is based on complete combustion of methane to CO_2 and H_2O, the fact that combustion is not complete has no influence on the calculation of air and excess air (amount of air that enters the combustion process over and above that required for complete combustion).

All of the information for the problem statement has been placed on Figure(A.1).

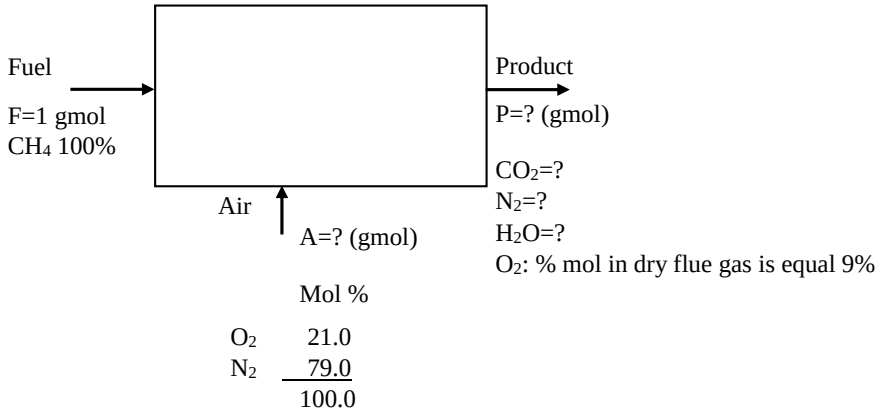

Figure A.1: problem statment

To find out of whether a problem is solvable or not determine the degree of freedom is helpful.

degree-of- freedom analysis for problem is:

Variable: 11

F, A, P, $\overset{A}{n}_{N_2}$, $\overset{A}{n}_{O_2}$, $\overset{P}{n}_{N_2}$, $\overset{p}{n}_{O_2}$, $\overset{p}{n}_{CO_2}$, $\overset{p}{n}_{H_2O}$, $\overset{p}{n}_{CH_4}$, ξ

where:

n_i is number of moles of component i in air or product
ξ is reaction conversion of methane

Equations: 11

- **Basis**: F=1 gmol
- **Species balance**: 5
  CH_4, O_2, N_2, CO_2, H_2O
- **Implicit equation** : 2
  $\sum \overset{p}{n}_i = P$
  $\sum \overset{A}{n}_i = A$
- **Specification**: 3
  $\xi = 1$
  $\overset{A}{n}_{N_2} = \frac{79}{21} \overset{A}{n}_{O_2}$
  $\frac{\overset{p}{n}_{O_2}}{P_{dry}} \times 100 = 9\%$

The degree of freedom is zero. So, there is unique solution for the problem.

The species material balance are:

Compound	Out		In		$\nu_i \times \xi$		gmol
CH_4:	$\overset{p}{n}_{CH_4}$	=	1	-	1×1	=	0
O_2:	$\mathrm{n}\overset{p}{n}_{O_2}$	=	$A \times 0.21$	-	2×1	=	$0.21A - 2$
N_2:	$\overset{p}{n}_{N_2}$	=	$A \times 0.79$	-	0×1	=	$0.79A$
CO_2:	$\overset{p}{n}_{CO_2}$	=	0	+	1×1	=	1.0
H_2O:	$\overset{p}{n}_{H_2O}$	=	0	+	2×1	=	2.0

and $\sum \overset{p}{n}_i = P_{wet}$, So:

$P_{wet} = A + 1$

and $P_{dry} = P_{wet} - n^{p}_{H_2O} = A - 1$

$\%mol\ n^{p}_{O_2} \quad in \quad dry \quad flue \quad gas = 9\%$

Then;

$$\frac{n^{p}_{H_2O}}{P_{dry}P} \times 100 = 9\% \Longrightarrow \frac{0.21A - 2}{A - 1} = 0.09 \Longrightarrow A = 15.92gmol$$

And $P_{dry} = 14.92$, $P_{wet} = 16.92$

Also, The amount of excess air is obtained:

$$\%\quad excess\quad air = 100 \times \frac{(entering\quad air\quad -\quad required\quad air)}{required\quad air} = 100 \times \frac{15.92-9.52}{9.52}$$

$$\%\quad excess\quad air = 67.22\%$$

The composition of flue gas from combustion of 1gmole methane with 67.22% excess air is listed for dry and wet flue gas in Table(A.2).

Table A.2: gmoles and gmol percent of combustion of 1gmol methane with 67.22 % excess air

	Wet		**Dry**	
Compound	**gmol**	**% gmol**	**gmol**	**% gmol**
$\mathbf{CH_4}$	0	0	0	
$\mathbf{O_2}$	1.34	7.93	1.34	9.00
$\mathbf{N_2}$	12.57	74.33	12.57	84.30
$\mathbf{CO_2}$	1	5.91	1	6.7
H_2O	2	11.82	0	0
Total	16.91	100	14.91	100

The same procedure and same assumption is applied to calculate results for real case with more real natural gas composition (Table(A.1)), air composition (Table(A.3))) with 10% relative humidity in air. The results of calculation is listed in Table(A.4) for $16.7Nl/min$ which is equal 44.15 $gmol/hr$ and final must be 9% O2 concentration in dry flue gas.

Calculation results show, the combustion must be done with 74% excess air.

Table A.3: Dry air composition

Composition	gmol%
CO_2	0.03
N_2	78.09
Ar	0.93
O_2	20.95
H_2O	0.00
Total(dry)	100.00

Table A.4: Calculation results of 44.15 *gmol/hr* natural gas combustion to get 9% O_2 concentration in dry flue gas with 10% RH

Composition	%gmol in NG[1]	%gmol in air	gmol/hr in NG	gmol/hr in air	gmol O_2 consummed	gmol CO_2 produced	gmol H_2O produced	gmol in Flue gas	%gmol(wet) Flue gas	%gmol(dry)
CH_4	88.64	0.00	39.13	0.00	78.27	39.13	78.27	0.00	0.00	0.00
C_2H_6	6.11	0.00	2.70	0.00	9.44	5.40	8.09	0.00	0.00	0.00
C3H_8	2.45	0.00	1.08	0.00	5.41	3.25	4.33	0.00	0.00	0.00
C_4H_{10}	1.1	0.00	0.49	0.00	3.16	1.94	2.43	0.00	0.00	0.00
C_5H_{12}	0.22	0.00	0.10	0.00	0.78	0.49	0.58	0.00	0.00	0.00
C6H_{14}	0.04	0.00	0.02	0.00	0.17	0.11	0.12	0.00	0.00	0.00
CO_2	1.11	0.03	0.49	0.27	0.00	0.00	0.00	51.07	5.72	6.41
N_2	0.33	78.09	0.15	629.7	0.00	0.00	0.00	674.2	75.57	84.60
Ar	0	0.93	0.00	7.53	0.00	0.00	0.00	0.00	0.00	0.00
O_2	0	20.95	0.00	168.9	0.00	0.00	0.00	71.69	8.04	9.00
H_2O	0	0.00	0.00	1.34	0.00	0.00	0.00	95.16	10.67	0.00
Total(dry)	100.0	100.0	44.15	806.4	97.22	50.31	93.82	797.0	0.00	100.0
Total(wet)	100.0	100.0	44.15	807.7	97.22	50.31	93.82	892.2	100.0	0.00

Appendix B

User Defined Function

A UDF [1] is a C function that can be dynamically loaded with the FLUENT solver to enhance the standard features of the code. For example, a UDF can be used to define specified boundary conditions, material properties, and source terms for flow regime, as well as specify customized model parameters (e.g., DPM, multiphase models), initialize a solution, or enhance post-processing.

In this study, to over come the non-uniformity of temperature in outer surface of cyclone reactor, UDF (DEFINE-PROFILE-FLUX) is used to explicitly set the heat flux along a wall. In y-direction heat flux is divided in 6 level with different heat flux values.

The UDF presented below, generate a heat lost rate profile for a cyclone wall. Once interpreted or compiled, it can br activate this UDF in the Wall boundary condition panel in ANSYS-FLUENT.

[1] User Defined Function

```
#include "udf.h"

DEFINE_PROFILE(heat_flux,thread,i)
{
 real x[ND_ND];

 face_t f;

 begin_f_loop(f,thread)

  {
   F_CENTROID (x,f,thread);

    if(x[1] <= 0.062)

   F_PROFILE(f,thread,i) =-700;

     else if(x[1] <= 0.137 && x[1] > 0.062)

   F_PROFILE(f,thread,i) =-2500;

    else if(x[1] <= 0.212 && x[1] > 0.137)

   F_PROFILE(f,thread,i) =-4600;

    else if(x[1] <= 0.275 && x[1] > 0.212)

   F_PROFILE(f,thread,i) =-5000;

    else if(x[1] <= 0.337 && x[1] > 0.275)

   F_PROFILE(f,thread,i) =-5300;

    else if(x[1] <= 0.392 && x[1] > 0.337)

   F_PROFILE(f,thread,i) =-5500;

    else if(x[1] <= 0.447 && x[1] > 0.392)

   F_PROFILE(f,thread,i) =-5000;

    else if(x[1] <= 0.475 && x[1] > 0.447)

   F_PROFILE(f,thread,i) =-7500;

    else if(x[1] <= 0.502 && x[1] > 0.475)

   F_PROFILE(f,thread,i) =-9000;

    else if(x[1] <= 0.6 && x[1] > 0.502)

   F_PROFILE(f,thread,i) =-7000;

    else

   F_PROFILE(f,thread,i) =-5000;

  }

end_f_loop(f,thread);

 }
```

The overall height of cyclone is divided into 11 unequal parts with different amount of heat loss as it is shown in Figure(B.1).

To obtain the heat loss values, first value were obtained by calculation with experimental results, then they optimized by changing the values to get good results regarding to temperature profiles.

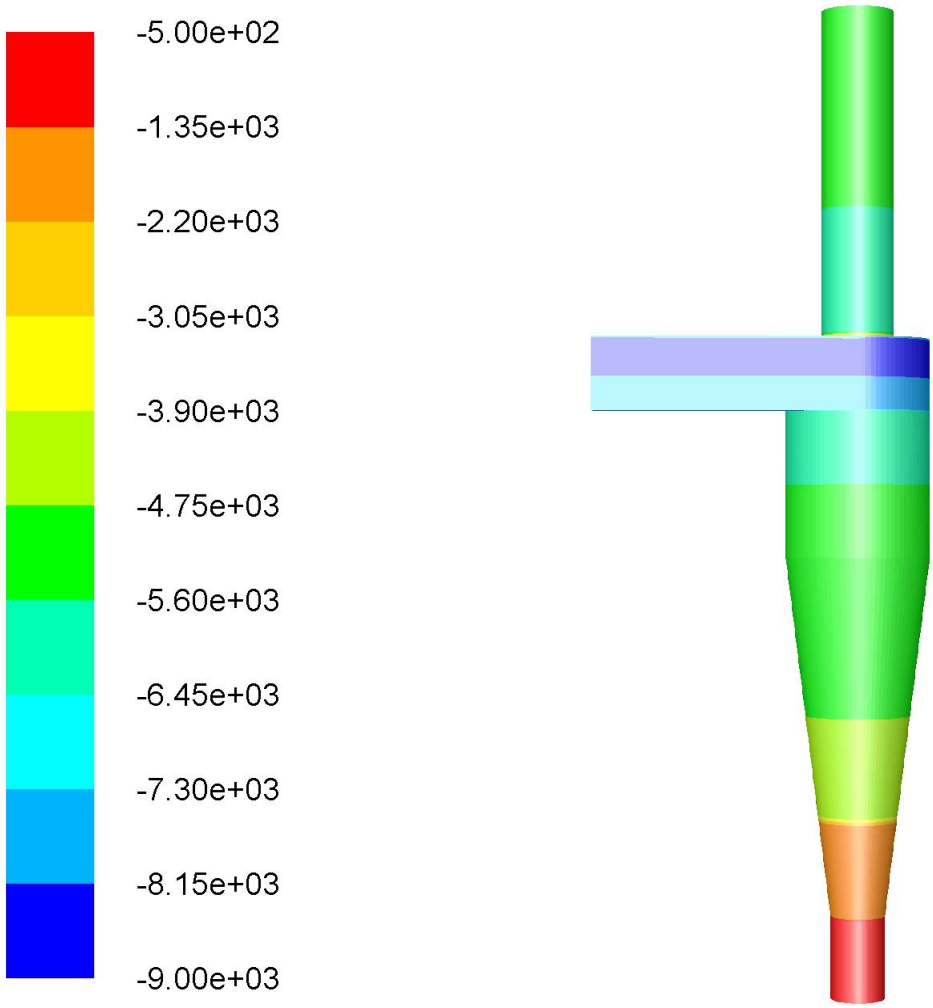

Figure B.1: Heat loss flux profile along the cyclone body

Appendix C

Binary Diffusion Coefficients for Flue gas composition

For predicting binary mass diffusion coefficient, the method presented by Reid et. al [166] is used. The methodology is based on the Chapman–Enskog theoretical description of binary mixtures of gases at low to moderate pressures. In this method, the binary diffusion coefficient for the species pair A and B is calculated by:

$$D_{AB} = \frac{3}{16} \frac{(4\pi k_B T/MW_{AB})^{1/2}}{(P/RT)\,\pi\sigma_{AB}^2\Omega_D} f_D \tag{C.1}$$

Where; k_B is the Boltzmann constant, T is the temperature in Kelvin, P is the pressure in Pascal, R is the universal gas constant, f_D is a theoretical correction factor whose value is sufficiently close to 1 to be assumed to be the same. The other terms are defined as below:

$$MW_{AB} = \frac{2}{(1/MW_A) + (1/MW_B)} \tag{C.2}$$

Where, MW_A and MW_B are the molecular weights of species A and B.

$$\sigma_{AB} = \frac{\sigma_A + \sigma_B}{2} \tag{C.3}$$

Where, σ_A and σ_B are the hard-sphere collision diameter of species A and B. Values of which are listed in Table(C.1) for used species in ANSYS-FLUENT [173].

The collision integral, Ω_D, is a dimensionless quantity calculated using the following expression:

$$\Omega_D = \frac{A}{(T^*)^B} + \frac{C}{exp(DT^*)} + \frac{E}{exp(FT^*)} + \frac{G}{exp(HT^*)} \tag{C.4}$$

Where;

A=1.06036 E=1.03587
B=0.15610 F=1.52996
C=0.03587 G=1.76474
D=0.47635 H=3.89411

and the dimensionless temperature T^* id defined by:

$$T^* = \frac{k_B T}{\varepsilon_{AB}} = \frac{k_B T}{(\varepsilon_A \varepsilon_B)^{1/2}} = \frac{T}{\left[\left(\frac{\varepsilon_A}{k_B}\right)\left(\frac{\varepsilon_B}{k_B}\right)\right]^{1/2}} \tag{C.5}$$

Values of the characteristic Lennard-Jones energy, ε/k_B are also listed in Table(C.1) for considering species in this project.

Table C.1: Lennard-Jones parameters and molecular weigh of species [173]

Species	$\sigma(^\circ A)$	$\varepsilon/k_B(K)$	$MW(gr/mol)$
Air	3.71	78.60	28.97
CO	3.69	91.70	28.01
CO_2	3.94	195.2	44.01
H_2O	2.64	809.1	18.02
NH_3	2.90	558.3	17.03
NO	3.49	116.7	30.01
N_2	3.80	71.40	28.01
N_2O	3.83	232.4	44.01
O_2	3.47	106.7	15.99

Substituting numerical values for the constants in Eq(C.1) results the below equation:

$$D_{AB} = \frac{0.0266T^{3/2}}{PMW_{AB}^{1/2}\sigma_{AB}^{2}\Omega_{D}} \tag{C.6}$$

With the following units:

D_{AB} :	m^2/s
T :	K
P :	Pa
σ_{AB} :	$^{\circ}A$

Bibliography

[1] D. Leith and D. Mehta. Cyclone performance and design. *Atmos. Environ.*, 7(5):527–549, May 1973.

[2] P.R. Taylor and R.W. Bartlett. Reduction of taconite concentrates in a cyclone reactor. *Minerals & metallurgical processing*, 11(4):203–209, 1994.

[3] N.W. Green, K. Duraiswamy, and R.E. Lumpkin. Pyrolysis with cyclone burner, July 1978. US Patent 4,102,773.

[4] L. Araujo and J. Campos. Gasification of pine and cork suspensions in a cyclone reactor. *Combustion Technologies for a Clean Environment*, 1:479, 1995.

[5] J.S. Barnhart and N.M. Laurendeau. Pulverized coal combustion and gasification in a cyclone reactor. 1. Experiment. *Ind. Eng. Chem. Process Des. Dev.*, 21(4):671–680, October 1982.

[6] Y.c. Zhang, Z.b. Wang, and Y.h. Jin. Simulation and experiment of gas–solid flow field in short-contact cyclone reactors. *Chem. Eng. Res. Des.*, 91(9):1768–1776, September 2013.

[7] V.V. Ranade. *Computational Flow Modeling for Chemical Reactor Engineering*. Process systems engineering. Academic Press, 2002.

[8] A.J. ter Linden. Investigations into cyclone dust collectors. *Arch. Proc. Inst. Mech. Eng. 1847-1982 (vols 1-196)*, 160(1949):233–251, January 1949.

[9] R. Parker, R. Jain, S. Calvert, D. Drehmel, and J. Abbott. Particle collection in cyclones at high temperature and high pressure. *Environ. Sci. Technol.*, 15(4):451–458, April 1981.

[10] J. Chen and M. Shi. Analysis on cyclone collection efficiencies at high temperatures. *China Particuology*, 1(1):20–26, April 2003.

[11] R. Dewil, J. Baeyens, and B. Caerts. CFB cyclones at high temperature: Operational results and design assessment. *Particuology*, 6(3):149–156, 2008.

[12] M. Trefz and E. Muschelknautz. Extended cyclone theory for gas flows with high solids concentrations. *Chem. Eng. Technol.*, 16(3):153–160, June 1993.

[13] J.L. Smith. An Analysis of the Vortex Flow in the Cyclone Separator. *J. Basic Eng.*, 84(4):609, 1962.

[14] A.C. Hoffmann and L.E. Stein. *Gas Cyclones and Swirl Tubes: Principles, Design, and Operation.* Springer-Verlag Berlin Heidelberg, 2007.

[15] H. Mothes and F. Löffler. Motion and deposition of particles in cyclones. *German chemical engineering*, 8(4):223–233, 1985.

[16] J. Gimbun, T.G. Chuah, A. Fakhru'l-Razi, and T.S.Y. Choong. The influence of temperature and inlet velocity on cyclone pressure drop: a CFD study. *Chem. Eng. Process. Process Intensif.*, 44(1):7–12, January 2005.

[17] M. Azadi, M. Azadi, and A. Mohebbi. A CFD study of the effect of cyclone size on its performance parameters. *J. Hazard. Mater.*, 182(1-3):835–41, October 2010.

[18] K. Elsayed and C. Lacor. The effect of cyclone inlet dimensions on the flow pattern and performance. *Appl. Math. Model.*, 35(4):1952–1968, April 2011.

[19] J.J. Derksen, S. Sundaresan, and H.E.A. van den Akker. Simulation of mass-loading effects in gas–solid cyclone separators. *Powder Technol.*, 163(1-2):59–68, April 2006.

[20] W. Peng, A.C. Hoffmann, P.J.A.J. Boot, A. Udding, H.W.A. Dries, A. Ekker, and J. Kater. Flow pattern in reverse-flow centrifugal separators. *Powder Technol.*, 127(3):212–222, November 2002.

[21] J. Szekely, J. Evans, and S. H.Y. *Gas-solid reactions.* Academic Press, 1976.

[22] J. Lede, F. Verzaro, B. Antoine, and J. Villermaux. Flash pyrolysis of wood in a cyclone reactor. *Chem. Eng. Process. Process Intensif.*, 20(6):309–317, November 1986.

[23] R. Galiasso, Y. González, and M. Lucena. New inverted cyclone reactor for flash hydropyrolysis. *Catal. Today*, 220-222:186–197, 2014.

[24] E. Bramer and G. Brem. A novel technology for fast pyrolysis of biomass: PyRos reactor. In *Twelfth European Biomass Conference: Biomass for Energy, Industry and Climate Protection*, 2002.

[25] L.C. Lin, F.V. Hanson, A.G. Oblad, and J.D. Westhoff. The Pyrolysis of Bitumen-Impregnated Sandstone in Short Contact Time Reactors, I. Cyclone reactor. *Fuel Process. Technol.*, 16(2):173–190, April 1987.

[26] S. Luidold, H. Antrekowitsch, and R. Ressel. Production of niobium powder by magnesiothermic reduction of niobium oxides in a cyclone reactor. *Int. J. Refract. Met. Hard Mater.*, 25(5-6):423–432, September 2007.

[27] J.S. Barnhart, J.F. Thomas, and N.M. Laurendeau. Pulverized coal combustion and gasification in a cyclone reactor. 2. Model and comparison with experiment. *Ind. Eng. Chem. Process Des. Dev.*, 21(4):681–689, October 1982.

[28] G. Manenti and M. Masi. Simulation study of production of fine ceramic powders in a cyclone reactor. *Chemical Engineering and Processing: Process Intensification*, 50(2):151–159, February 2011.

[29] W. Barth. Design and layout of the cyclone separator on the basis of new investigations. *Brenn. Warme Kraft*, 8(1), 1956.

[30] R.M. Alexander. Fundamentals of cyclone design and operation. *Proc. Aus. Inst. Min. Met. NS*, 152(3):152–153, 1949.

[31] E. Muschelknautz and W. Krambrock. Design of cyclone separators in the engineering practice. *Staub-Reinhalt. Luft*, 30(5):1–12, 1970.

[32] C.B. Shepherd and C.E. Lapple. Flow Pattern and Pressure Drop in Cyclone Dust Collectors. *Ind. Eng. Chem.*, 31(8):972–984, August 1939.

[33] C.B. Shepherd and C.E. Lapple. Flow Pattern and Pressure Drop in Cyclone Dust Collectors Cyclone without Intel Vane. *Ind. Eng. Chem.*, 32(9):1246–1248, September 1940.

[34] *The collection efficiency of cyclone type particle collectors: a new theoretical approach*, volume 68, 1972.

[35] D. Morgan, M. Biffin, S.Y. No, and N. Syred. An anlysis of the behaviour of non-slagging, coal fired, cyclone combustors using a phenomenological model. *Symp. Combust.*, 22(1):175–182, January 1989.

[36] C.R. Brunner. National ambient air quality standards. In *Hazardous Air Emissions from Incineration*, pages 27–37. Springer, 1985.

[37] Agency European Environment. European Union emission inventory report 1990–2014 under the UNECE Convention on Long-range Transboundary Air Pollution (LRTAP), 2014.

[38] Y.B. Zeldovich, D.A. Frank-Kamenetskii, and P. Sadovnikov. *Oxidation of nitrogen in combustion*. Publishing House of the Acad of Sciences of USSR, 1947.

[39] K.B. Schnelle and C.A. Brown. *Air Pollution Control Technology Handbook*. Mechanical engineering handbook series. CRC Press, 2002.

[40] D.W. Pershing and J.O.L. Wendt. Relative Contributions of Volatile Nitrogen and Char Nitrogen to NO_x Emissions from Pulverized Coal Flames. *Ind. Eng. Chem. Process Des. Dev.*, 18(1):60–67, January 1979.

[41] S. Mahmoudi, J. Baeyens, and J.P.K. Seville. NOx formation and selective non-catalytic reduction (SNCR) in a fluidized bed combustor of biomass. *Biomass and Bioenergy*, 34(9):1393–1409, September 2010.

[42] Elsevier. *Reduction of sulfur trioxide and nitrogen oxides by secondary fuel injection*, volume 14, 1973.

[43] S.C. Wood. Select the Right NOx Control Technology. *Chemical Engineering Progress*, page 33, 1994.

[44] J.J. Van Eerden, C.F. Gottschlich, and W.C. Gensler. Low NOx burner, September 1991. US Patent 5,044,931.

[45] A. Garg. Specify better low-NOx burners for furnaces. *Chemical Engineering Progress;(United States)*, 90(1), 1994.

[46] X. Hu, J.J. Zhang, S. Mukhnahallipatna, J. Hamann, M.J. Biggs, and P. Agarwal. Transformations and destruction of nitrogen oxides - NO, NO_2 and N_2O - In a pulsed corona discharge reactor. *Fuel*, 82(13):1675–1684, 2003.

[47] H. Lin, X. Gao, Z. Luo, K. Cen, and Z. Huang. Removal of NOx with radical injection caused by corona discharge. *Fuel*, 83(10):1349–1355, July 2004.

[48] A.a. Basfar, O.I. Fageeha, N. Kunnummal, S. Al-Ghamdi, A.G. Chmielewski, J. Licki, A. Pawelec, B. Tyminski, and Z. Zimek. Electron beam flue gas treatment (EBFGT) technology for simultaneous removal of SO_2 and NOx from combustion of liquid fuels. *Fuel*, 87(8-9):1446–1452, 2008.

[49] T.w. Chien and H. Chu. Removal of SO_2 and NO from flue gas by wet scrubbing using an aqueous $NaClO_2$ solution. *J. Hazard. Mater.*, 80(1-3):43–57, December 2000.

[50] D.S. Jin, B.R. Deshwal, Y.S. Park, and H.K. Lee. Simultaneous removal of SO_2 and NO by wet scrubbing using aqueous chlorine dioxide solution. *J. Hazard. Mater.*, 135(1-3):412–417, 2006.

[51] K. Chandrasekara Pillai, S.J. Chung, T. Raju, and I.S. Moon. Experimental aspects of combined NOx and SO_2 removal from flue-gas mixture in an integrated wet scrubber-electrochemical cell system. *Chemosphere*, 76(5):657–664, July 2009.

[52] G. Busca, L. Lietti, G. Ramis, and F. Berti. Chemical and mechanistic aspects of the selective catalytic reduction of NO<SUB align=right>x by ammonia over oxide catalysts: A review. *Applied Catalysis B: Environmental*, 18(1):1–36, 1998.

[53] R.M. Heck. Catalytic abatement of nitrogen oxides–stationary applications. *Catalysis Today*, 53(4):519–523, 1999.

[54] D. Yang, J. Li, M. Wen, and C. Song. Selective catalytic reduction of NOx with methane over indium supported on tungstated zirconia. *Catal. Commun.*, 8(12):2243–2247, December 2007.

[55] K.i. Shimizu and A. Satsuma. Hydrogen assisted urea-SCR and NH_3-SCR with silver–alumina as highly active and SO_2-tolerant de-NOx catalysis. *Appl. Catal. B: Environ.*, 77(1-2):202–205, November 2007.

[56] G. Carja, Y. Kameshima, K. Okada, and C.D. Madhusoodana. Mn–Ce/ZSM_5 as a new superior catalyst for NO reduction with NH_3. *Appl. Catal. B: Environ.*, 73(1-2):60–64, April 2007.

[57] W. Xu, Y. Yu, C. Zhang, and H. He. Selective catalytic reduction of NO by NH_3 over a Ce/TiO_2 catalyst. *Catal. Commun.*, 9(6):1453–1457, March 2008.

[58] X. Wang, S. Zhang, Q. Yu, and H. Yang. Tungsten promoted HZSM-5 in the SCR of NO by acetylene. *Microporous Mesoporous Mater.*, 109(1-3):298–304, March 2008.

[59] Y. Li and Q. Zhong. The characterization and activity of F-doped vanadia/titania for the selective catalytic reduction of NO with NH_3 at low temperatures. *J. Hazard. Mater.*, 172(2-3):635–640, December 2009.

[60] M. Fu, C. Li, P. Lu, L. Qu, M. Zhang, Y. Zhou, M. Yu, and Y. Fang. A review on selective catalytic reduction of NOx by supported catalysts at 100–300 °C—catalysts, mechanism, kinetics. *Catal. Sci. Technol.*, 4(1):14–25, 2014.

[61] K. Cheng, W. Song, Y. Cheng, J. Liu, Z. Zhao, and Y. Wei. Selective catalytic reduction over size-tunable rutile TiO_2 nanorod microsphere-supported CeO_2 catalysts. *Catal. Sci. Technol.*, 2016.

[62] R.K. Lyon. Method for the reduction of the concentration of NO in combustion effluence using ammonia, August 19 1975. US Patent 3,900,554.

[63] J.a. Caton and Z. Xia. The Selective Non-Catalytic Removal (SNCR) of Nitric Oxides From Engine Exhaust Streams: Comparison of Three Processes. *J. Eng. Gas Turbines Power*, 126(2):234, 2004.

[64] J.A. Miller and C.T. Bowman. Mechanism and modeling of nitrogen chemistry in combustion. *Prog. Energy Combust. Sci.*, 16(4):347, January 1990.

[65] F. Birkhold, U. Meingast, P. Wassermann, and O. Deutschmann. Modeling and simulation of the injection of urea-water-solution for automotive SCR DeNOx-systems. *Appl. Catal. B Environ.*, 70(1-4):119–127, 2007.

[66] R.K. Lyon. The NH_3-NO-O_2 reaction. *Int. J. Chem. Kinet.*, 8(2):315–318, March 1976.

[67] R.k. Lyon. Kinetics and Mechanism of thermal DeNOx: A Review. *194th Annu. ACS Meet. Div. Fuel Chem.*, (15):433–443, 1987.

[68] L.J. Muzio, J.K. Arand, and D.P. Teixeira. Gas phase decomposition of nitric oxide in combustion products. *Symposium (International) on Combustion*, 16(1):199–208, January 1977.

[69] D. Lucas and N.J. Brown. Characterization of the selective reduction of NO by NH_3. *Combust. Flame*, 47:219–234, January 1982.

[70] C.P. Fenimore. Destruction of NO by NH_3 in lean burnt gas. *Combust. Flame*, 37(3):245–250, January 1980.

[71] M.A. Kimball-Linne and R.K. Hanson. Combustion-driven flow reactor studies of thermal DeNOx reaction kinetics. *Combust. Flame*, 64(3):337–351, June 1986.

[72] L.J. Muzio, K.L. Maloney, and J.K. Arand. Reactions of NH_3 with NO in coal-derived combustion products. *Symposium (International) on Combustion*, 17(1):89–96, January 1979.

[73] S.M. Banna and M.C. Branch. Mixing and reaction of NH_3 with NO in combustion products. *Combust. Flame*, 42(2):173–181, January 1981.

[74] P. Lodder and J.B. Lefers. Effect of natural gas, C_2H_6 and CO on the homogeneous gas phase reduction of NOx by NH_3. *Chem. Eng. J.*, 30(3):161–167, June 1985.

[75] M. Jødal, C. Nielsen, T. Hulgaard, and K. Dam-Johansen. Pilot-scale experiments with ammonia and urea as reductants in selective non-catalytic reduction of nitric oxide. *Symp. Combust.*, 23(1):237–243, January 1991.

[76] R.M. Iron, H.J. Price, and R.T. Squires. Tailoring Ammonia-based SNCR for instalation on power station boilers. In *Jt. Symp. Station. Combust. NOx Control*, pages 99–118. Electronic Power Research Instiute, 1991.

[77] B. Leckner, M. Karlsson, K. Dam-Johansen, C.E. Weinell, P. Kilpinen, and M. Hupa. Influence of additives on selective noncatalytic reduction of NO with NH_3 in circulating fluidized bed boilers. *Ind. Eng. Chem. Res.*, 30(11):2396–2404, November 1991.

[78] J.A. Caton, J.K. Narney, C. Cariappa, and W.R. Laster. The Selective Non-Catalytic Reduction of Nitric Oxide Using Ammonia at up to 15% Oxygen. *Can. J. Chem. Eng.*, 73, 1995.

[79] M. Østberg, K. Dam-Johansen, and J.E. Johnsson. Influence of mixing on the SNCR process. *Chem. Eng. Sci.*, 52(15):2511–2525, August 1997.

[80] M.U. Alzueta, H. Røjel, P.G. Kristensen, P. Glarborg, and K. Dam-Johansen. Laboratory Study of the $CO/NH_3/NO/O_2$ System: Implications for Hybrid Reburn/SNCR Strategies. *Energy & Fuels*, 11(3):716–723, May 1997.

[81] L. Liang, S. Hui, S. Pan, T. Shang, C. Liu, and D. Wang. Influence of mixing, oxygen and residence time on the SNCR process. *Fuel*, 120:38–45, March 2014.

[82] S. Salimian and R.K. Hanson. A Kinetic Study of NO Removal from Combustion Gases by Injection of NH_i-Containing Compounds. *Combust. Sci. Technol.*, 23(5-6):225–230, September 1980.

[83] J. Miller, M. Branch, and R. Kee. A chemical kinetic model for the selective reduction of nitric oxide by ammonia. *Combust. Flame*, 43:81–98, 1981.

[84] A. Dean, J. Hardy, and R.K. Lyon. Kinetics and mechanism of NH_3 oxidation. *Symp. Combust.*, 19(1):97–105, January 1982.

[85] J.A. Silver and C.E. Kolb. Kinetic measurements for the reaction of amidogen + nitric oxide over the temperature range 294-1215K. *J. Phys. Chem.*, 86(16):3240–3246, August 1982.

[86] R.K. Lyon and J.E. Hardy. Discovery and development of the thermal DeNOx process. *Ind. Eng. Chem. Fundam.*, 25(1):19–24, February 1986.

[87] W. Duo, K. Dam-Johansen, and K. Østergaard. Kinetics of the gas-phase reaction between nitric oxide, ammonia and oxygen. *Can. J. Chem. Eng.*, 70(5):1014–1020, October 1992.

[88] M.C. Branch, R.J. Kee, and J.A. Miller. A Theoretical Investigation of Mixing Effects in the Selective Reduction of Nitric Oxide by Ammonia. *Combust. Sci. Technol.*, 29(3-6):147–165, December 1982.

[89] H. Røjel, A. Jensen, P. Glarborg, and K. Dam-Johansen. Mixing Effects in the Selective Noncatalytic Reduction of NO. *Ind. Eng. Chem. Res.*, 39(9):3221–3232, 2000.

[90] M. Oliva, M.U. Alzueta, A. Millera, and R. Bilbao. Theoretical study of the influence of mixing in the SNCR process. Comparison with pilot scale data. *Chem. Eng. Sci.*, 55(22):5321–5332, November 2000.

[91] E. Hampartsoumian and B. Gibbs. The influence of NH_3 addition on the NO emissions from a coal fired fluidised bed combustor. *Symp. Combust.*, 19(1):1253–1262, January 1982.

[92] M. Østberg and K. Dam-Johansen. Empirical modeling of the selective non-catalytic reduction of NO: comparison with large-scale experiments and detailed kinetic modeling. *Chem. Eng. Sci.*, 49(12):1897–1904, June 1994.

[93] M. Østberg and K. Dam-Johansen. The droplet diffusion model—An empirical model for micromixing in reacting gas phase systems. *Chem. Eng. Sci.*, 50(13):2061–2067, July 1995.

[94] J. Brouwer, M. Heap, D. Pershing, and P. Smith. A model for prediction of selective noncatalytic reduction of nitrogen oxides by ammonia, urea, and cyanuric acid with mixing limitations in the presence of CO. *Symp. Combust.*, 26(2):2117–2124, 1996.

[95] J.A. Caton and D.L. Siebers. Comparison of Nitric Oxide Removal by Cyanuric Acid and by Ammonia. *Combust. Sci. Technol.*, 65(4-6):277–293, June 1989.

[96] J.L. Lumley. Computational modeling of turbulent flows. *Advances in applied mechanics*, 18:123–176, 1979.

[97] S. Jakirlic, K. Hanjalic, and C. Tropea. Modeling Rotating and Swirling Turbulent Flows: A Perpetual Challenge. *AIAA J.*, 40(10):1984–1996, October 2002.

[98] M.A. LESCHZINER and S. HOGG. Computation of highly swirling confined flow with a Reynolds stress turbulence model. *AIAA J.*, 27(1):57–63, January 1989.

[99] F. Boysan, W.H. Ayers, and J. Swithenbank. A fundamental mathematical modelling approach to cyclone design. *Trans. Inst. Chem. Eng.*, 60a:222–230, 1982.

[100] F. Boysan, B.C.R. Ewan, J. Swithenbank, and W.H. Ayers. Experimental and theoretical studies of cyclone separation aerodynamics. In *Powtech '83 Part. Technol.*, number 69, pages 305–319. Elsevier, 1983.

[101] A.J. Hoekstra, J.J. Derksen, and H.E.A. Van Den Akker. An experimental and numerical study of turbulent swirling flow in gas cyclones. *Chem. Eng. Sci.*, 54(13-14):2055–2065, July 1999.

[102] K. Pant, C.T. Crowe, and P. Irving. On the design of miniature cyclones for the collection of bioaerosols. *Powder Technol.*, 125(2-3):260–265, June 2002.

[103] M. Sommerfeld and C.A. Ho. Numerical calculation of particle transport in turbulent wall bounded flows. *Powder Technol.*, 131(1):1–6, March 2003.

[104] H.F. Meier and M. Mori. Anisotropic behavior of the Reynolds stress in gas and gas–solid flows in cyclones. *Powder Technol.*, 101(2):108–119, February 1999.

[105] R.B. Xiang and K.W. Lee. Numerical study of flow field in cyclones of different height. *Chem. Eng. Process. Process Intensif.*, 44(8):877–883, August 2005.

[106] F. Qian, Z. Huang, G. Chen, and M. Zhang. Numerical study of the separation characteristics in a cyclone of different inlet particle concentrations. *Comput. Chem. Eng.*, 31(9):1111–1122, September 2007.

[107] G. Wan, G. Sun, X. Xue, and M. Shi. Solids concentration simulation of different size particles in a cyclone separator. *Powder Technol.*, 183(1):94–104, March 2008.

[108] F. Kaya and I. Karagoz. Numerical investigation of performance characteristics of a cyclone prolonged with a dipleg. *Chem. Eng. J.*, 151(1-3):39–45, August 2009.

[109] H.M. El-Batsh. Improving cyclone performance by proper selection of the exit pipe. *Appl. Math. Model.*, 37(7):5286–5303, April 2013.

[110] H. Safikhani, M.A. Akhavan-Behabadi, M. Shams, and M.H. Rahimyan. Numerical simulation of flow field in three types of standard cyclone separators. *Adv. Powder Technol.*, 21(4):435–442, July 2010.

[111] K. Elsayed and C. Lacor. The effect of the dust outlet geometry on the performance and hydrodynamics of gas cyclones. *Comput. Fluids*, 68:134–147, September 2012.

[112] S.K. Shukla, P. Shukla, and P. Ghosh. The effect of modeling of velocity fluctuations on prediction of collection efficiency of cyclone separators. *Appl. Math. Model.*, 37(8):5774–5789, April 2013.

[113] H. Grotjans. Application of higher order turbulence models to cyclone flows. *Vdi-Berichte*, pages 175 – 182, 1999.

[114] G. Gronald and J.J. Derksen. Simulating turbulent swirling flow in a gas cyclone: A comparison of various modeling approaches. *Powder Technol.*, 205(1-3):160–171, January 2011.

[115] J.J. Derksen and H.E.A. Van den Akker. Simulation of vortex core precession in a reverse-flow cyclone. *AIChE J.*, 46(7):1317–1331, July 2000.

[116] H. Shalaby, K. Pachler, K. Wozniak, and G. Wozniak. Comparative study of the continuous phase flow in a cyclone separator using different turbulence models. *Int. J. Numer. Methods Fluids*, 48(11):1175–1197, August 2005.

[117] H. Shalaby, K. Wozniak, and G. Wozniak. Numerical Calculation of Particle-Laden Cyclone Separator Flow Using LES. *Eng. Appl. Comput. Fluid Mech.*, 2(4):382–392, January 2008.

[118] J.J. Derksen. Separation performance predictions of a Stairmand high-efficiency cyclone. *AIChE J.*, 49(6):1359–1371, June 2003.

[119] F.J. de Souza, R. de Vasconcelos Salvo, and D.A. de Moro Martins. Large Eddy Simulation of the gas–particle flow in cyclone separators. *Sep. Purif. Technol.*, 94:61–70, June 2012.

[120] H. Mikulčić, M. Vujanović, M.S. Ashhab, and N. Duić. Large eddy simulation of a two-phase reacting swirl flow inside a cement cyclone. *Energy*, 75:89–96, October 2014.

[121] A.J. Hoekstra. *Gas Flow Field and Collection Efficiency of Cyclone Separators*. Phd thesis, Delft University of Technology, 2000.

[122] S. Elghobashi. On predicting particle-laden turbulent flows. *Appl. Sci. Res.*, 52(4):309–329, June 1994.

[123] M. Sommerfeld. Theoretical and Experimental Modelling of Particulate Flows.-Lecture Series 2000-06, 2000.

[124] M. Chiesa, V. Mathiesen, J.a. Melheim, and B. Halvorsen. Numerical simulation of particulate flow by the Eulerian–Lagrangian and the Eulerian–Eulerian approach with application to a fluidized bed. *Comput. Chem. Eng.*, 29(2):291–304, January 2005.

[125] E. Loth. Numerical approaches for motion of dispersed particles, droplets and bubbles. *Prog. Energy Combust. Sci.*, 26(3):161–223, June 2000.

[126] C. Anh Ho and M. Sommerfeld. Modelling of micro-particle agglomeration in turbulent flows. *Chem. Eng. Sci.*, 57(15):3073–3084, August 2002.

[127] S.A. Morsi and A.J. Alexander. An investigation of particle trajectories in two-phase flow systems. *J. Fluid Mech.*, 55(02):193, September 1972.

[128] S. Yuu, T. Jotaki, Y. Tomita, and K. Yoshida. The reduction of pressure drop due to dust loading in a conventional cyclone. *Chem. Eng. Sci.*, 33(12):1573–1580, January 1978.

[129] B. Wang, D.L. Xu, K.W. Chu, and A.B. Yu. Numerical study of gas–solid flow in a cyclone separator. *Appl. Math. Model.*, 30(11):1326–1342, November 2006.

[130] C.T. Crowe, M.P. Sharma, and D.E. Stock. The Particle-Source-In Cell (PSI-CELL) Model for Gas-Droplet Flows. *J. Fluids Eng.*, 99(2):325, 1977.

[131] J.J. Derksen, H.E.A. van den Akker, and S. Sundaresan. Two-way coupled large-eddy simulations of the gas-solid flow in cyclone separators. *AIChE J.*, 54(4):872–885, April 2008.

[132] D. Rong and M. Horio. Behavior of particles and bubbles around immersed tubes in a fluidized bed at high temperature and pressure: a DEM simulation. *Int. J. Multiph. Flow*, 27(1):89–105, January 2001.

[133] M. Narasimha, R. Sripriya, and P.K. Banerjee. CFD modelling of hydrocyclone—prediction of cut size. *Int. J. Miner. Process.*, 75(1-2):53–68, January 2005.

[134] M.S. Brennan. Multiphase cfd simulations of dense medium and classifying hydrocyclones. In *Proceedings of the 3rd International Conference on CFD in the Minerals and Process Industries, CSIRO Melbourne Australia*, volume 10, pages 59–63, 2003.

[135] M. Narasimha, M.S. Brennan, and P.N. Holtham. Numerical simulation of magnetite segregation in a dense medium cyclone. *Miner. Eng.*, 19(10):1034–1047, August 2006.

[136] M.S. Brennan, M. Narasimha, and P.N. Holtham. Multiphase modelling of hydrocyclones – prediction of cut-size. *Miner. Eng.*, 20(4):395–406, April 2007.

[137] S.A. Grady, G.D. Wesson, M. Abdullah, and E.E. Kalu. Prediction of 10-mm Hydrocyclone Separation Efficiency Using Computational Fluid Dynamics. *Filtr. Sep.*, 40(9):41–46, November 2003.

[138] H.F. Meier and M. Mori. Gas-solid flow in cyclones: The Eulerian-Eulerian approach. *Comput. Chem. Eng.*, 22(98):S641–S644, March 1998.

[139] J. Gao, Y. Zhao, S. Sun, H. Che, G. Zhao, and J. Wu. Experiments and numerical simulation of sawdust gasification in an air cyclone gasifier. *Chem. Eng. J.*, 213:97–103, December 2012.

[140] D.W.F. Michels, G. Gnaedig, and J.R. Comparato. The Application of Computational Fluid Dynamics in the NOxOUT Process for Reducing NOx Emissions from Stationary Combustion Sources. In *Am. Flame Res. Comm. 1990 Fall Int. Symp.*, San Francisco, California, 1990. Digitized by: J. Willard Marriott Library, University of Utah.

[141] M.A. Cremer, C.J. Montgomery, D.H. Wang, M.P. Heap, and J.Y. Chen. Development and implementation of reduced chemistry for computional fluid dynamics modeling of selective non-catalytic reduction. *Proc. Combust. Inst.*, 28(2):2427–2434, January 2000.

[142] M.S. Skjøth-Rasmussen, O. Holm-Christensen, M. Østberg, T.S. Christensen, T. Johannessen, A.D. Jensen, P. Glarborg, and H. Livbjerg. Post-processing of detailed chemical kinetic mechanisms onto CFD simulations. *Comput. Chem. Eng.*, 28(11):2351–2361, October 2004.

[143] T.D.B. Nguyen, Y.I. Lim, S.J. Kim, W.H. Eom, and K.S. Yoo. Experiment and Computational Fluid Dynamics (CFD) Simulation of Urea-Based Selective Noncatalytic Reduction (SNCR) in a Pilot-Scale Flow Reactor. *Energy & Fuels*, 22(6):3864–3876, November 2008.

[144] J. Chen. Development of reduced mechanisms for numerical modelling of turbulent combustion. In *Workshop on Numerical Aspects of Reduction in Chemical Kinetics, France*, 1997.

[145] W. Zhou, A. Marquez, D. Moyeda, S. Nareddy, J. Frato, G. Yu, S. Knarvik, and V. Froseth. Design and test of a selective noncatalytic reduction (SNCR) system for full-scale refinery CO boilers to achieve high NOx removal. *Energy and Fuels*, 24(7):3936–3941, 2010.

[146] N. Modlinski. Numerical simulation of SNCR (selective non-catalytic reduction) process in coal fired grate boiler. *Energy*, 40:1–10, 2015.

[147] T. Blejchař and D. Dolníčková. Numerical Simulation of SNCR Technology with Simplified Chemical Kinetics Model. *EPJ Web Conf.*, 45:01015, 2013.

[148] A.A.B. Musa, X.W. Zeng, Q.Y. Fang, and H.C. Zhou. Numerical simulation on improving NOx reduction efficiency of SNCR by regulating the 3-D temperature field in a furnace. *Adv. Mater. Res.*, 807-809(X):1505–1513, 2013.

[149] M. Ghamri, S. Vats, and A. Ratner. Numerical modeling of urea injection and no emission in a stoker boiler. In *8th US national combustion meeting organized by the western states section of the combustion Institute and hosted by the university of Utah (May 19–22, 2013)*, 2013.

[150] P.E. Burström, D. Antos, T.S. Lundström, and B.D. Marjavaara. A CFD-based evaluation of selective non-catalytic reduction of nitric oxide in iron ore grate-kiln plants. *Prog. Comput. Fluid Dyn. An Int. J.*, 15(1):32, 2015.

[151] Z. Xia, J. Li, T. Wu, C. Chen, and X. Zhang. CFD simulation of MSW combustion and SNCR in a commercial incinerator. *Waste Manag.*, 34(9):1609–1618, 2014.

[152] P.E. Burström, T.S. Lundstrom, B.D. Marjavaara, and S. Toyra. CFD-modelling of Selective Non-Catalytic Reduction of NOx in grate-kiln plants. *Prog. Comput. Fluid Dyn. An Int. J.*, 10(5/6):284, 2010.

[153] B. Ljungdahl and J. Larfeldt. Optimised NH3 injection in CFB boilers. *Powder Technol.*, 120(1-2):55–62, October 2001.

[154] W.G. Huang, J.J. Li, and H.R. Yang. DeNOx Technology Selection and Optimal Design of SNCR System for a 300MWe CFB Boiler. *Appl. Mech. Mater.*, 492:7–12, 2014.

[155] ENERGINET/DK. https://energinet.dk/Gas/Gaskvalitet/Gaskvalitet-maaned-for-maaned.

[156] S. Sun, Y. Zhao, F. Ling, and F. Su. Experimental research on air staged cyclone gasification of rice husk. *Fuel Process. Technol.*, 90(4):465–471, 2009.

[157] H.K. Versteeg and W. Malalasekera. *An introduction to computational fluid dynamics: the finite volume method*. Pearson Education, 2007.

[158] R.B. Bird, W.E. Stewart, and E.N. Lightfoot. Transport phenomena, rev. *Wiley, New York*, 2007.

[159] G.K. Batchelor. *An introduction to fluid dynamics*. Cambridge University Press., 1991.

[160] C.J. Stairmand. The design and performance of cyclone separators. *Trans. Inst. Chem. Eng*, 29:356–383, 1951.

[161] *Ansys Fluent Theory' Guide, Release 15.0*. 2015.

[162] *Ansys Fluent Users' Guide, Release 15.0*. 2015.

[163] J.P. Van Doormaal and G.D. Raithby. ENHANCEMENTS OF THE SIMPLE METHOD FOR PREDICTING INCOMPRESSIBLE FLUID FLOWS. *Numer. Heat Transf.*, 7(2):147–163, April 1984.

[164] S.K. Shukla, P. Shukla, and P. Ghosh. Evaluation of numerical schemes using different simulation methods for the continuous phase modeling of cyclone separators. *Adv. Powder Technol.*, 22(2):209–219, March 2011.

[165] Increase Performance.

[166] R. Reid, J. Prausnitz, and T. Sherwood. *The Properties of Gases and Liquids*. McGraw-Hill,, 1977.

[167] B..F. Magnussen and B.H. Hjertager. On mathematical modeling of turbulent combustion with special emphasis on soot formation and combustion. *Symp. Combust.*, 16(1):719–729, January 1977.

[168] D. Wenli, K. Dam-Johansen, and K. Øtergaard. Widening the temperature range of the thermal DeNOx process. An experimental investigation. *Symp. Combust.*, 23(1):297–303, 1991.

[169] F. Kasuya, P. Glarborg, J.E. Johnsson, and K. Dam-Johansen. The thermal DeNOx process: Influence of partial pressures and temperature. *Chem. Eng. Sci.*, 50(9):1455–1466, May 1995.

[170] D.B.. Spalding. Mixing and chemical reaction in steady confined turbulent flames. *Symp. Combust.*, 13(1):649–657, January 1971.

[171] D. Stropky, K. Pougatch, P. Nowak, M. Salcudean, P. Pagoria, I. Gartshore, and J. Yuan. RTD (residence time distribution) predictions in large mechanically aerated lagoons. *Water Sci. Technol.*, 55(11):29, June 2007.

[172] Rtd prediction, modelling and measurement of gas flow in reactor. *Nukleonika*, 43(1):95–114, 1998.

[173] S. Turns. *An Introduction to Combustion: Concepts and Applications w/Software*. McGraw-Hill Companies,Incorporated, 1999.